Location-Aware Adaptive Vehicle Dynamics System: Linear Chassis Predictions

Rebecca Anne Bandy

Thesis submitted to the faculty of the Virginia Polytechnic Institute and State University
in partial fulfillment of the requirements for the degree of

Master of Science
In
Mechanical Engineering

John B. Ferris
Jan Helge Bøhn
Alexander Leonessa

May 1, 2014
Blacksburg, Virginia

Keywords: vehicle dynamics, active safety, predictive dynamics, perturbation theory

Location-Aware Adaptive Vehicle Dynamics System: Linear Chassis Predictions

Rebecca Anne Bandy

Abstract

One seminal question that faces a vehicle's driver (either human or computer) is predicting the capability of the vehicle as it encounters upcoming terrain. A Location-Aware Adaptive Vehicle Dynamics (LAAVD) System is being developed to assist the driver in maintaining vehicle handling capabilities through various driving maneuvers. In contrast to current active safety systems, this system is predictive, not reactive. The LAAVD System employs a predictor-corrector method in which the driver's input commands (throttle, brake, steering) and upcoming driving environment (terrain, traffic, weather) are predicted. An Intervention Strategy uses a novel measure of handling capability, the Performance Margin (PM), to assess the need to intervene. The driver's throttle and brake control are modulated to affect desired changes to the PM in a manner that is minimally intrusive to the driver's control authority. This system depends heavily on an understanding of the interplay between the vehicle's longitudinal, lateral, and vertical forces, as well as their resulting moments. These vehicle dynamics impact the PM metric and ultimately the point at which the Intervention Strategy will modulate the throttle and brake controls. Real-time implementation requires the development of computationally efficient predictive models of the vehicle dynamics.

In this work, a method for predicting future vehicle states, based on current states and upcoming terrain, is developed using perturbation theory. An analytical relationship between the change in the spindle forces and the resulting change in the PM is derived, and the inverse relationship, between change in PM and resulting changes in longitudinal forces, is modeled. This model is implemented in the predictor-corrector algorithm of the Intervention Strategy. Corrections to the predicted states are made at each time step using a detailed, full, non-linear vehicle model. This model is run in real-time and is intended to be replaced with a drive-by-wire vehicle. Finally, the impact of this work on the automotive industry is discussed and recommendations for future work are given.

Dedication

To my parents, for teaching me that life is a journey, not a race.

Acknowledgements

First and foremost, I would like to thank my advisor, Dr. John Ferris for his support throughout my graduate career. This thesis would not have been possible without his patience, guidance, and technical expertise. In addition to his support of my thesis research, Dr. Ferris graciously allowed me to pursue other opportunities during my studies, and in doing so, has provided me with a unique perspective of the automotive engineering sector. I am also indebted to my other committee members: Dr. Jan Helge Bøhn, for providing me with opportunities to study in Germany and for broadening my horizons, and Dr. Alexander Leonessa, who initially welcomed me to Blacksburg and has kept me on my toes during my time here.

Special thanks are also due to Volkswagen Group of America for sponsoring the LAAVD research and to the National Science Foundation for sponsorship of the REU program that has been integral to my graduate studies.

I would also like to recognize the role that my fellow graduate students, from the Vehicle Terrain Performance Laboratory, to Darmstadt, to Blacksburg at large, have played in keeping my spirits up throughout this experience.

Lastly, I am forever thankful for my extensive family. You all have been the driving force behind all of my adventures, and I would have accomplished none of this without your constant encouragements to follow my dreams. Thank you.

Table of Contents

List of Figures

List of Tables

Nomenclature

Abbreviations

ABS	-	Antilock Braking System
ADAS	-	Advanced Driver Assistance System
CAS	-	Collision Avoidance System
CG	-	Center of Gravity
ESC	-	Electronic Stability Control
IS	-	Intervention Strategy
LAAVD	-	Location-Aware Adaptive Vehicle Dynamics
LKS	-	Lane-Keeping System
PM	-	Performance Margin
SAE	-	Society of Automotive Engineers
VTPL	-	Vehicle Terrain Performance Laboratory
VDC	-	Vehicle Dynamics Control
VSC	-	Vehicle Stability Control
V2I	-	Vehicle-to-Infrastructure
V2V	-	Vehicle-to-Vehicle
TCS	-	Traction Control Systems

Symbols

a	-	Distance from front axle to vehicle center of gravity
b	-	Distance from rear axle to vehicle center of gravity
d	-	½ of vehicle track width
F_{xij}	-	Longitudinal force measured at station *i* and tire *j*
F_{yij}	-	Lateral force measured at station *i* and tire *j*
F_{zij}	-	Vertical force measured at station *i* and tire *j*
m	-	Vehicle mass
m_s	-	Vehicle sprung mass
t	-	Time
u	-	Path vector
v_x	-	Longitudinal velocity
v_z	-	Vertical velocity
$\dot{v}_y$	-	Lateral acceleration
X	-	Global longitudinal coordinate
Y	-	Global lateral coordinate
Z	-	Global vertical coordinate
ΔF_x	-	Change in longitudinal force
ΔF_y	-	Change in lateral force
ΔF_z	-	Change in vertical force
ΔPM	-	Change in Performance Margin

η	-	Roll stiffness ratio
μ	-	Friction coefficient
ρ	-	Radius of curvature of track profile
ω_y	-	Lateral rotational velocity
ω_z	-	Vertical rotational velocity

1 Introduction

Autonomous vehicles have been an active area of research for over 30 years; steady progress has resulted in many impressive contributions [1] [2] [3] [4]. As noted by Matthews, one seminal question that faces the vehicle's driver (either human or computer) is predicting the capability of the vehicle as it encounters upcoming terrain [5]. A model of the vehicle (either a conceptual model developed in the mind of a human based on previous driving experience, or a mathematical model in which the complex multi-body dynamics are calculated by the computer) and the excitation of this model must both be considered when predicting the resulting vehicle performance. In this way, the driver can make informed decisions about the manner in which the vehicle should be driven.

Of course, when a human drives the vehicle, the computer is still of great assistance. Anti-Lock Braking Systems (ABS) typically stop the vehicle in a shorter distance than a human driver and Electronic Stability Control (ESC) systems apply different braking forces to each of the four wheels to help maintain stability during agile cornering. However, most of the current Driver Assistance Systems are reactive and only act to control the vehicle based on the current vehicle state and very little information about the local driving environment. Presently, more Advanced Driver Assistance Systems (ADAS), such as Collision Avoidance Systems (CAS) and Lane-Keeping Systems (LKS) are being developed that are predictive, rather than reactive. These new ADAS capabilities rely on the ever increasing amount of information available about the driving environment and vehicle state, as communicated by new vehicle-to-vehicle (V2V) and vehicle-to-infrastructure (V2I) systems.

1.1 Motivation

The focus of LAAVD research is to provide even greater assistance to the human driver as another step in the evolution to autonomous driving. The research focus of this work is the development of a system to avoid situations in which the vehicle exceeds its handling capabilities. The proposed method is predictive, estimating the ability of the

vehicle to successfully navigate upcoming terrain, not reactive. It is assumed that the proposed system has the luxury of knowing the future vehicle states and local driving environment. The strategy by which the system should intervene must be determined. That is, an Intervention Strategy must be developed that is minimally intrusive to the human driver's control authority, yet through modest changes to the driver's commands (and possible changes to the suspension) allow the vehicle to be navigated successfully through a corner. In addition, the Intervention Strategy must accomplish this task in a manner that is in harmony with the driver's intentions and not in a distracting or irritating manner.

This approach is unique in that the driver drives the vehicle (as opposed to autonomous driving), yet the system is predictive rather than reactive. The goal of this research is to enhance (not replace) existing ADAS. For example, the proposed system would predict that the vehicle is approaching a curve at a high rate of speed for the given conditions, alert the driver to the issue, then make modest corrections to the driver's brake and throttle commands. The intent is to avoid the situation in which systems such as ESC would become active. The ESC system is envisioned to have higher control authority than the proposed system and would take over control of the vehicle if the situation cannot be avoided.

Integrating the information about the local driving environment into these ADAS control strategies is becoming a possibility and with it comes the necessity for a predictive Intervention Strategy to control the vehicle. The purpose of this work is to extend the Location-Aware Adaptation of Vehicle Dynamics research to take advantage of this new information, especially in the following areas:

- ***Vehicle to Vehicle Communication*** **–** Several automotive manufacturers are developing systems that allow vehicles to collect and share data about terrain conditions, weather, traffic, and other information that may be helpful for drivers. The LAAVD System would use such systems to better anticipate upcoming terrain features and conditions.
- ***Collision Avoidance Systems*** **–** Cooperation with collision avoidance systems is twofold. First, the combination of sensor technologies employed by collision avoidance systems to detect and maneuver around obstacles can be used by the

LAAVD System to identify hazardous conditions. Second, the LAAVD System would pass control authority back to existing collision avoidance systems if the obstacles detected cannot be safely traversed by the Intervention Strategy alone.

- ***Lane Keeping Systems –*** Similar to collision avoidance systems, lane keeping systems utilize a variety of sensors to help the vehicle stay within the bounds of its current lane. These sensors provide valuable path prediction information which would lead to more accurate calculations of longitudinal force and handling capabilities throughout upcoming terrain by the LAAVD System.

1.2 LAAVD System Project Overview

The feasibility of this proposed research is dependent on the ability to predict future vehicle states and the availability of information about the local driving environment (e.g., bank angle, elevation changes, curvature, and friction coefficient). Clearly then, this research relies on the numerous new technologies being developed to capture and convey such information back to the vehicle and driver [6] [7]. It is therefore important to consider the scope of the proposed LAAVD System research within the broader spectrum of vehicle safety and driver assistance systems.

Current and developing systems can be organized on a plot such as Figure 1, with the passive to active spectrum on the vertical axis and the safety to convenience or comfort spectrum on the horizontal axis [7]. Each of the quadrants then encompasses a set of systems with similar end goals. The Active Safety quadrant includes collision avoidance and automatic emergency braking – two very unique systems which both take action to maintain some element of the vehicle's safety when the driver is unable to do so. In contrast, the Driver Alert quadrant includes such systems as Blind Spot Monitoring and Lane Change Warning. These systems do not actively control the vehicle's dynamics, but instead survey the immediate surroundings to build a more complete view for the driver. At the center of such a plot are the sensors that all of these varied systems are built upon.

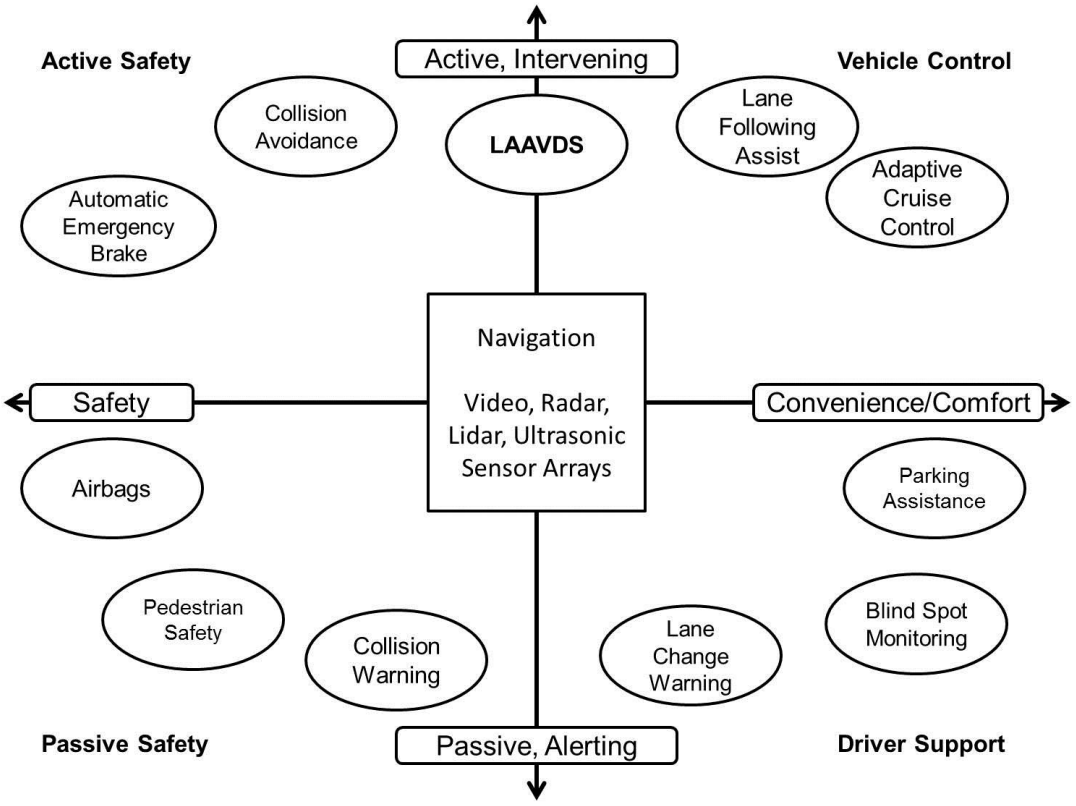

Figure 1: Map of Driver Assistance Systems

The LAAVD System under development straddles the line between safety and control, the goal of the research being to maintain safe handling capabilities through control of the longitudinal forces at the individual tire contact patches.

While the present scope of the LAAVD System research is to develop one active safety system, it is being developed with the intention of future incorporation into a fully autonomous vehicle. To ease such incorporation, standard SAE notation is used throughout the development of this system [8].

1.2.1 Intervention Strategy

This research first requires the determination of a metric which is both simple to calculate and fully captures information about when the tires (front or rear) will become saturated. This metric must be continuously estimated for upcoming driving conditions to identify when it exceeds a user defined threshold, thus triggering the Intervention Strategy. The immediate goal of the Intervention Strategy (IS) then is to bring the metric

back within an acceptable range by making modest adjustments to the throttle and brake commands.

1.2.2 Performance Margin

Matthews [5] defines the Performance Margin (PM) as the ratio of required tractive effort to complete a maneuver to the available tractive effort at the front and rear axles respectively. A PM value of unity corresponds to tire saturation and to a loss of handling. A suitable threshold for the PM can be set according to individual needs; a threshold of 0.3 is used in this research. The calculation of the PM for the front and rear axles are given by Equations 1 and 2 below where the front tires are indexed by $i = 1, 2$ and the rear tires by $i = 3, 4$. Figure 2 illustrates this tire numbering scheme. The forces F_{xi}, $F_{yi,}$ and F_{zi} correspond to the longitudinal, lateral, and vertical forces respectively as measured at each tire contact patch.

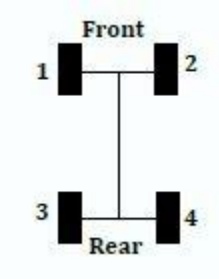

Figure 2: Tire Indexing

$$PM_{front} = \sum_{i=1}^{2} \frac{\sqrt{F_{xi}^2 + F_{yi}^2}}{\mu F_{zi}} \quad (1)$$

$$PM_{rear} = \sum_{i=3}^{4} \frac{\sqrt{F_{xi}^2 + F_{yi}^2}}{\mu F_{zi}} \quad (2)$$

1.2.3 Design Philosophy of the Intervention Strategy

The design goals for the Intervention Strategy are presented here in terms of a design optimization problem where the variable being monitored is the PM at the front and rear axles and the variable being controlled is the longitudinal force on each tire. It is assumed that the longitudinal force at each tire can be controlled separately. In a typical

passenger vehicle equipped with an internal combustion engine and ESC, this can be achieved by managing the throttle and brake directly at each wheel. The overarching assumption that the ultimate control authority resides with the driver still remains. Only modifications to the throttle and brake commands are considered here; changes to steering and vehicle dynamics (e.g. damping rates) are future considerations.

The following constraints are placed on the Intervention Strategy design problem:

1. $PM_{front} < PM_{threshold}, \forall t < T$
2. $PM_{rear} < PM_{threshold}, \forall t < T$

Where T is the preview window of near-future times being predicted (e.g., 12 seconds)

The objective function becomes:

1. Calculate ΔF_{xi}, such that the effect is minimally intrusive to the driver.

1.2.4 Overview of Intervention Strategy Implementation

At each time step, a single simulation is conducted on a full, non-linear vehicle model. This simulation is based on the current vehicle state, the driver commands (brake, throttle, steering), and the upcoming terrain. The full, non-linear simulation is conducted for some time period, T, into the future (e.g. T = 12 sec). The vehicle responses at the tire patch for this time period ($0 < t < T$) are then recovered and the PM is then calculated from the tire forces and friction according to Equations 1 and 2. This full, non-linear simulation is shown in the upper box in Figure 3.

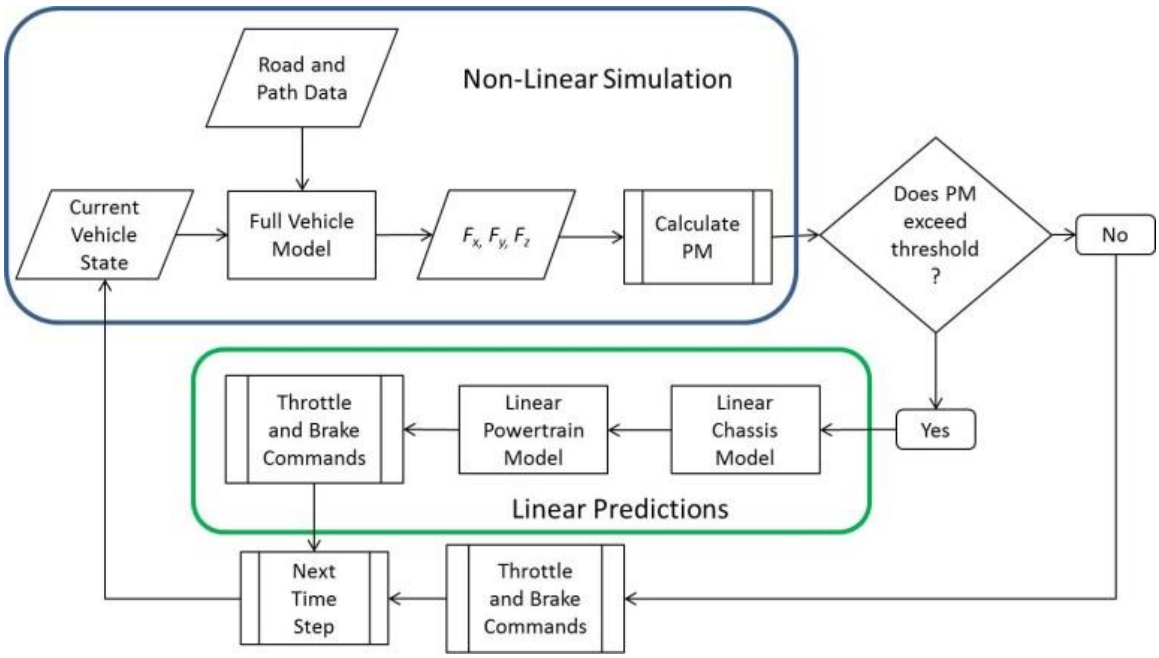

Figure 3: Overview of Intervention Strategy Implementation in Simulation

The vehicle states considered during simulation include the vehicle speed, longitudinal and lateral accelerations, yaw rates, suspension displacements and velocities. Road surface characteristics used in the full, non-linear simulation include elevation changes, bank angle, rutting, crowning, and the friction coefficient. The vehicle responses retrieved from the full model are the forces and moments at each tire contact patch and a prediction of these states at each subsequent time step.

If the PM exceeds the prescribed threshold within the preview time, then a linear prediction of the necessary changes to the longitudinal forces and subsequently to the throttle and brake commands is calculated (shown in the lower box in Figure 3). In this way, at each time step a linear predictor and non-linear corrector is used to implement the Intervention Strategy.

The strategy outlined in Figure 3 is a high-level view of the intervening process and there are several technical issues which must be further addressed. In order to determine how desired changes in the PM drive the required changes in the longitudinal force, and thus in the vehicle's handling capabilities, the effect of changes in longitudinal force on the PM must be studied. This requires a model of the full vehicle dynamics so that the interplay between longitudinal, lateral, and vertical forces and their resulting moments can be understood. This will be accomplished in two steps, first through a first-

principles approach followed by a linear predictor of the optimum changes to the longitudinal force that should affect the desired changes to the PM. When the forward problem has been solved, the backwards problem can be addressed by the linear chassis model shown in Figure 3.

Next, a linearized model must be developed to predict how changes to the throttle and brake commands affect changes to the longitudinal forces. Again, once the linear relationship between changes to the brake and throttle commands and resulting changes to the longitudinal forces is developed, then the optimum changes to the brake and throttle commands can be calculated to affect the desired changes to the longitudinal forces. This is shown as the Throttle and Brake Commands box within the lower box in Figure 3.

While the interdependence of the vehicle forces can be solved by first principles, two difficult challenges remain, namely estimating the friction and the changes to the vertical forces when the brake and throttle commands are being changed. The product of these terms composes the available traction (see the denominator in Equations 1 and 2). Predicting changes to the vertical forces due to prescribed changes in the longitudinal forces is in itself a complex task since prescribing a change in the longitudinal force requires a change in the vehicle speed and consequently the timing with which the vehicle will encounter events in the road (e.g., potholes). In addition to their dependence on terrain excitation, vertical forces are also dependent on changes to the roll and pitch motions of the vehicle. These factors must be combined to understand the full impact of vertical force on the PM.

1.3 Thesis Statement and Scope of Work

A linear relationship between changes in the longitudinal force and the resulting changes in the PM metric can be analytically derived for any vehicle operating state. This simplified relationship between ΔPM and ΔF_x will allow for computationally efficient modeling and support the real-time integration of a predictor-corrector Intervention Strategy into the proposed LAAVD System architecture.

The scope of this thesis is the linear perturbation of the longitudinal forces at the tires and the resulting change in the PM. It is assumed that the driver's intentions are

known (throttle, brake, steering, and gear selection) as is the driving environment (elevation, bank angle, friction, radius of curvature). Changes in gear selection are outside the scope of this work. Also outside the scope of this work are specifics of the tire model used within the CarSim environment. A linear point-follower model is assumed and can be expanded on in the future.

1.4 Main Contributions

The specific contributions of this thesis are listed below.

1. The determination of a linear relationship between ΔF_x and ΔPM through:
    a. A simple vehicle model consisting of the relationships
        i. $\Delta F_{z,roll} \rightarrow \Delta F_x$
        ii. $\Delta F_{z,pitch} \rightarrow \Delta F_x$
        iii. $\Delta F_{y,yaw\ and\ velocity} \rightarrow \Delta F_x$
    b. The solution to the backwards problem $\Delta PM \rightarrow \Delta F_x$
    c. The expansion of the PM equation to include varying friction coefficients
    d. The linear relationship between terrain excitations and F_z (the relationship $\Delta F_{z,terrain} \rightarrow \Delta F_x$ is left to be validated as future work)
2. Algorithmic implementation of these relationships in code and demonstration of the effectiveness through an example as a proof-of-concept

1.5 Publications

The following journal articles have been accepted for publication.

1. Bandy, R. A., Cho, S., Matthews, C., Celli, J., et al., "Location-Aware Adaptive Vehicle Dynamics System: Concept Development," *SAE Int. J. Passeng. Cars – Mech. Syst.* 7(1):2014, doi:10.2471/2014-01-0121.

2. Cho, S., Bandy, R. A., Ferris, J., Schlinkheider, J., et al., "Location-Aware Adaptive Vehicle Dynamics System: Throttle Modulation," *SAE Int. J. Passeng. Cars – Mech. Syst.* 7(1):2014, doi:10.4271/2014-01-0105.

3. Cho, S., Bandy, R. A., Ferris, J., Schlinkheider, J., et al., "Location-Aware Adaptive Vehicle Dynamics System: Brake Modulation," *SAE Int. J. Passeng. Cars – Mech. Syst.* 7(2):2014, doi:10.4271/2014-01-0079.

The following conference paper has been submitted to the DSCC 2014 Automotive and Transportation System invited session.

1. Bandy, R. A., Cho, S., Ferris, J., Schlinkheider, J., et al, "Location-Aware Adaptive Vehicle Dynamics System: Linear Chassis Predictions."

1.6 Thesis Outline

The rest of this thesis is organized as follows. First, several background topics are explored, including the LAAVD System, commercially available safety systems, vehicle dynamics, and the future of semi-autonomous vehicles. Next, the individual contributions are discussed – first a simple vehicle model related the change in lateral and vertical force back to a corresponding change in longitudinal force, then the influence of terrain excitations on vertical and ultimately longitudinal force, and finally the overall relationship between the PM metric and changes in longitudinal force at the tire contact patches. The predictive dynamics theory presented here is validated against an integrated MATLAB/Simulink – CarSim model. Finally, conclusions and the potential for future work are presented.

2 Background

2.1 Vehicle Dynamics

The vehicle dynamics which form a basis for this work begin with traditional roll, pitch, and yaw models that are derived almost entirely from first principles. Several texts in particular are helpful and are highlighted in the next section. Using perturbation theory and assuming knowledge about upcoming terrain, these traditional dynamics are expanded to form the linear chassis predictions that make up the bulk of this thesis.

2.1.1 Traditional

The SAE J670 standard on vehicle terminology [8] is followed in the development of the LAAVD System. This standard combines the previous SAE Standard J670e and the ISO Standard 8855 to recognize both Z-Up and Z-Down coordinate systems and defines five axis systems. In addition, suspension and steering components not covered in the previous ISO Standard are defined and inclined, non-uniform road surfaces are accommodated. Without the use of this standard as the basis for the LAAVD System terminology, there would be no way to ensure proper connection between the linear chassis and powertrain models or to expand this work to interface with other commercially available systems.

Several texts are referenced during the derivation of the roll, pitch, and yaw models to ensure that all of the chassis dynamics are properly accounted for. The details of the perturbations of roll, pitch, and yaw relationships are developed in Chapter 3, and a discussion of Newton's Second Law is omitted here for brevity. In particular, Greenwood [9] and Beer [10] are referenced for their fundamental explanations of Newtonian dynamics. Milliken [11], Stone and Ball [12] and Heissing [13] are referenced for their descriptions of quarter-car, single-track, and full vehicle models. Wong [14] and Pacejka [15] are of particular use when the impact of terrain excitations are included in the final model.

2.1.2 Predictive

There are several existing systems which are capable of providing information about the driving environment upon which the LAAVD System depends. In addition to more commonly available driver assistance systems (which will be discussed later), Vehicle-to-Vehicle and Vehicle-to-Infrastructure communications are becoming ever more of a possibility, thanks to technologies such as the "euroFOT" program described by Benmimoun, et al [16]. This test used data collected from over 1000 instrumented vehicles to automate incident detection. The SimTD program, coordinated through several automotive manufacturers in central Germany, tested the feasibility of large scale V2V and V2I communications and declared the technology ready for market [17]. Most recently, the U.S. Department of Transportation's (DOT) National Highway Traffic Safety Administration (NHTSA) announced that it will begin taking steps to enable V2V communication technology for light vehicles [18].

In addition to communication technologies that allow for real-time estimates of future terrain conditions and thus the prediction of vehicle handling, much headway has been made in the area of predictive modeling for either collision avoidance or steering control. Like the LAAVD System, these research projects use standard sensors and develop methods to negotiate treacherous driving conditions. In particular, Cole, et al [19] use predictive and linear quadratic control methods to model driver steering control. Steering control is not incorporated into the LAAVD System at this time, but would be another valuable tool in assessing future vehicle handling. Another project very similar to the LAAVD System is that designed by Ali, et al [20] which also aims to avoid roadway departures as well as collisions with moving or stationary objects. In addition to predicting the vehicle's tractive forces at future states, this research incorporates prediction and control of the vehicle's position within the operating lane. These types of functionalities can be added to the LAAVD System.

2.2 Terrain Measurement and Influence

Terrain is the fundamental excitation to every vehicle; terrain measurement and classification has been an area of interest to vehicle manufacturers for decades. Sayers and Karamihas [21] discuss the evolution of road profilers at length – from the first

inertial profilometer developed by the General Motors Research Laboratory up to 1998. At its simplest, a profile can be defined as a sequence of heights along a longitudinal path on the road surface, and a profiler is a device to measure such profiles. The Vehicle Terrain Measurement System (VTMS) of the VTPL was first constructed in 2006 and has seen several iterations as technologies have evolved. Described in depth by Rainey [22], the VTMS consists of a scanning laser coupled with an inertial measurement system. This allows for high fidelity representations of the road and for the body motion of the host vehicle to be completed removed from the data. What remains is a three dimensional point cloud of data which represents the elevation of the road surface. The data points are not equally spaced along the terrain surface however, due to the dependence on velocity at which the data were taken, which makes comparing the data from different runs difficult. The solution is to introduce a path coordinate, u, and a perpendicular coordinate, v, thus forming a curved regular grid (CRG) coordinate system in the horizontal plane [23]. Figure 4 is comprised of two individual graphs. The upper represents the point cloud of data immediately after collection by a profiler such as the VTMS. The data points are equally spaced with respect to time, not necessarily longitudinal distance, and the specific trajectory of the measured terrain is evident. The lower graph represents the same point cloud of data in the CRG coordinate system with equal longitudinal spacing. While the trajectory of the path is no longer immediately clear, this coordinate system allows for two runs measured at different velocities to be compared directly to one another. The CRG format will be used extensively in this work, since it allows for the vehicle response at two different velocities to be compared side by side at points u_i along the path coordinate.

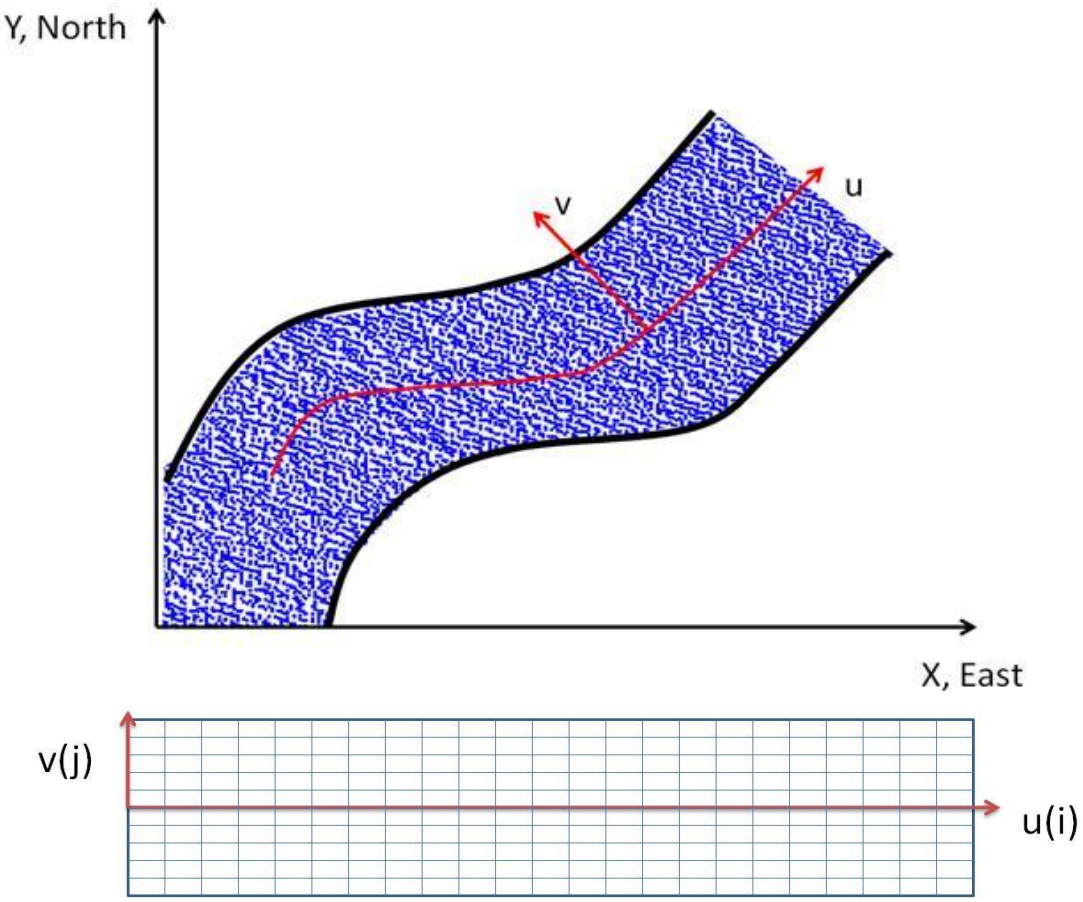

Figure 4: CRG Format [24]

This measured terrain is used as the excitation to vehicle ride, handling, and durability simulations. The relationship between these terrain excitations and vehicle response has been studied extensively, and is especially important to the predictive aspect of this work. Robson has written a series of papers that show the feasibility of estimating vehicle response spectra from known road profile excitations [25], the response of individual components to the same excitations [26], and even the response of accelerating vehicles to road undulations [27]. He goes even further to describe the roughness of the road surface, to characterize it as a stochastic process, and to relate that roughness back to the vehicle's response [28] [29] [30]. Unfortunately, Robson and his colleagues rely on describing the terrain excitations and corresponding vehicle responses in terms of power spectral density. The Intervention Strategy in its current configuration surveys vehicle states in the spatial domain, and switching between the frequency and spatial domains would not be computationally efficient enough for real-time implementation.

Nevertheless, these works are fundamental to the understanding of the interplay between terrain excitations and vehicle response, particularly at the tire contact patch.

2.3 Vehicle Safety and Driver Assistance

In addition to SAE J670, which lays out standard terms for vehicle dynamics, the SAE J2564 report is pertinent to the LAAVD System [31]. Since each vehicle manufacturer and OEM has copyrighted their own name for what are admittedly similar safety systems, this standard sets out to define common terminology which can be used to discuss current technology and any new safety technologies that may become available. Beginning with an extensive list of currently used acronyms, SAE J2564 sorts these systems into three main groups – ABS, Traction Control Systems (TCS), and ESC systems – and gives minimum requirements for such systems. For example, all ESC systems are assumed to include ABS as well as additional functionality. Vehicle Dynamics Control (VDC) patented by Bosch [6] and Vehicle Stability Control (VSC) patented by Ford [32] are both classified as ESC systems.

Again, the LAAVD System described in this work assumes that certain sensors and predictive capabilities will be available. In particular, collision avoidance, lane keeping, and V2V communication would all help position the vehicle within the lane and with respect to any upcoming maneuvers that may trigger the IS. Since the ultimate goal of the LAAVD System is to improve vehicle safety through control of its handling, recent work in the field of vehicle stabilization is of particular interest. Tjonnas [33] presents a method for yaw stabilization through brake control, longitudinal slip control, friction parameter estimation, and steering angle corrections. Anubi [34] develops a roll stabilization model based on variable suspension stiffness. Davoudi [35] also seeks to maintain stability through brake, steering, and suspension control. Looking forward, steering predictions [36], steering control [37], and path fitting [38] could all be included in the IS currently being developed. These works show that stability control by means of brake, throttle, and steering control is possible and lend credence to the viability of the proposed IS.

2.4 LAAVD System Project

The LAAVD System Project of the Vehicle Terrain Performance Laboratory (VTPL) is a multi-year research endeavor funded by Volkswagen Group of America. In addition to the broad overview given in the previous chapter, there are several key developments that deserve more discussion.

In his thesis, Celli lays out the fundamental aspect of the LAAVD System Project – the use of a simple yet inclusive metric to determine vehicle handling capacity [39]. Relying heavily on the Milliken Moment Method [40], Celli suggests the PM in its current form (Equations 1 and 2). He also lays out the tire indexing notation that is used in this thesis and shown in Figure 2 in Chapter 1.

In addition to the determination of the PM equation, Celli takes a look at friction measurement techniques, since road surface friction is an integral component to vehicle handling capability. Particularly interesting are several of the lateral dynamics based models, including Pasterkamp and Pacejka, who use neural networks and tire data to measure friction coefficients [41], Hsu, Law, and Gerdes, who estimate friction coefficients by measurements of steering torque [42].

Matthews, Cho, et al. give background on the LAAVD System and use a computer simulation to demonstrate the efficacy of using the PM as a handling metric in a vehicle control system. They demonstrate that a set of specific intervention strategies are useful in preventing loss of traction for the defined initial conditions. Future research is suggested, including the development of a computationally efficient model capturing how changes in longitudinal force impact changes on the PM [5].

Cho has also made valuable contributions to the LAAVD System Project over the past year. In his paper, "LAAVD System: Throttle Modulation," he develops a method by which desired changes in engine torque can be affected by modest throttle modulations. The desired changes in engine torque are based on changes in longitudinal force necessary to keep the PM within user defined values [43]. Even further, Cho develops a method by which similar modulations can be made to the brake commands, in the even that throttle modulations alone are not sufficient to retain a safe PM level [44].

Most recently, a driving simulator has been developed to showcase the Intervention Strategy. As detailed in [45], this simulator relies on a 7 degree-of-freedom

Simulink vehicle model, steering, throttle, and brake inputs from the user, and performs real time PM calculations. Ultimately, this simulator will be expanded to include a full, non-linear vehicle model and the predictive chassis and powertrain calculations outlined by this work and Cho [46].

3 Efficient Prediction of Vehicle Response (the Forward Problem)

The purpose of this work, within the LAAVD research framework, is to estimate future vehicle states by a linear, computationally efficient model. The work developed here is best described in terms of Figure 3, specifically the "linear chassis model" box. As initially described in Chapter 1, there are two major components to the Intervention Strategy (IS) – the full non-linear vehicle simulation (upper box) and the linear predictions (lower box). At each time step, a single simulation is conducted on a full non-linear vehicle model. The simulation is based on the current vehicle state (vehicle speed, accelerations, yaw rate, suspension displacements), driver commands (brake, throttle, steering), and information about the upcoming terrain. The vehicle model is simulated for a future time period, T. The vehicle responses at the tire contact patches are used to calculate the Performance Margin (PM) values over this simulation time period. If the PM exceeds the user defined threshold at any point in the simulation, the linear predictions in the lower box are taken into account.

The linear chassis model is developed in this work as a sequence – at each point along the track the vehicle model is linearized about the predicted trajectory and the previous vehicle state. By solving the analytical, instead of numerical, solution, the impact of each individual longitudinal force on the overall PM value becomes apparent. This model determines the relationship between changes in the PM metric resulting from changes in longitudinal force at the tire contact patches (the forward problem: estimation). This allows for a connection from the *desired* changes in PM through necessary changes in longitudinal force at each of the tires (the backward problem: prediction). This is the point at which the linear chassis prediction and linear powertrain predictions interface in Figure 3. The actual interface and relationship between changes in longitudinal force and changes in throttle are outside the scope of this work.

Cho [43] [44] determined the cutoff frequency of the powertrain to be 0.7 Hz, thus the chassis dynamics can be modeled as a linear, steady state, two-track model. Standard SAE notation and z-up orientation is used throughout the LAAVD Research [8].

Figure 5 shows a top down view of the modeled vehicle with dimensions and the tire numbering scheme used throughout this work.

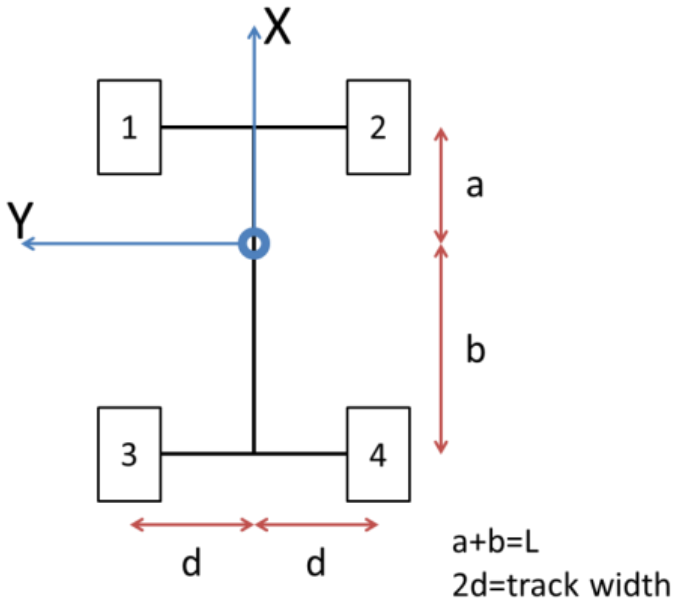

Figure 5: Vehicle Orientation and Numbering Scheme

3.1 ΔPM as a function of ΔF_x, ΔF_y, and ΔF_z

Since a standard industry test is to run over split-mu conditions, Equations 1 and 2 need to be expanded to allow for such conditions. This is accomplished by modifying the denominator in the definition of the Performance Margin to allow for different friction coefficients at the left and right tires. When μ_{left} is equal to μ_{right}, these new equations are reduced to the original form. Equations 3 and 4 are the expanded PM equations.

$$PM_{front} = \frac{\sqrt{F_{x1}^2 + F_{y1}^2} + \sqrt{F_{x2}^2 + F_{y2}^2}}{\mu_1 F_{z1} + \mu_2 F_{z2}} \quad 3$$

$$PM_{rear} = \frac{\sqrt{F_{x3}^2 + F_{y3}^2} + \sqrt{F_{x4}^2 + F_{y4}^2}}{\mu_3 F_{z3} + \mu_4 F_{z4}} \quad 4$$

In order to connect these linear predictions to the existing powertrain model in the lower box of Figure 3, an equation of the form $\Delta PM = f(\Delta F_x)$ is necessary. Consider a vector of changes to the Performance Margin and a vector of changes to the longitudinal force, ΔF_x, then the relationship being sought is simply $\Delta PM = R\Delta F_x$, where R is a

matrix whose elements are updated at each time step. Capturing all of the vehicle states in a single matrix and expressing the vehicle dynamics in terms of longitudinal force alone allows for simpler interfacing with the linear powertrain model. The solution to the backward problem is then the relationship $\Delta F_x = R^{-1}\Delta PM$ and will be discussed later in this chapter.

Taking the equations for PM given in Equations 3 and 4 and performing a Taylor Series approximation gives the first order perturbations to the system.

$$\Delta PM_{front} = \alpha_1\Delta F_{x1} + \alpha_2\Delta F_{x2} + \beta_1\Delta F_{y1} + \beta_2\Delta F_{y2} + \gamma_1\Delta F_{z1} + \gamma_2\Delta F_{z2} \quad (5)$$

Where:

$$\alpha_1 = \frac{\partial PM_f}{\partial F_{x1}} \approx F_{x1}\frac{\left[F_{x1}^2 + F_{y1}^2\right]^{-\frac{1}{2}}}{\mu_1 F_{z1} + \mu_2 F_{z2}} \quad (6)$$

$$\alpha_2 = \frac{\partial PM_f}{\partial F_{x2}} \approx F_{x2}\frac{\left[F_{x2}^2 + F_{y2}^2\right]^{-\frac{1}{2}}}{\mu_1 F_{z1} + \mu_2 F_{z2}} \quad (7)$$

$$\beta_1 = \frac{\partial PM_f}{\partial F_{y1}} \approx F_{y1}\frac{\left[F_{x1}^2 + F_{y1}^2\right]^{-\frac{1}{2}}}{\mu_1 F_{z1} + \mu_2 F_{z2}} \quad (8)$$

$$\beta_2 = \frac{\partial PM_f}{\partial F_{y2}} \approx F_{y2}\frac{\left[F_{x2}^2 + F_{y2}^2\right]^{-\frac{1}{2}}}{\mu_1 F_{z1} + \mu_2 F_{z2}} \quad (9)$$

$$\gamma_1 = \frac{\partial PM_f}{\partial F_{z1}} \approx -\mu_1\frac{PM_f}{\mu_1 F_{z1} + \mu_2 F_{z2}} \quad (10)$$

$$\gamma_2 = \frac{\partial PM_f}{\partial F_{z2}} \approx -\mu_2\frac{PM_f}{\mu_1 F_{z1} + \mu_2 F_{z2}} \quad (11)$$

Similarly, the perturbed equation for changes in PM at the rear axle is:

$$\Delta PM_{rear} = \alpha_3\Delta F_{x3} + \alpha_4\Delta F_{x4} + \beta_3\Delta F_{y3} + \beta_4\Delta F_{y4} + \gamma_3\Delta F_{z3} + \gamma_4\Delta F_{z4} \quad (12)$$

$$\alpha_3 = \frac{\partial PM_r}{\partial F_{x3}} \approx F_{x3}\frac{\left[F_{x3}^2 + F_{y3}^2\right]^{-\frac{1}{2}}}{\mu_3 F_{z3} + \mu_4 F_{z4}} \quad (13)$$

$$\alpha_4 = \frac{\partial PM_r}{\partial F_{x4}} \approx F_{x4}\frac{\left[F_{x4}^2 + F_{y4}^2\right]^{-\frac{1}{2}}}{\mu_3 F_{z3} + \mu_4 F_{z4}} \quad (14)$$

$$\beta_3 = \frac{\partial PM_r}{\partial F_{y3}} \approx F_{y3} \frac{\left[F_{x3}^2 + F_{y3}^2\right]^{-\frac{1}{2}}}{\mu_3 F_{z3} + \mu_4 F_{z4}} \quad (15)$$

$$\beta_4 = \frac{\partial PM_r}{\partial F_{y4}} \approx F_{y4} \frac{\left[F_{x4}^2 + F_{y4}^2\right]^{-\frac{1}{2}}}{\mu_3 F_{z3} + \mu_4 F_{z4}} \quad (16)$$

$$\gamma_3 = \frac{\partial PM_r}{\partial F_{z3}} \approx -\mu_3 \frac{PM_r}{\mu_3 F_{z3} + \mu_4 F_{z4}} \quad (17)$$

$$\gamma_4 = \frac{\partial PM_r}{\partial F_{z4}} \approx -\mu_4 \frac{PM_r}{\mu_3 F_{z3} + \mu_4 F_{z4}} \quad (18)$$

These equations are more succinctly represented as:

$$\begin{bmatrix} \Delta PM_{front} \\ \Delta PM_{rear} \end{bmatrix} = A\Delta F_x + B\Delta F_y + C\Delta F_z \quad (19)$$

$$A = \begin{bmatrix} \alpha_1 & \alpha_2 & 0 & 0 \\ 0 & 0 & \alpha_3 & \alpha_4 \end{bmatrix} \quad (20)$$

$$B = \begin{bmatrix} \beta_1 & \beta_2 & 0 & 0 \\ 0 & 0 & \beta_3 & \beta_4 \end{bmatrix} \quad (21)$$

$$C = \begin{bmatrix} \gamma_1 & \gamma_2 & 0 & 0 \\ 0 & 0 & \gamma_3 & \gamma_4 \end{bmatrix} \quad (22)$$

$$\Delta F_x = \begin{bmatrix} \Delta F_{x1} \\ \Delta F_{x2} \\ \Delta F_{x3} \\ \Delta F_{x4} \end{bmatrix} \quad (23)$$

$$\Delta F_y = \begin{bmatrix} \Delta F_{y1} \\ \Delta F_{y2} \\ \Delta F_{y3} \\ \Delta F_{y4} \end{bmatrix} \quad (24)$$

$$\Delta F_z = \begin{bmatrix} \Delta F_{z1} \\ \Delta F_{z2} \\ \Delta F_{z3} \\ \Delta F_{z4} \end{bmatrix} \quad (25)$$

3.1.1 Validation of the Taylor Series Approximation to ΔPM

In order to validate the equations derived in Section 3.1, several simulations are run in CarSim which involve the same vehicle traversing the same track at different velocities. The vehicle responses are processed in pairs, with the lower velocity results assumed to be the known value from which the higher velocity results would be

estimated. Because the aim of the LAAVD Research is to reduce single vehicle accidents in urban driving situations, velocities of 20 to 75 km/h are initially simulated.

The vehicle model used throughout this LAAVD Research is a sedan with a 205.94 kW engine and 6 speed automatic transmission which was previously built in a commercially available modeling environment. The specifics are presented in Appendix A.1.1 Vehicle Setup. The vehicle properties used in the roll, pitch, and yaw models are shown in
Table 1.

Table 1: Vehicle Properties

a, distance from CG to front axle	1402 mm
b, distance from CG to rear axle	1308 mm
L, wheelbase	2710 mm
d, ½ track width	800.5 mm
Track width	1601 mm
h, CG height	590 mm
m_s, sprung mass	1536 kg
η, roll stiffness ratio	0.48

To validate the Taylor Series as an approximation of changes in the Performance Margin, this vehicle is simulated driving on the track used by Matthews [5] – a length of pavement with a right hand turn, radius of 50 m, and no changes in elevation or bank angle. The coefficient of friction remains constant at 0.85 throughout the length of the test track. This track is defined according to the Curved Regular Grid (CRG) format, which defines a path vector, u, and can be sampled at equally spaced stations u_i along the length of the track. This track is later expanded to include a section of variable friction as well as a series of terrain excitation events for the validation of the roll, pitch, and yaw models developed in this chapter. Figure 6 shows the geometry of the first track tested.

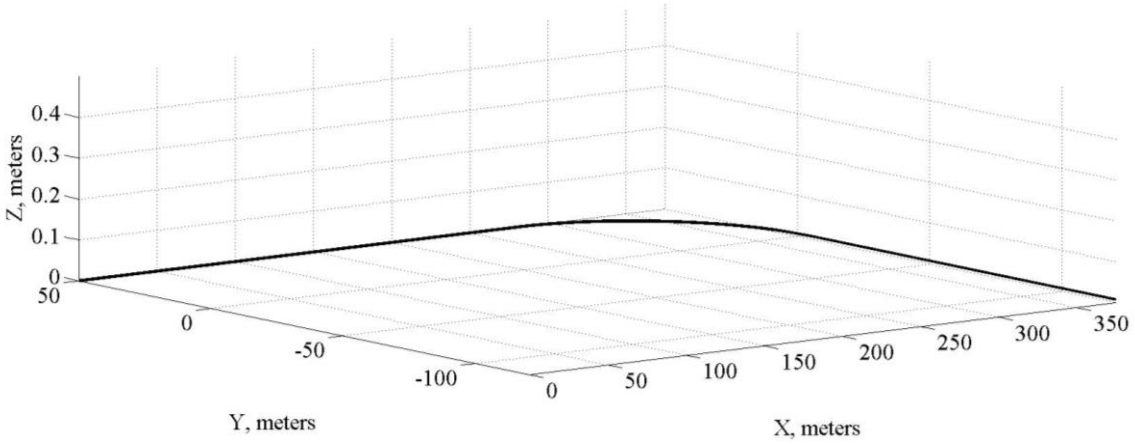

Figure 6: Track 1 - Flat Right Hand Turn

The peak PM values at the front and rear axles are evaluated for each velocity, and it is found that 60 km/h is the velocity for which the front tires reach saturation for this particular track, and higher velocities need not be investigated further. Table 2 shows the peak PM values for the front and rear axles at each velocity tested on the initial track. Note that at speeds greater than 60 km/h the peak PM value decreases. This occurs when the tire is saturated and the friction at the tire contact patch becomes dynamic, rather than static. The tire has less ability to generate lateral force and the PM, which is based on the static friction, is developed for non-limit handling. In fact, the Intervention Strategy is developed in order to maintain the vehicle in a non-limit handling operating regime.

Table 2 : Peak PM Values

Velocity (km/h)	PM value, Front	PM value, Rear
20	.2171	.2471
25	.2577	.2472
30	.3105	.2930
35	.4145	.3903
40	.5299	.4986
45	.6572	.6180
50	.7857	.7357
55	.9141	.8582
60	.9712	.9135
65	.9694	.9108
75	.9669	.9060

These results are compared in MATLAB, following the guide provided in Appendix C. In short, a Track structure is built which contains all pertinent information about the test track. Similarly, a Vehicle structure is constructed of the original CarSim results, and a Driver structure will be added in the future to allow brake, throttle, and steering commands into the algorithm. The 12 forces at the four tire contact patches are stored and indexed with respect to the station, u_i, along the test track in CarSim. These forces are interpolated to the stations in the corresponding Track structure. By organizing the vehicle, terrain, and driver information at stations along the track instead of time, it is possible to directly compare data from two different velocity tests. That is, the time dependency discussed by Bandy [47] is negated and the force response from specific excitations is clearly expressed.

The coefficients α, β, and γ are calculated for the run with lower speed using these new station-based forces. For this first simulation, the change in forces F_x, F_y, and F_z are calculated by subtracting the forces of the lower speed run from the forces of the higher speed run at each station along the track. The change in PM is then estimated from the known coefficients and changes in force.

Consider an example in which an initial simulation at 25 km/h is used to estimate the PM for a simulation at 30km/h. This example is shown in Figure 7. The PM for the initial run at 25 km/h is plotted as a blue dotted line and the estimated PM for the run at 30 km/h is plotted as a red dashed line. To compare the actual and estimated PM values at 30 km/h, the actual PM for the run at 30km/h is also plotted as a solid black line. These three plots allow for evaluation of the efficacy of the PM estimation; it is apparent how closely the estimation tracks the actual value. The relative difference in PM between the two runs, the magnitude of the PM, and rate of change of the PM can all be seen in one concise figure. After some initial settling of the vehicle simulation in the first 30 centimeters of the track, the simulated change in the value of the Performance Margin is accurate to within 3% of the actual change in PM at the front axle and 5% at the rear axle.

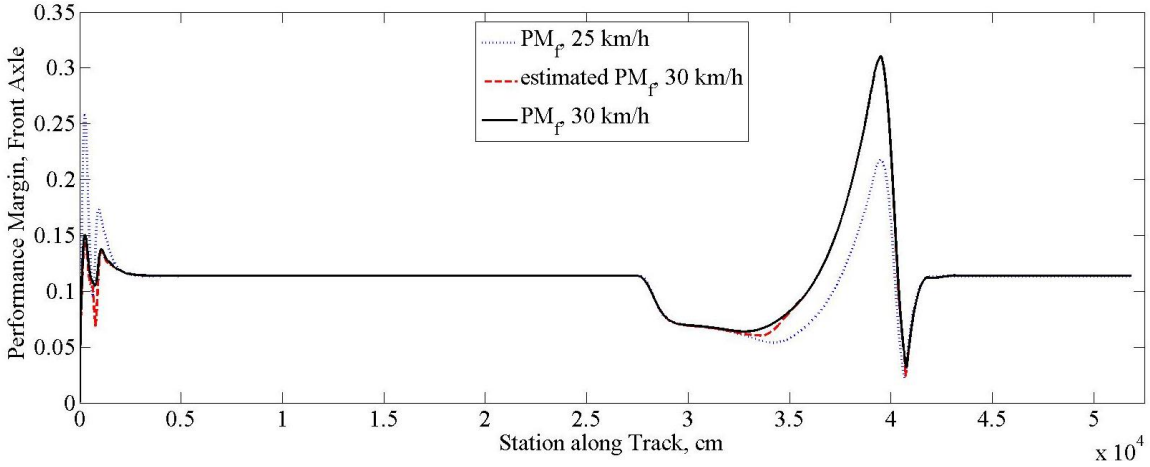

Figure 7: Estimated and Actual PM, Front Axle, 25 to 30 km/h, 1 cm spacing

This initial driving maneuver and overall estimation of PM is used to validate several parameters that will be used throughout the remainder of this analysis. In Figure 7 the track is sampled at a 1 cm spacing along the *u* coordinate (the longitudinal coordinate). This produces excellent results, but is computationally expensive in later estimation schemes. When the same simulations are run at an increased spacing of 25 cm, drastically reducing the number of stations along the track, negligible accuracy is sacrificed as shown in Figure 8 where the spacing is 25 cm. Figure 9 and Figure 10 show the absolute error between the estimated and actual changes in PM between 25 and 30 km/h. Compared side to side, it is apparent that the accuracy of the simulation does not decrease when the spacing is increased to 25 cm.

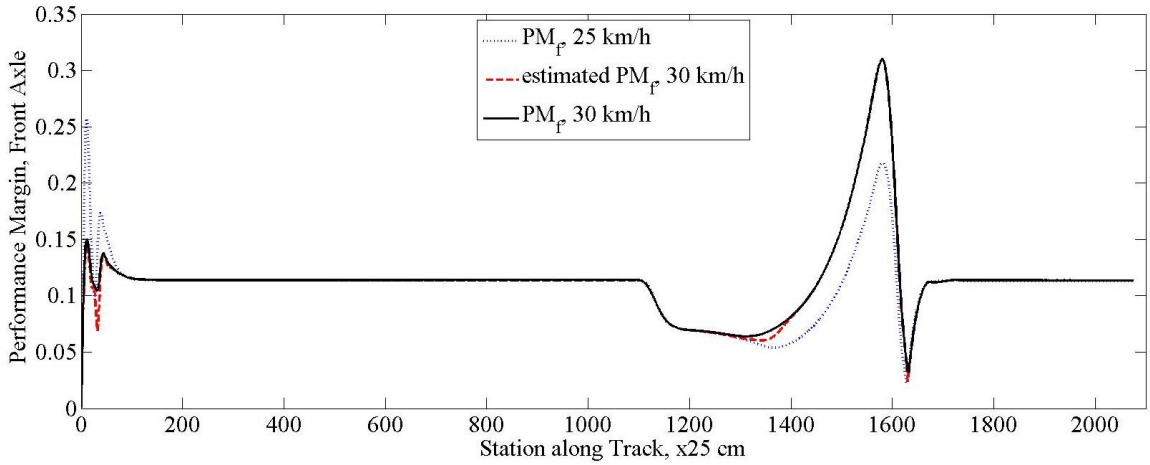

Figure 8: Estimated and Actual PM, Front Axle, 25 to 30 km/h, 25 cm spacing

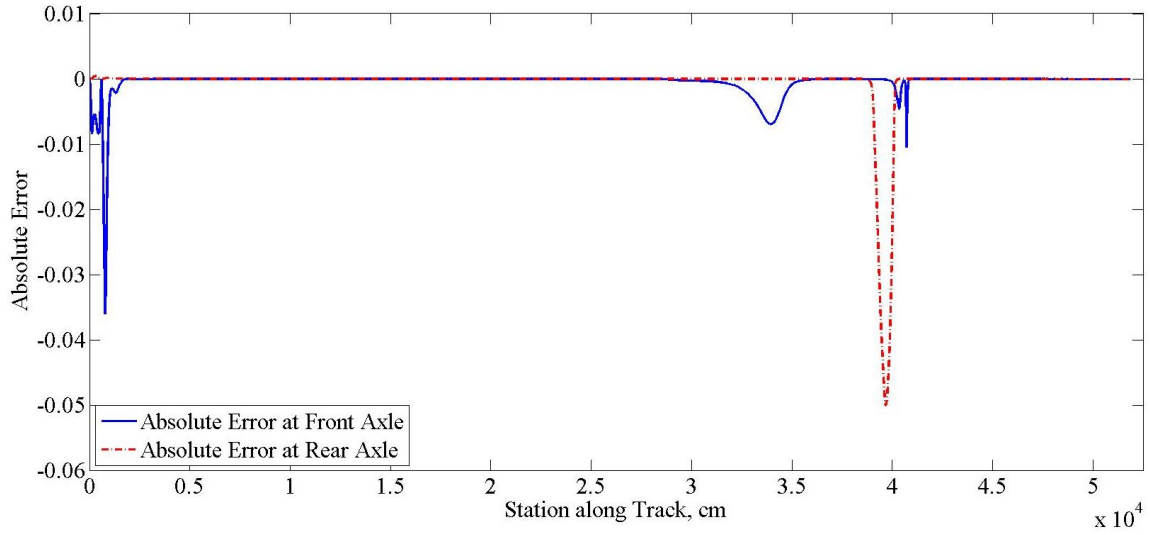

Figure 9: Absolute Error between Estimated and Actual Change in PM, 25 to 30 km/h, 1 cm spacing

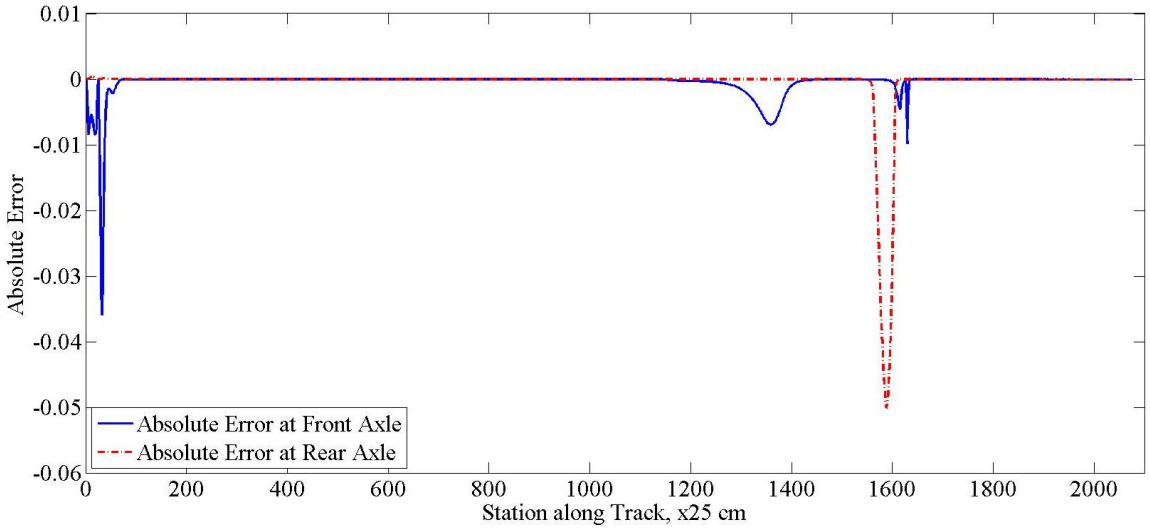

Figure 10: Absolute Error between Estimated and Actual Change in PM, 25 to 30 km/h, 25 cm spacing

Next, it is important to test the impact of relative difference between the "known" and "perturbed" velocities on the estimation accuracy. Understanding the range of speed variations over which the PM can be accurately estimated is critical in developing an Intervention Strategy (IS). Intuitively, smaller differences in velocity should produce more accurate estimations. Figure 11 and Figure 12 show the actual and estimated PM values at the front axle for 30 km/h perturbed to 45 km/h and for 40 km/h perturbed to 45 km/h respectively. These plots focus on the response to the excitation event and clearly illustrate that the estimation of PM, the red dotted line, tracks the actual PM value much

more closely with a corresponding reduction in velocity difference. That is, the estimation of the perturbed PM is more accurate when based on a velocity closer to the perturbed value. In both cases, the estimated PM performs well at values well above the cutoff value of 0.3; the error at the peak of the turning maneuver is within 1% at both cases. The magnitude of the sharp change in PM at station 1150 in the first case is too drastic for the linear simulation to capture, and the error reaches 5% by station 1300. The second case includes the same sharp change but at a smaller magnitude and the error between stations 1150 and 1300 peaks at 0.3%.

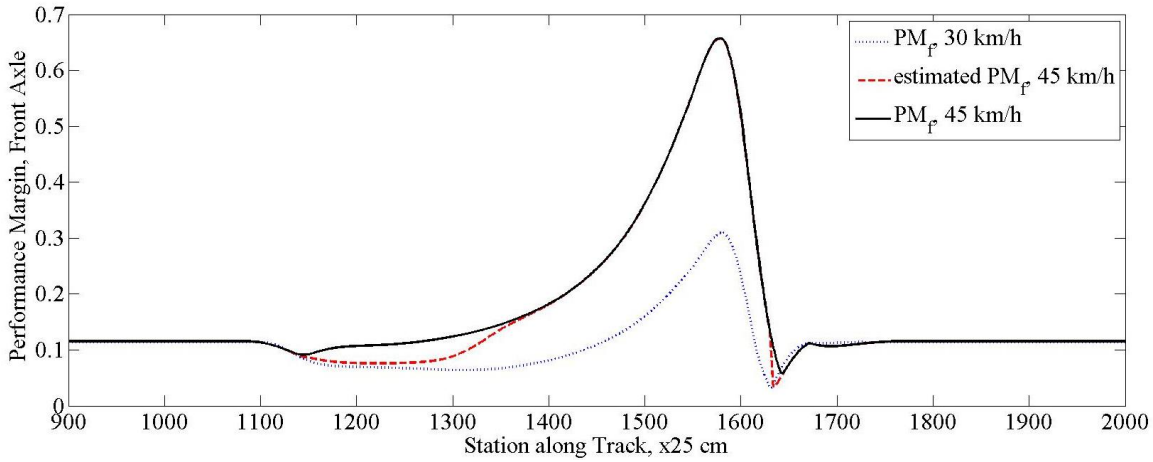

Figure 11: Estimated and Actual PM, Front Axle, 30 to 45 km/h

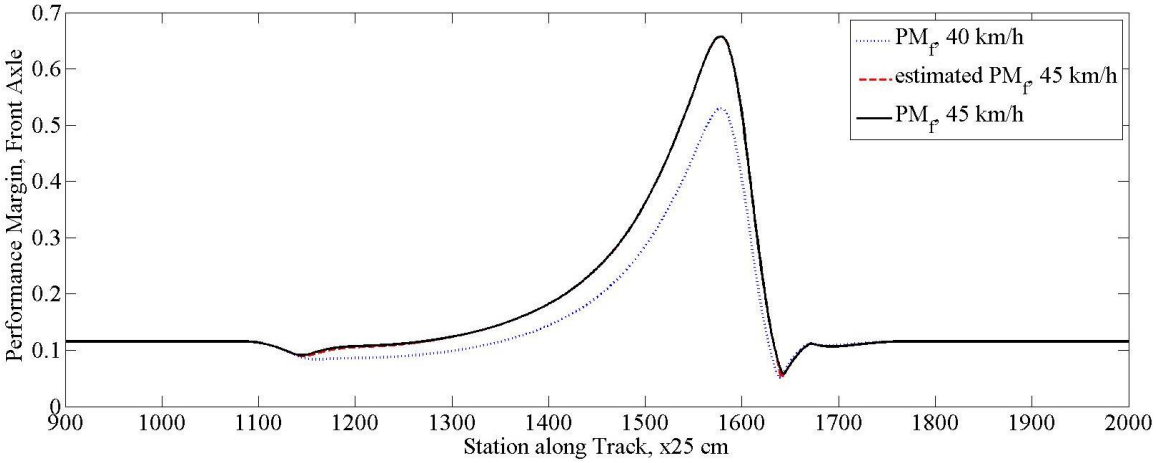

Figure 12: Estimated and Actual PM, Front Axle, 40 to 45 km/h

The effect of estimating over a range of different initial speeds is also investigated. The results of 25 km/h perturbed to 30 km/h and 55 km/h perturbed to 60 km/h are shown in Figure 13 through Figure 16. These figures focus on the response to the excitation event. Results of intermediate velocities are presented in Appendix C: Additional Results. Note

that in Figure 14 the estimated PM, shown as a dashed red line, does not track well to the actual PM, shown as a solid black line, through the turning maneuver. The error is almost 6% through the peak of the turn. Potential sources of this anomaly are discussed in Appendix B: Lateral Force Anomaly.

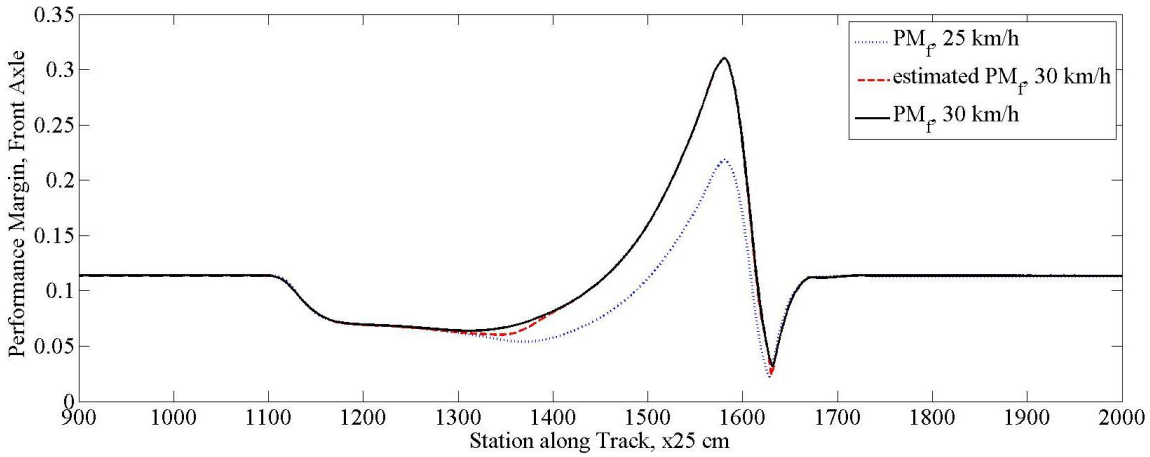

Figure 13: Estimated and Actual PM, Front Axle, 25 to 30 km/h

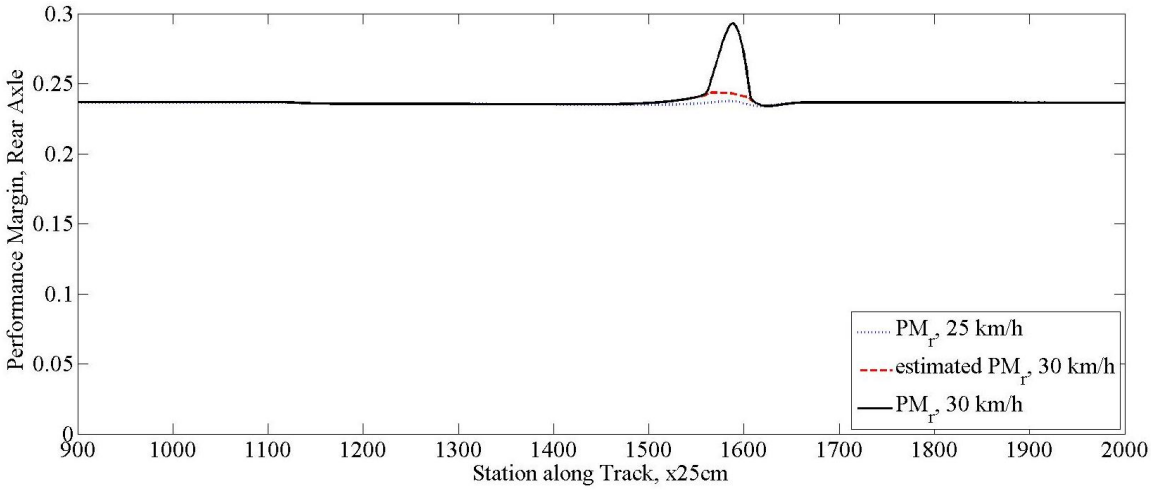

Figure 14: Estimated and Actual PM, Rear Axle, 25 to 30 km/h

Figure 15 and Figure 16 illustrate the accuracy of the Taylor Series approximation even to the limits of the PM. The case of the front axle is particularly telling, as the PM reaches a maximum of 0.9712, far above the cutoff value for this research. Through the center of the turn (station 1500), the error is below 5% at both the front and rear axles. Just prior to station 1650, the error at the front axle reaches a maximum of 10% and the rear axle exhibits almost 40% error. The PM value corresponding to this maximum error at the rear axle is 0.7037, more than double the cutoff value for this simulation. This

means that the Intervention Strategy would be triggered well before the simulation errors grow above even 5%.

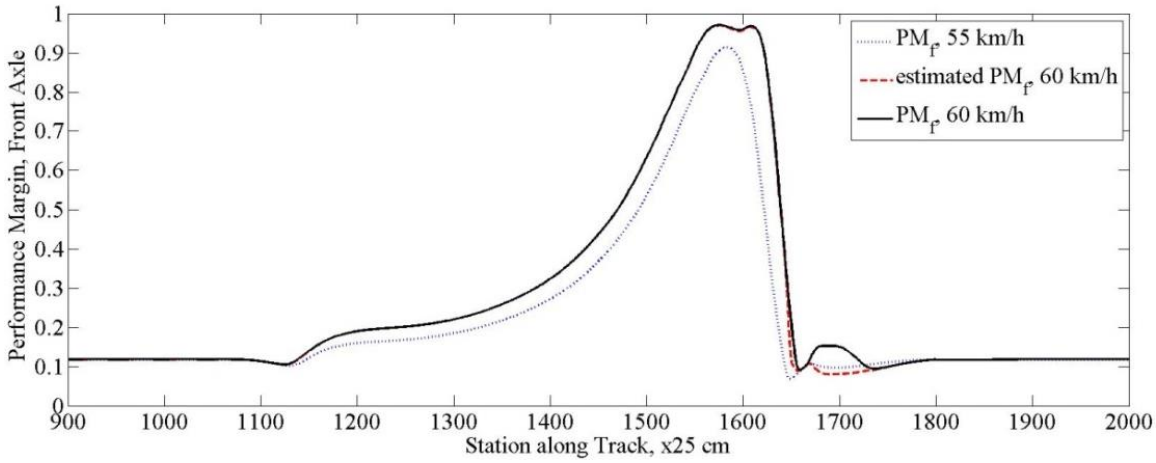

Figure 15: Estimated and Actual PM, Front Axle, 55 to 60 km/h

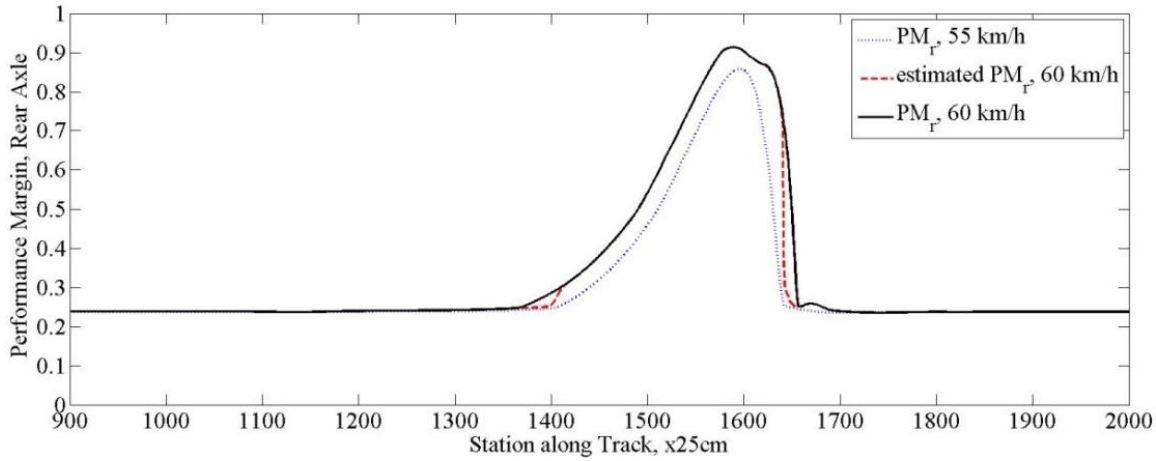

Figure 16: Estimated and Actual PM, Rear Axle, 55 to 60 km/h

These results show the validity and the acceptability of the Taylor Series approximation to changes in PM if the changes in the tire forces are known. Next, the changes in lateral force (ΔF_y) and the vertical force (ΔF_z) are estimated solely in terms of changes in the longitudinal force (ΔF_x). In this way, only one control variable, ΔF_x, is required to predict the change in PM. Similarly, the desired outcome from the powertrain model can be developed in terms of one variable, again ΔF_x. Note that ΔF_z is dependent on the roll and pitch motions of the vehicle and the direct excitation from the track (the terrain surface). ΔF_y is likewise dependent on the velocity at which the vehicle travels around a curve producing the yaw motion of the vehicle. It is assumed here that the changes in the roll, pitch, and yaw motions can be reasonably represented through steady-

state perturbations. This assumption is reasonable since there is a frequency constraint on the powertrain model, as stated by Cho [43]. Simply, if the powertrain model cannot respond instantly, it is not necessary that the chassis responds instantly.

3.2 ΔF_z due to Roll and Pitch

First, a roll model is used to find ΔF_z in terms of ΔF_y. Figure 17 shows the orientations of the forces and moments in this model as they correspond to SAE J670 [8].

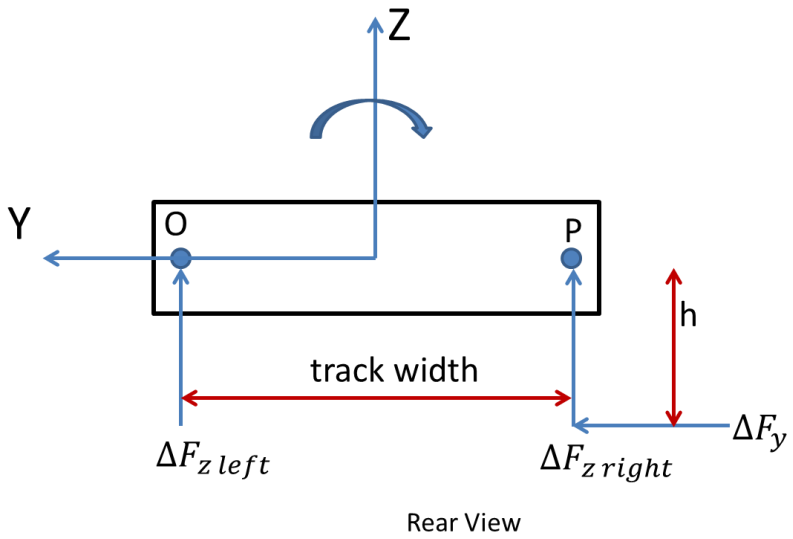

Figure 17: Vehicle Roll Model

Summing the moments about point O gives:

$$h\Delta F_y = track\Delta F_{z\,right} \tag{26}$$

While summing the moments about point P gives:

$$h\Delta F_y = -track\Delta F_{z\,left} \tag{27}$$

This gives the total roll equations:

$$\Delta F_{z1} + \Delta F_{z3} = -\frac{h}{track}\sum_{i=1}^{4} F_{yi} \tag{28}$$

$$\Delta F_{z2} + \Delta F_{z4} = \frac{h}{track}\sum_{i=1}^{4} F_{yi} \tag{29}$$

The ΔF_y term is solved in terms of ΔF_x using a yaw model in Section 3.3. Next, the portion of ΔF_z due to pitch is solved in terms of ΔF_x. Again, the SAE coordinate system is used and the orientation of forces is shown in Figure 18.

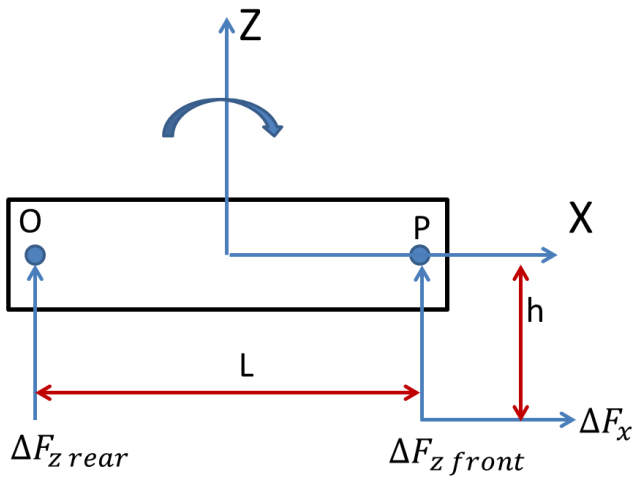

Figure 18: Vehicle Pitch Model

Summing the moments about O gives:

$$h\Delta F_x = -L\Delta F_{z\,front} \tag{30}$$

And summing the moments about P gives:

$$h\Delta F_x = L\Delta F_{z\,rear} \tag{31}$$

In total, the pitch equations are:

$$\Delta F_{z1} + \Delta F_{z2} = -\frac{h}{L}\sum_{i=1}^{4} F_{xi} \tag{32}$$

$$\Delta F_{z3} + \Delta F_{z4} = \frac{h}{L}\sum_{i=1}^{4} F_{xi} \tag{33}$$

The roll and pitch equations are underconstrained, therefore it is further assumed that the vertical load transfer left to right is biased front/rear by the ratio η and that the pitching load transfer is equal left/right. Given these constraints, and knowing that ΔF_z is comprised of roll, pitch, and road effects, the following overall equations are derived:

$$\Delta F_z = \Delta F_{z\,pitch} + \Delta F_{z\,roll} + \Delta F_{z\,road} \tag{34}$$

$$\Delta F_{z1} = -\frac{h}{2L}\Delta F_x - \frac{\eta h}{track}\Delta F_y + \Delta F_{z\,road} \quad (35)$$

$$\Delta F_{z2} = -\frac{h}{2L}\Delta F_x + \frac{\eta h}{track}\Delta F_y + \Delta F_{z\,road} \quad (36)$$

$$\Delta F_{z3} = \frac{h}{2L}\Delta F_x - (1-\eta)\frac{h}{track}\Delta F_y + \Delta F_{z\,road} \quad (37)$$

$$\Delta F_{z4} = \frac{h}{2L}\Delta F_x + (1-\eta)\frac{h}{track}\Delta F_y + \Delta F_{z\,road} \quad (38)$$

Expanding this to all stations, u_i, along the track and combining with the overall equation for PM gives the following matrix equations.

$$\begin{Bmatrix}\Delta F_{z1}\\ \Delta F_{z2}\\ \Delta F_{z3}\\ \Delta F_{z4}\end{Bmatrix}_{roll\ and\ pitch} = \frac{h}{2L}\begin{bmatrix}-1 & -1 & -1 & -1\\ -1 & -1 & -1 & -1\\ 1 & 1 & 1 & 1\\ 1 & 1 & 1 & 1\end{bmatrix}\begin{Bmatrix}\Delta F_{x1}\\ \Delta F_{x2}\\ \Delta F_{x3}\\ \Delta F_{x4}\end{Bmatrix} + \frac{h}{track}\begin{bmatrix}-\eta & -\eta & -\eta & -\eta\\ \eta & \eta & \eta & \eta\\ -(1-\eta) & -(1-\eta) & -(1-\eta) & -(1-\eta)\\ (1-\eta) & (1-\eta) & (1-\eta) & (1-\eta)\end{bmatrix}\begin{Bmatrix}\Delta F_{y1}\\ \Delta F_{y2}\\ \Delta F_{y3}\\ \Delta F_{y4}\end{Bmatrix} \quad (39)$$

$$\Delta F_{z\,roll\ and\ pitch} = D\Delta F_x + E\Delta F_y \quad (40)$$

$$\Delta PM = A\Delta F_x + B\Delta F_y + C\left(D\Delta F_x + E\Delta F_y + \Delta F_{z\,road}\right) \quad (41)$$

$$\Delta PM = (A + CD)\Delta F_x + (B + CE)\Delta F_y + C\Delta F_{z\,road} \quad (42)$$

3.2.1 Validation of ΔF_z due to Roll and Pitch

In order to isolate the impacts of roll and pitch, the equations derived above are validated on the flat right hand turn shown in Figure 6. As before, the results are sampled at 25 centimeter intervals along the track, the estimated and actual PM are plotted on the same graph, and the results are compared in pairs with a 5 km/h difference in "known" and "perturbed" velocity. Figure 19 and Figure 20 depict the results from 55 km/h perturbed to 60 km/h, again illustrating the accuracy of this method at the uppermost

limit of the PM. The error between estimated and actual changes in PM at the front axle stays belows 10% for the entire track, even when the value of the PM reaches above 0.9. The estimation at the rear axle does not perform as well – with the error between estimated and actual changes in PM reaching almost 40% through the center of the turn. Additional results (from 20 km/h up to 55 km/h) are presented in Appendix C: Additional Results.

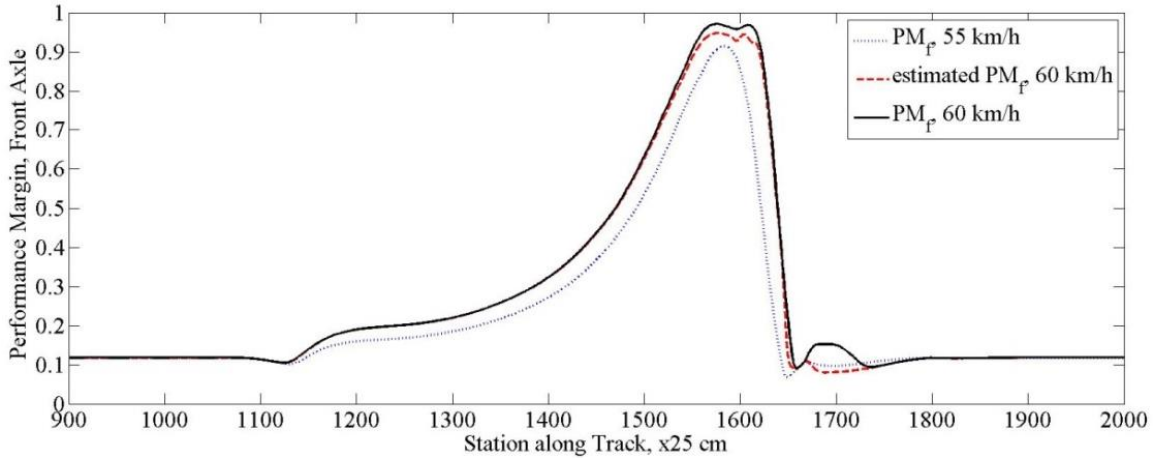

Figure 19: Estimated and Actual PM, Front Axle, 55 to 60 km/h

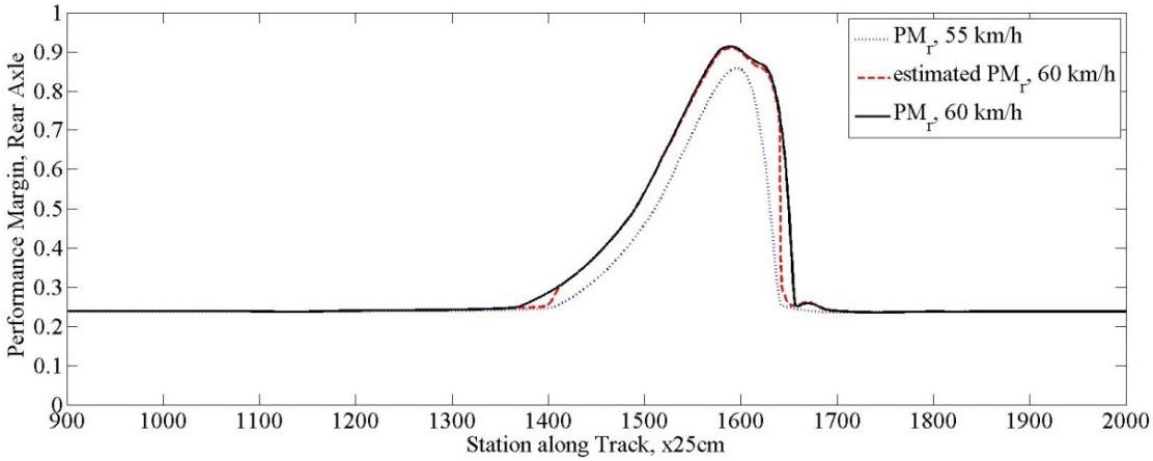

Figure 20: Estimated and Actual PM, Rear Axle, 55 to 60 km/h

As previously stated, the PM cutoff value for this simulation is 0.3, and the Intervention Strategy will be triggered well before the simulations lose their accuracy.

3.3 ΔF_y due to Velocity and Yaw

Next, a yaw model is employed to determine the relationship between ΔF_y and ΔF_x. Figure 21 shows the orientation of forces referenced in the following derivations.

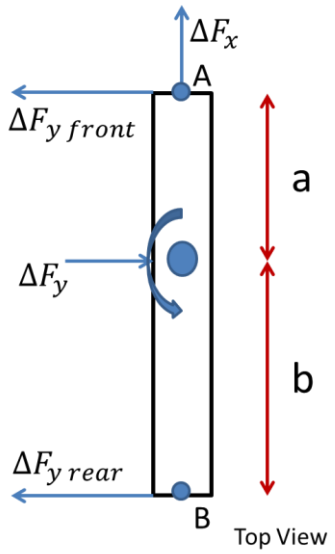

Figure 21: Vehicle Yaw Model

Summing the moments about points A and B give the following equations for the yaw motion of the vehicle.

$$\Delta F_{y\ front} = \Delta F_{y1} + \Delta F_{y2} = \frac{b}{L}\Delta F_y \quad (43)$$

$$\Delta F_{y\ rear} = \Delta F_{y3} + \Delta F_{y4} = \frac{a}{L}\Delta F_y \quad (44)$$

In order to put these equations solely in terms of longitudinal force, it is necessary to return to the definition of lateral force given by Greenwood [9] and shown below.

$$F_y = m(\dot{v}_y + v_x\omega_z - v_z\omega_y) \quad (45)$$

Neglecting the influence of road excitations, which are addressed separately, allows the vertical velocity, v_z, and the entire vertical acceleration term to be set to zero. The lateral acceleration term, $\dot{v}_y$, can also be set to zero, since the vehicle is modeled as rotating about an instantaneous center, as described by Beer [10]. The following substitution for the longitudinal acceleration allows for the replacement of the rotational term with the radius of curvature of the track – which can be calculated for each station u_i.

$$v_x \omega_z = \frac{v_x^2}{\rho} \tag{46}$$

This gives the overall form of lateral force solely in terms of longitudinal velocity.

$$\Delta F_y = \frac{2m}{\rho} v_x \Delta v_x \tag{47}$$

Beginning with the definitions of longitudinal force and velocity from first principles, the following manipulations can be made to solve for lateral force in terms of longitudinal force.

$$F_{x(i)} = \frac{m\left(v_{x(i)} - v_{x(i-1)}\right)}{t_i - t_{i-1}} \tag{48}$$

$$\Delta v_{x(i)} = \frac{\Delta F_{x(i)} \Delta t_i}{m} + \Delta v_{x(i-1)} \tag{49}$$

$$\Delta v_{x(i)} = \frac{\Delta t_i}{m} \Delta F_{x(i)} + \frac{\Delta t_{i-1}}{m} \Delta F_{x(i-1)} + \frac{\Delta t_{i-2}}{m} \Delta F_{x(i-2)} + \cdots \tag{50}$$

$$\Delta F_{x(i)} = (\Delta F_{x1} + \Delta F_{x2} + \Delta F_{x3} + \Delta F_{x4})_i \tag{51}$$

$$\Delta v_{x(i)} = \frac{1}{m} \sum_{j=1}^{i} \Delta t_j \left[\Delta F_{x1(j)} + \Delta F_{x2(j)} + \Delta F_{x3(j)} + \Delta F_{x4(j)}\right] \tag{52}$$

$$[\Delta v_{x(1)} \quad \Delta v_{x(2)} \quad \cdots \quad \Delta v_{x(n)}] = \frac{1}{m} \left[\Delta t_1 \Delta F_{x(1)} \quad \sum_{i=1}^{2} \Delta t_i \Delta F_{x(i)} \quad \cdots \quad \sum_{i=1}^{n} \Delta t_i \Delta F_{x(i)}\right] \tag{53}$$

$$[\Delta v_{x(1)} \quad \Delta v_{x(2)} \quad \cdots \quad \Delta v_{x(n)}] = \frac{1}{m} [1 \quad 1 \quad 1 \quad 1] * \begin{bmatrix} \Delta F_{x1(1)} & \Delta F_{x1(2)} & \cdots & \Delta F_{x1(n)} \\ \Delta F_{x2(1)} & \Delta F_{x2(2)} & \cdots & \Delta F_{x2(n)} \\ \Delta F_{x3(1)} & \Delta F_{x3(2)} & \cdots & \Delta F_{x3(n)} \\ \Delta F_{x4(1)} & \Delta F_{x4(2)} & \cdots & \Delta F_{x4(n)} \end{bmatrix} \begin{bmatrix} \Delta t_1 & 0 & 0 & 0 \\ 0 & \Delta t_2 & 0 & 0 \\ 0 & 0 & \ddots & 0 \\ 0 & 0 & 0 & \Delta t_n \end{bmatrix} * \begin{bmatrix} 1 & 1 & \cdots & 1 \\ 0 & 1 & \cdots & 1 \\ \vdots & 0 & \ddots & 1 \\ 0 & 0 & 0 & 1 \end{bmatrix} \tag{54}$$

First, the definition of velocity is expanded as a recursive series. The definition of longitudinal force is also expanded as a sum of the force at each tire. These are combined in Equation 52 and expanded to each station along the road in Equation 54.

$$[\Delta v_{x(1)} \quad \Delta v_{x(2)} \quad \cdots \quad \Delta v_{x(n)}] = \frac{1}{m} [I \; I \; I \; I] [\Delta F_X] [T] [U] \tag{55}$$

$$\Delta F_{y1(i)} = \frac{2bm}{2L\rho_i} v_{x(i)} \Delta v_{x(i)} = \frac{bm}{L\rho_i} v_{x(i)} \Delta v_{x(i)} \quad (56)$$

$$\delta_i = \frac{m v_{x(i)}}{\rho_i} \quad (57)$$

$$\Delta F_{y2(i)} = \frac{b}{L} \delta_i \Delta v_{x(i)} \quad (58)$$

$$\Delta F_{y3(i)} = \frac{a}{L} \delta_i \Delta v_{x(i)} \quad (59)$$

$$\Delta F_{y4(i)} = \frac{a}{L} \delta_i \Delta v_{x(i)} \quad (60)$$

$$\begin{bmatrix} \Delta F_{y1} \\ \Delta F_{y2} \end{bmatrix} = \frac{b}{L} \begin{bmatrix} \delta_1 & \ddots & 0 \\ 0 & & \delta_n \\ \delta_1 & \ddots & 0 \\ 0 & & \delta_n \end{bmatrix} [I\ I\ I\ I] \begin{bmatrix} \Delta F_{x1} \\ \Delta F_{x2} \\ \Delta F_{x3} \\ \Delta F_{x4} \end{bmatrix} [T][U] \quad (61)$$

$$\begin{bmatrix} \Delta F_{y3} \\ \Delta F_{y4} \end{bmatrix} = \frac{a}{L} \begin{bmatrix} \delta_1 & \ddots & 0 \\ 0 & & \delta_n \\ \delta_1 & \ddots & 0 \\ 0 & & \delta_n \end{bmatrix} [I\ I\ I\ I] \begin{bmatrix} \Delta F_{x1} \\ \Delta F_{x2} \\ \Delta F_{x3} \\ \Delta F_{x4} \end{bmatrix} [T][U] \quad (62)$$

These equations are put in matrix form, with the matrices T and U acting to preserve the summations from the previous form. These new equations for velocity are substituted into the equation for lateral force at each tire. The lateral forces at the front and rear tires are grouped together, and are substituted into the overall PM equation in the following series of equations.

$$\Delta PM_{front} = \left(A_f + C_f D_f\right) \begin{bmatrix} \Delta F_{x1} \\ \Delta F_{x2} \end{bmatrix} + \left(B_f + C_f E_f\right) * \frac{b}{L} [\delta] \left[[I\ I\ I\ I] [\Delta F_x] [T] [U] \right]^T + C_f \Delta F_{z\,road\ front} \quad (63)$$

$$\Delta PM_{rear} = \left(A_r + C_r D_r\right) \begin{bmatrix} \Delta F_{x3} \\ \Delta F_{x4} \end{bmatrix} + \left(B_r + C_r E_r\right) * \frac{a}{L} [\delta] \left[[I\ I\ I\ I] [\Delta F_x] [T] [U] \right]^T + C_r \Delta F_{z\,road\ rear} \quad (64)$$

Equations 63 and 64 are sufficient for modeling the impact of roll, pitch, and yaw on the overall PM, but they need to be put in a simpler form in order to connect with the impact of road excitations and ultimately, the linear powertrain model as shown in Figure 3. This is accomplished in Section 3.4.

3.3.1 Validation of ΔF_y due to Velocity and Yaw

As in the previous two sections, the actual and estimated PM values for the "known" and "perturbed" velocities are plotted on the same axes. The results of the additional yaw estimation mirror those of the roll and pitch estimations completed in Section 3.2.1, namely that though some accuracy is lost due to the introduction of another estimated variable, the linear estimation is reasonably accurate at PM values above the linear range. Figure 22 and Figure 23 show the upper limits of the roll, pitch, and yaw estimations' accuracy. The error between estimated and actual changes in PM stays below 4% at both the front and rear axle until station 1500 – well into the turn. After that, the estimation accuracy falls off significantly, reaching a peak error of almost 50% at the rear axle by station 1640.

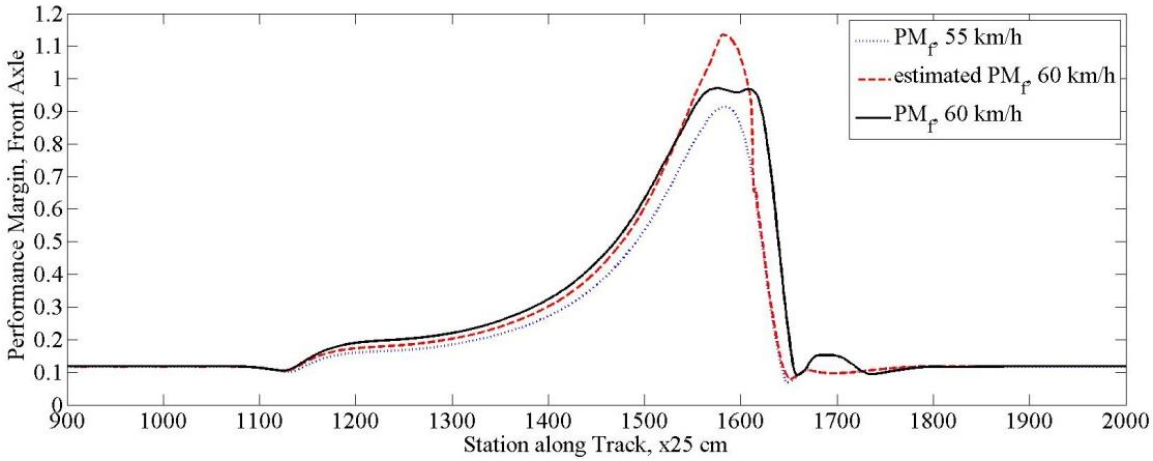

Figure 22: Estimated and Actual PM, Front Axle, 55 to 60 km/h

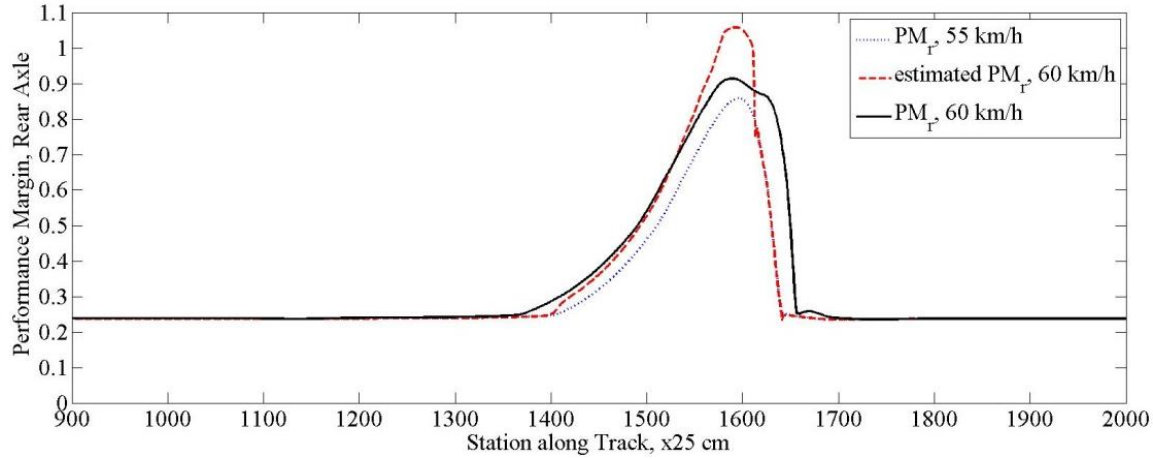

Figure 23: Estimated and Actual PM, Rear Axle, 55 to 60 km/h

The results of lower velocity runs are shown in Figure 77 to Figure 90 in Appendix C: Additional Results.

3.4 ΔPM as a function of ΔF_x

In order to connect the linear chassis model and linear powertrain model sections of Figure 3, it is necessary to have an equation of the form $\Delta PM = A * \Delta F_x$, where *A* is a matrix of size 2*n* by 4*n*, where *n* is the number of stations down the track. Beginning with Equations 63 and 64 from Section 3.3, the following manipulations are made. The *A*, *D*, and first *C* matrices are padded with zeroes, the first ΔF_x matrices are expanded to include forces from all tires, and a matrix *R* is defined such that:

$$R_f = \left(\left(A_{f_{expanded}} + C_{f_{expanded}} D_{f_{expanded}}\right) + \left(\left(B_f + C_{f_{original}} E_f\right) G_f U^T T[I\ I\ I\ I]\right)\right) \quad 65$$

$$R_r = \left(\left(A_{r_{expanded}} + C_{r_{expanded}} D_{r_{expanded}}\right) + \left(\left(B_r + C_{r_{original}} E_r\right) G_r U^T T[I\ I\ I\ I]\right)\right) \quad 66$$

The *G* matrix is a combination of the $\frac{b}{L}[\delta]$ and $\frac{a}{L}[\delta]$ terms for the front and rear axles respectively. The final formulation of the PM equation, neglecting the impact of road excitations on vertical force, is shown below.

$$\Delta PM_{front} = R_f \Delta F_x \quad 67$$

$$\Delta PM_{rear} = R_r \Delta F_x \quad 68$$

This should be expanded in the future to include the relationship $\Delta F_{z,terrain\ excitations} \rightarrow \Delta F_x$.

3.5 Efficient Prediction of Vehicle Response (the Backward Problem)

In order to incorporate the relationships between the lateral, longitudinal, and vertical forces into the Intervention Strategy, the backward problem $\Delta F_x = f(\Delta PM)$ must

be solved. The final form of the forward problem in Equations 67 and 68 is easily inverted to give the solution to the backward problem. Since the R matrices and ΔF_x vectors are indexed at stations along the track, it is now possible to pick out exactly which "active" stations correspond to where the Performance Margin crosses the threshold and where the Intervention Strategy needs to be initiated.

In the future, it is this solution to the backward problem which will directly interface with the linear powertrain model.

3.6 Validation of Split-Mu Condition

Using Equations 67 and 68, a test is also run to validate the split-mu conditions of the expanded PM equation. The track shown in Figure 6 is used again, but with a different friction profile. At 270 meters down the track, the friction coefficient changes from 0.85 across the entire track to 0.2 along the left hand side and 0.5 along the right hand side. At 280 meters, the friction changes again to 0.5 across the entire track, and at 281 meters, the friction is changed back to 0.85 for the duration of the track. The CarSim screen corresponding to these changes is shown in Figure 24. This modified version of Track 1 is called Track 2.

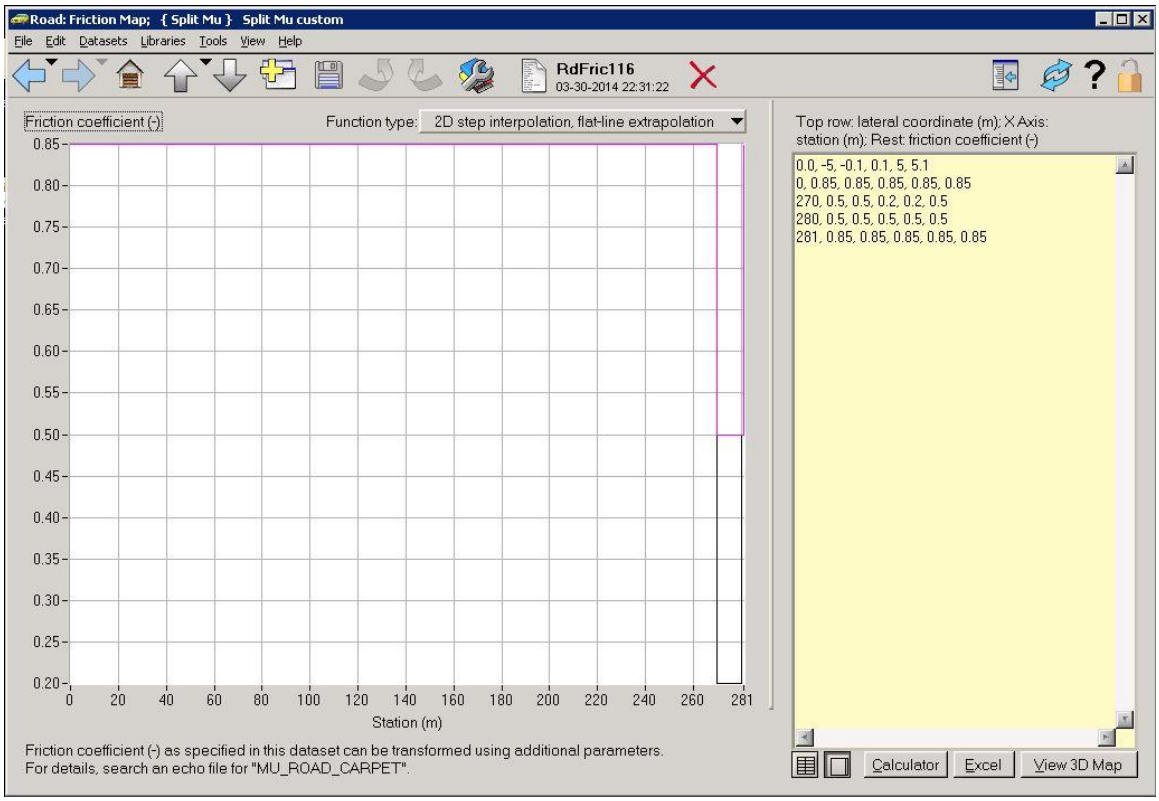

Figure 24: Friction Map for Track 2

Again, simulations are run from 20 km/h to 60 km/h in 5 km/h increments. The results are similar to those in the previous section, since the right hand turn has not been modified and generates a higher PM value than the change in friction coefficient. The results for the 50 km/h perturbed to 55 km/h case are presented here, the rest are shown in Appendix C: Additional Results. These results show that the expanded PM equation can accurately estimate the PM under split-mu conditions.

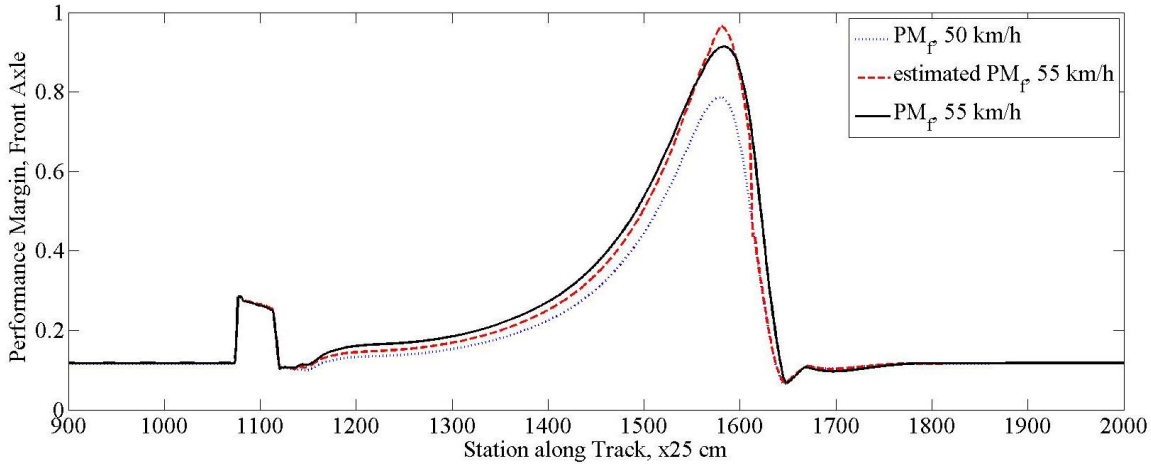

Figure 25: Estimated and Actual PM, Front Axle, 50 to 55 km/h

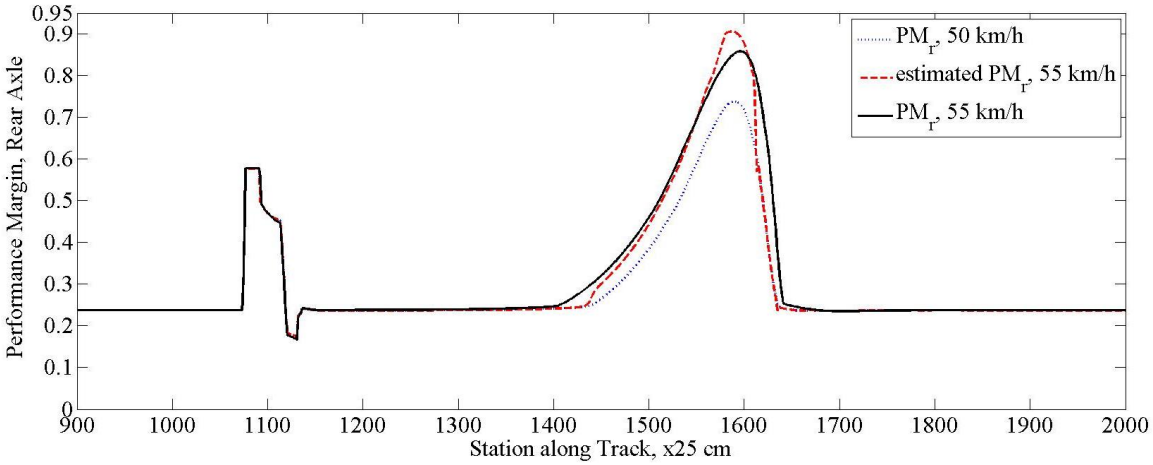

Figure 26: Estimated and Actual PM, Rear Axle, 50 to 55 km/h

4 ΔF_z due to Terrain Excitations

Much of the previous work concerning terrain excitations has dealt in the frequency domain. Constantly transforming between the temporal or spatial and frequency domains is not computationally efficient enough for this application, so a new method is developed here. The basic concept is to deal with terrain excitations as impulse functions which can be added together to simulate a smooth or rough surface. This chapter follows the development and validation of that theory, specifically that an impulse function is used to determine whether the response at one velocity can be predicted from the known response at a different velocity.

4.1 Impulse Response Function

In order to show that the vertical forces due to terrain excitations can be modeled as a series of impulse response functions, a brief study is made to first test the plausibility of estimating one impulse response from a similar, known response. As noted by Bandy [47], there is a phase shift in the timing or spacing of the vertical force response due to a sine wave excitation at higher velocities. This is somewhat assuaged by working only with lower velocities, as those in this study, and by indexing the response at stations along the road instead of time, but the feasibility of using one response to predict another was as yet unstudied. This then, is the natural progression of that previous work. Beginning with the standard equation for an impulse response function normalized over the area of the excitation, Equations 69 to 72 are derived.

$$F_z(t) = \int_0^t z(\tau)h(t-\tau)d\tau \quad (69)$$

$$d\tau = \frac{du}{v} \quad (70)$$

$$F_{zi} = uinc \sum_{j=1}^{i} \frac{z_j}{v_j} h(t_i - t_j) \quad (71)$$

$$F'_{zi} = uinc \sum_{j=1}^{i} \frac{z_j}{v'_j} h(t'_i - t'_j) \quad (72)$$

Here, F_{zi} is the vertical force response at a known velocity and $F_{zi}{}'$ is the response at a perturbed velocity. The response at the perturbed velocity is estimated by evaluating the response function $h(t_i - t_j)$ of the known velocity at the perturbed times $t'_i - t_j{}'$. These results are shown in Section 4.1.1.

4.1.1 Estimation of Impulse Response from a Known Response

Several issues are encountered with the physical representation of an impulse in CarSim before results which can be further manipulated are achieved. These issues are fully discussed in Appendix D: Impulse Response Anomaly. In short, CarSim is not able to interpolate the vehicle's response to bumps of very short duration (on the order of centimeters). A longer bump (duration of 25 cm) is used, but is found to be a step function instead of an approximation of an impulse. It is finally decided to move ahead with the results of the fourth excitation event, a bump with duration of 3 cm and a height of 10 mm, as defined in Figure 128 and Figure 134. This particular event gives physically plausible results at the 20 and 25 km/h cases, so the impulse response at 25 km/h is estimated here using the known response of the 20 km/h case. When the response function of the lower velocity run is evaluated at the timings of the higher velocity run, the following results are achieved. Figure 27 and Figure 28 show the response of the front tires focused on the excitation event. It is apparent from these figures that the estimation is close – coming within 8% of the peak value – but there still appears to be some lag in the timing of the peak force.

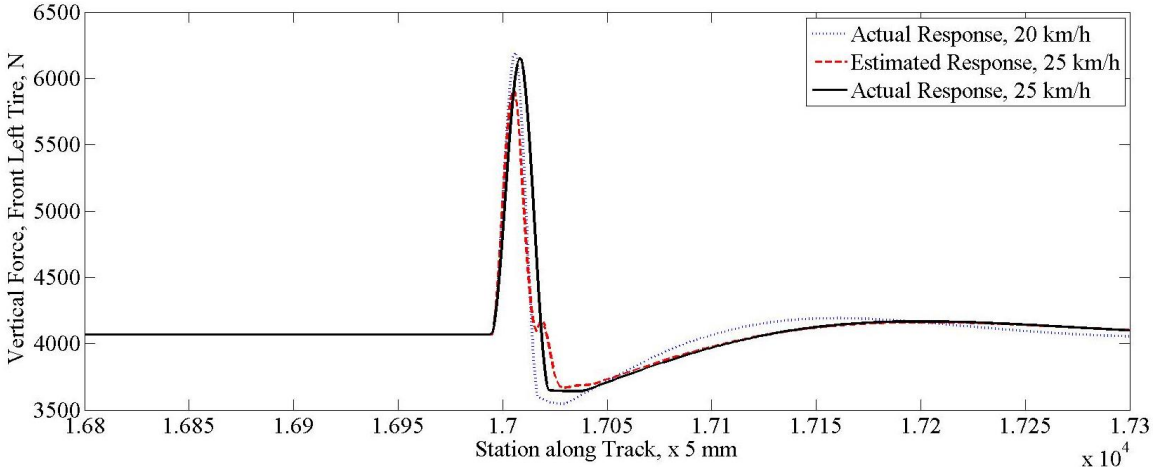

Figure 27: Estimated and Actual Impulse Response, Front Left Tire, 20 to 25 km/h

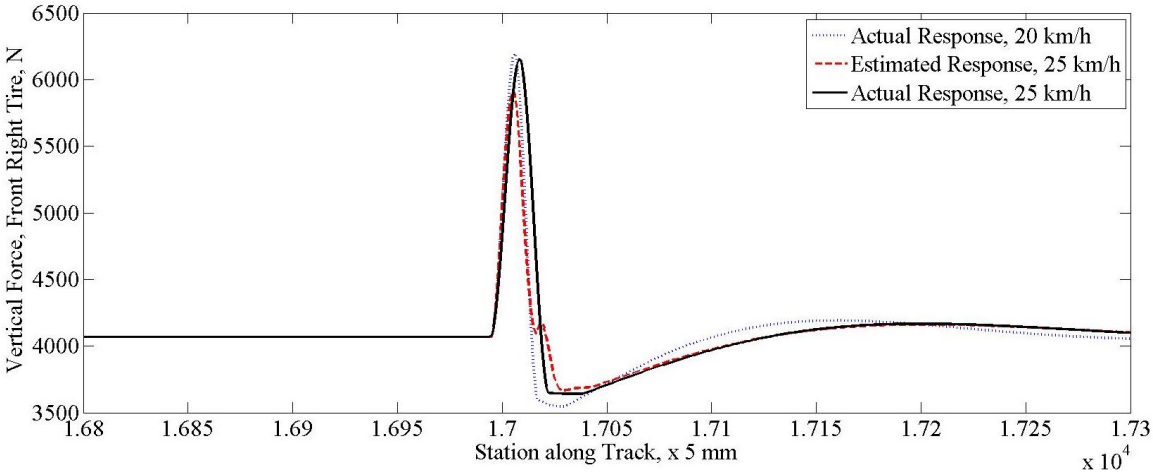

Figure 28: Estimated and Actual Impulse Response, Front Right Tire, 20 to 25 km/h

Figure 68 and Figure 69 show the estimated vertical force response at 25 km/h (the red dashed line) in comparison to the actual response at 20 km/h (dotted blue line) and 25 km/h (solid black line). There is an initial response in the correct direction, but it does not match the peak magnitude of the actual response, resulting in an error of approximately 23%. There is also a secondary estimated response that does not correlate to any of the actual results. Clearly more study is needed to determine where this second response is coming from. Unfortunately, CarSim does not contain a point-follower tire model and adding an analytical tire model into this impulse response algorithm would mean that the estimation is no longer linear, so neither potential fix is within the realm of this study and must be considered future work.

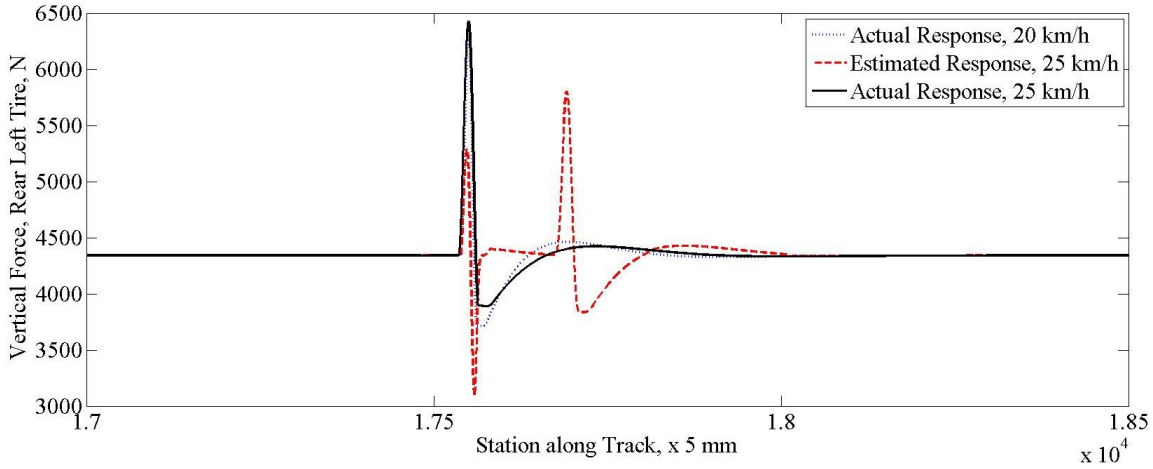

Figure 29: Estimated and Actual Impulse Response, Rear Left Tire, 20 to 25 km/h

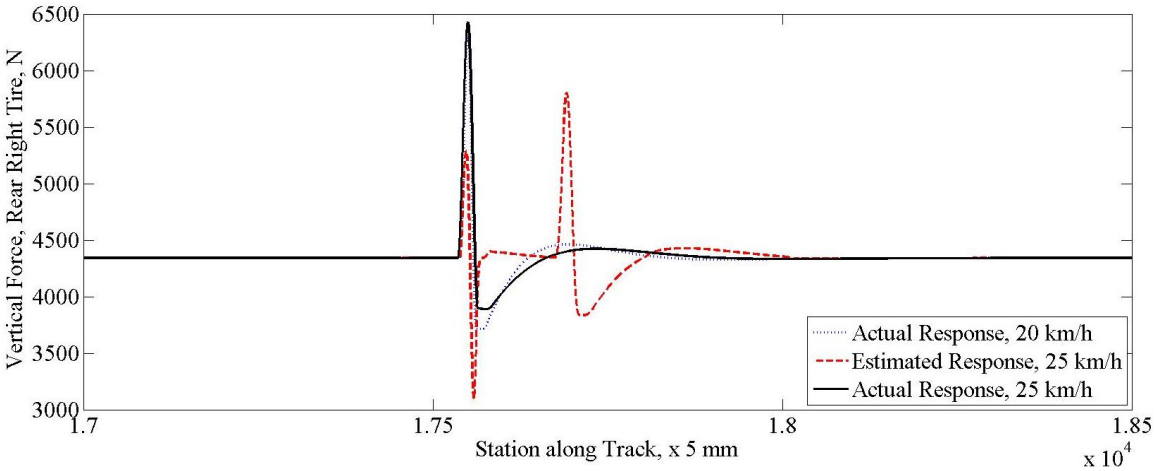

Figure 30: Estimated and Actual Impulse Response, Rear Right Tire, 20 to 25 km/h

The results at the front axle do however show that under the correct circumstances, one known response can be used to estimate another, and that achieves the goal of this particular experiment.

4.2 F_z due to Terrain Excitations

Now that the efficacy of using a known response to estimate the response at a perturbed velocity has been shown, the vertical force due to terrain excitations needs to be estimated by the vehicle's response to an impulse excitation and connected back to the longitudinal force at the tire contact patch so that this work can be connected with the existing powertrain model. The first step in this process is to validate that the form of the impulse response shown in Equation 71 can accurately estimate the vertical forces arising from a different track, not just the one on which it was measured. For this investigation,

the only set of physically plausible data resulting from the third impulse event described in Appendix D: Impulse Response Anomaly is used to quantify the vehicle's response to an impulse excitation event. This particular set of data is used because it was measured using the 225/60 R18 tires that are standard on the vehicle model used for the rest of the LAAVDS Research.

The track used to validate the expanded PM equation with varying friction conditions is updated to include three bumps, each with duration of 25 cm and a height of 10 mm, before the split-mu section. Figure 31 shows the profile of Track 3.

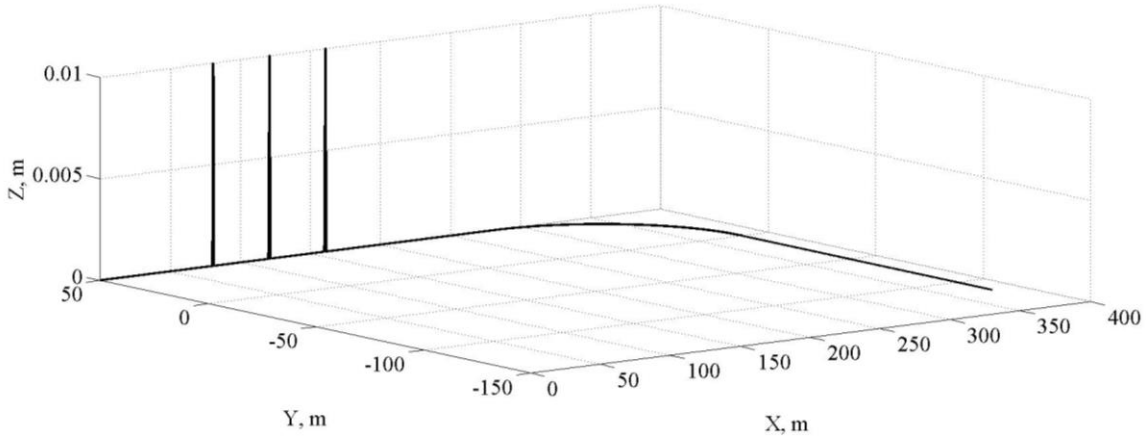

Figure 31: Track 3 Definition

The 3 cm long, 10 mm high excitation event is used to capture the impulse response at each of the four tire contact patches that are specific to this vehicle model. These impulse responses, the vector of heights from Track 3, and the velocities at which the simulations are run over Track 3 are substituted back into Equation 71 to estimate the vertical force resulting from terrain excitations alone. Figure 32 and Figure 33 show the estimated vertical force (dashed red line) and the actual vertical force (solid blue line) at the front tires at 25 km/h.

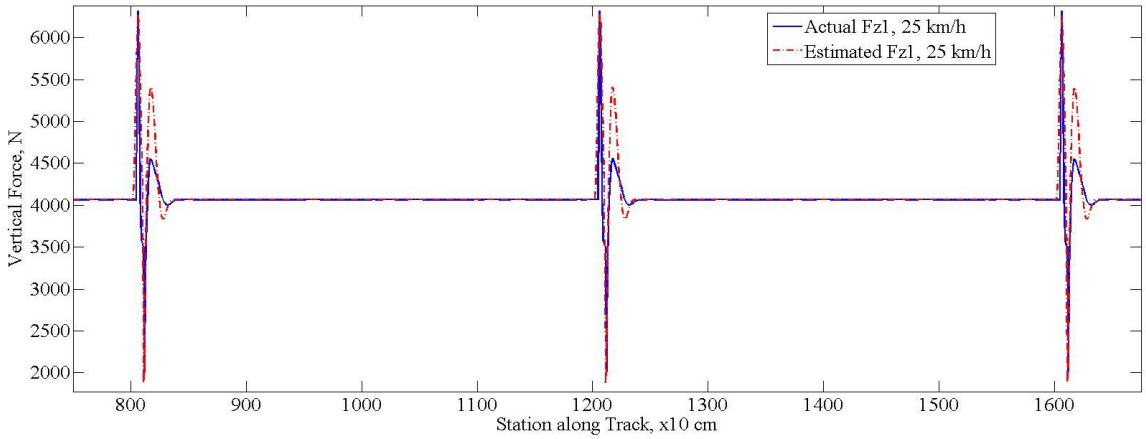

Figure 32: Estimated and Actual Vertical Force, Left Front Tire, 25 km/h

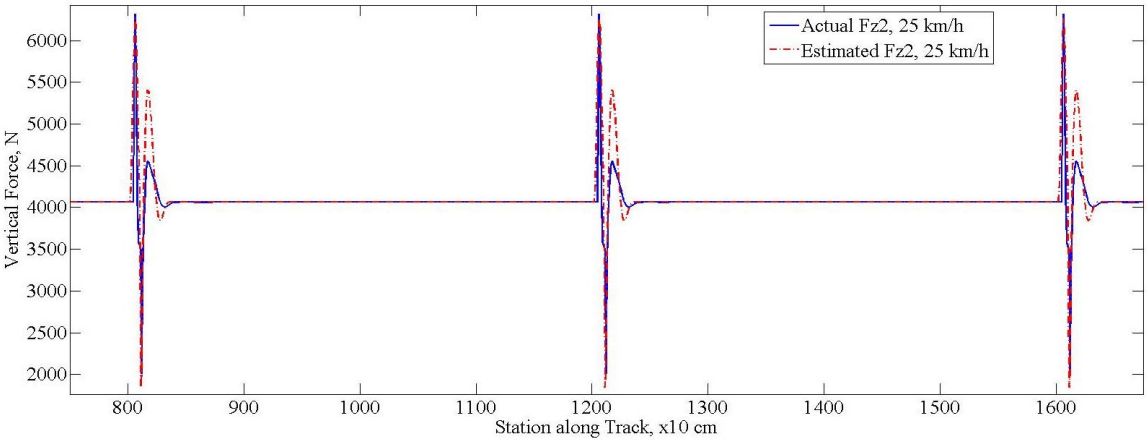

Figure 33: Estimated and Actual Vertical Force, Right Front Tire, 25 km/h

Initially, there is a lag between the estimated and actual responses which arises from the fact that the actual response is calculated with the native CarSim tire model, the leading edge of which interacts with the bump before the center of the contact patch. The number of stations between the CarSim tire reacting to the bump and the center of the contact patch reacting to the bump is calculated and the estimated response is shifted by this amount to better approximate the actual response from CarSim.

The first two peaks of the vertical force response are estimated within 0.6 and 6.2% of the peak values respectively, but the third peak is only estimated to within 18.8% of the peak value. The impact of this on the overall PM estimation remains to be seen.

Figure 34 and Figure 35 show the vertical force response at the rear tires. As with the front tires, the initial two peaks are more closely estimated than the third (7.9%, 3.9%,

and 15.6% respectively) and the estimation response is shifted to account for the tire model lag.

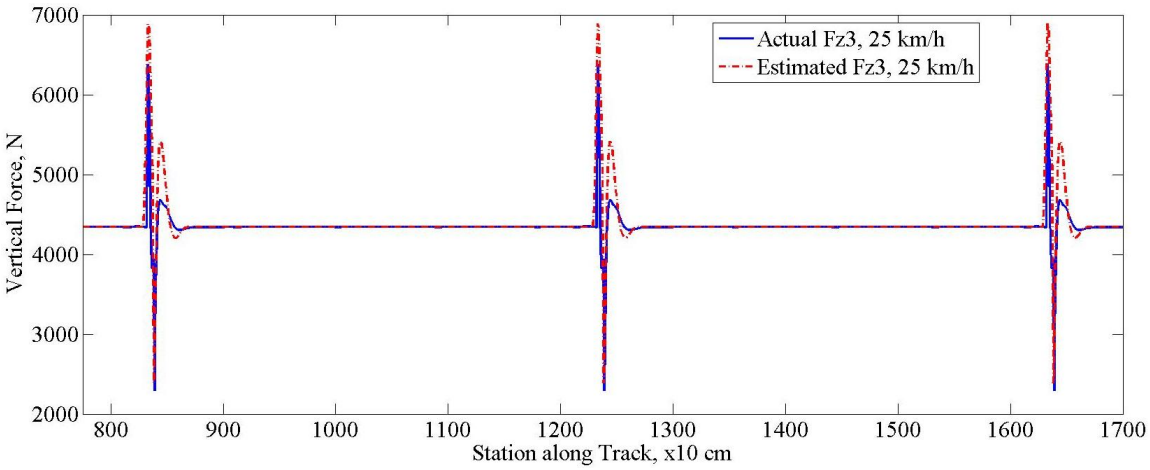

Figure 34: Estimated and Actual Vertical Force, Left Rear Tire, 25 km/h

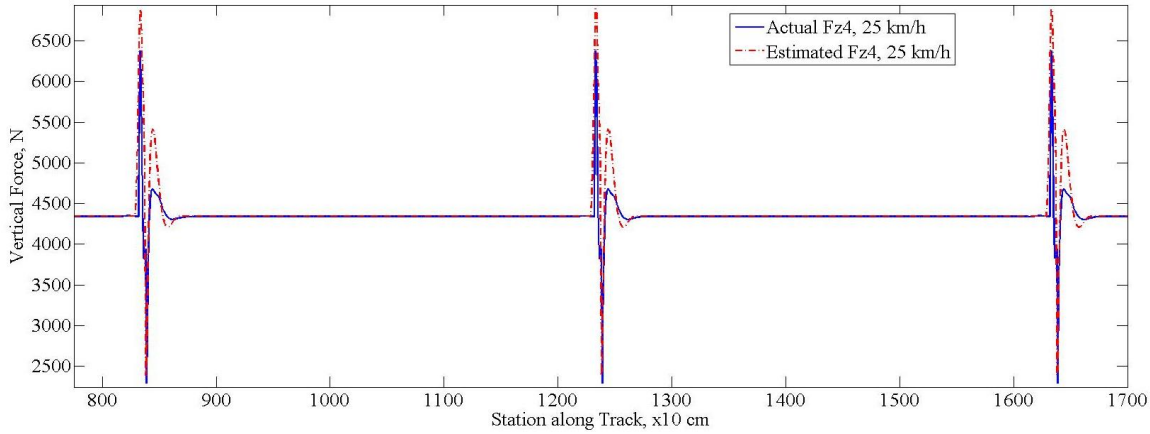

Figure 35: Estimated and Actual Vertical Force, Right Rear Tire, 25 km/h

The estimation of vertical forces due to terrain excitation at 30 km/h, 35 km/h, 45 km/h, and 55 km/h are included in Appendix C: Additional Results.

These results are promising, and the next steps towards incorporating the effect of terrain excitations into the overall PM equation are to estimate changes in vertical force with the impulse response function and to solve the relationship between $\Delta F_{z,terrain}$ and ΔF_x. Both of these steps are left as future work. However, a possible relationship between changes in vertical force due to terrain excitations and changes in longitudinal force is outlined in Appendix E: Relationship Between $\Delta \boldsymbol{F}_{\boldsymbol{z,terrain}}$ and $\Delta \boldsymbol{F}_{\boldsymbol{x}}$.

5 Conclusions

5.1 Summary of Research

The work contained in this thesis is only part of the LAAVD Research and is intended to further the development of the LAAVD System as a whole. The individual contributions, listed in the Section 5.2, are all valuable steps to understanding the relationship between the handling capabilities captured in the PM and the forces at the tire contact patch. The work contained in this thesis begins with a reworking of the existing PM equation to the form shown in Equations 3 and 4. These expanded PM equations allow for a more robust handling metric and particularly aim to capture situations where the coefficient of friction is not constant across the road surface. Beginning with first principles and continued with perturbation theory, a model is developed to succinctly represent the interplay between longitudinal, lateral and vertical forces. This model is easily inverted to obtain the relationship between necessary changes in longitudinal force and desired changes in PM, also known as the backward problem, and the method by which this work will be integrated into the Intervention Strategy. Once this integration, which is outside the scope of this thesis, is completed, work can begin on the integration of this IS into the driving simulator that was conceived of at the beginning of the LAAVDS Project. This work also includes a preliminary look into the possibility of estimating the vertical force due to terrain excitations as a series of impulse responses.

The results shown in this work illustrate clearly that linear predictions, particularly on flat terrain, can accurately capture some nonlinearities of the vehicle's dynamics. Looking below the PM cutoff value of 0.3, the error between estimated and actual changes in PM stays below 2.5% at the front axle and below 3.6% at the rear axle for all test cases discussed here. This accuracy should only improve as the refresh rates of the non-linear simulation and the IS as a whole are tuned to the driving simulator and ultimately to a test vehicle.

5.2 Main Contributions

The specific contributions of this thesis are listed below.

1. The determination of a linear relationship between ΔF_x and ΔPM through:
    a. A simple vehicle model consisting of the relationships
        i. $\Delta F_{z,roll} \rightarrow \Delta F_x$
        ii. $\Delta F_{z,pitch} \rightarrow \Delta F_x$
        iii. $\Delta F_{y,yaw\ and\ velocity} \rightarrow \Delta F_x$
    b. The solution to the backwards problem $\Delta PM \rightarrow \Delta F_x$
    c. The expansion of the PM equation to include varying friction coefficients
    d. The linear relationship between terrain excitations and F_z (the relationship $\Delta F_{z,terrain} \rightarrow \Delta F_x$ is left to be validated as future work)
2. Algorithmic implementation of these relationships in code and demonstration of the effectiveness through an example as a proof-of-concept

5.3 Future Work

There are several avenues for further work which stem from problems encountered during this thesis work. First, there are situations where a tire may momentarily leave the pavement but the handling of the vehicle is not necessarily lost. If any tire loses contact with the road surface, the vertical force at that instant goes to zero. When only one tire on each axle loses contact with the ground at a time, the PM can still be calculated in its current form. Figure 36 shows the resulting vertical forces at the left front (solid blue line) and right front (dashed red line) tires when the vehicle encounters a pothole 5 cm deep on the right hand side of the roadway while traveling at 20 km/h. The vertical force at the right front tire goes to zero immediately before the center of the tire drops into the pothole; this occurs at station 805. Figure 37 shows the corresponding value of the PM at the front axle over the duration of the pothole event.

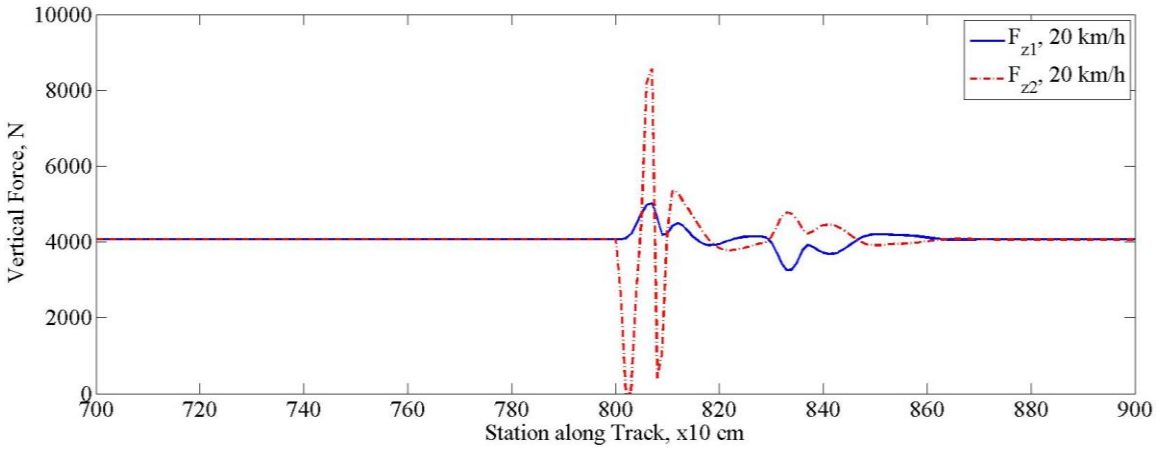

Figure 36: Vertical Force at Front Tires, 20 km/h, Pothole Excitation Event

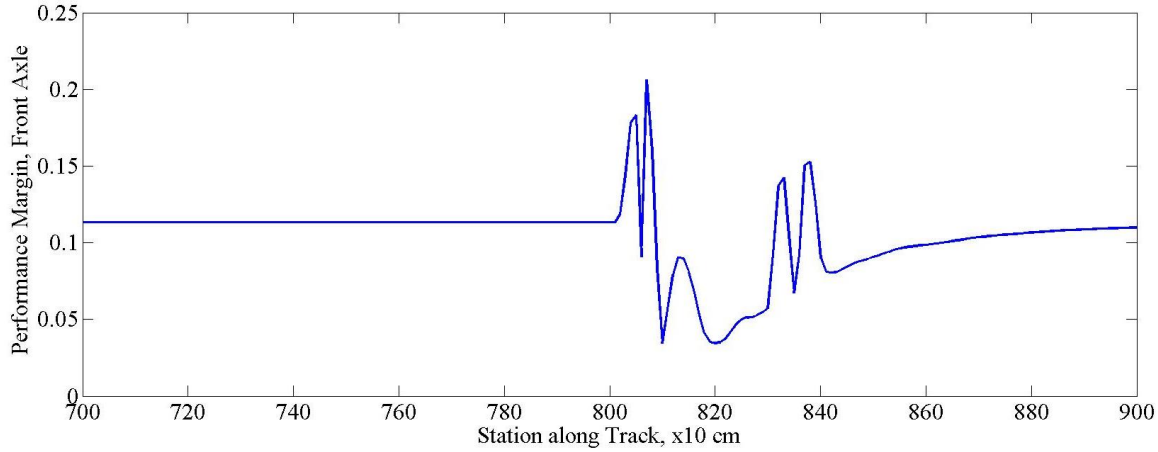

Figure 37: Performance Margin at Front Axle, 20 km/h, Pothole Excitation Event

When both tires on the same axle lose contact with the roadway, a new technique for measuring the vehicle's handling capabilities is necessary. Figure 38 shows the vertical force at the left front tire as the vehicle travels over a bump 10 cm in height at 20 km/h and Figure 39 shows the corresponding PM measurement. Note the holes in the plot of the PM after stations 800, 1200, and 1600 respectively. These correspond to the stations where the vertical force is zero, and the current formulation of the PM equation cannot be calculated.

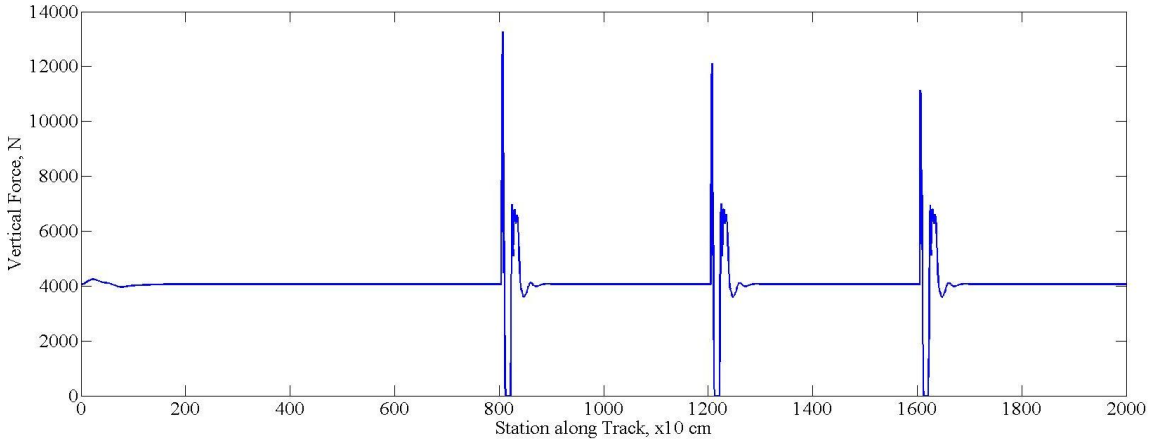

Figure 38: Vertical Force due to Traversing 10 cm Bump at 20 km/h

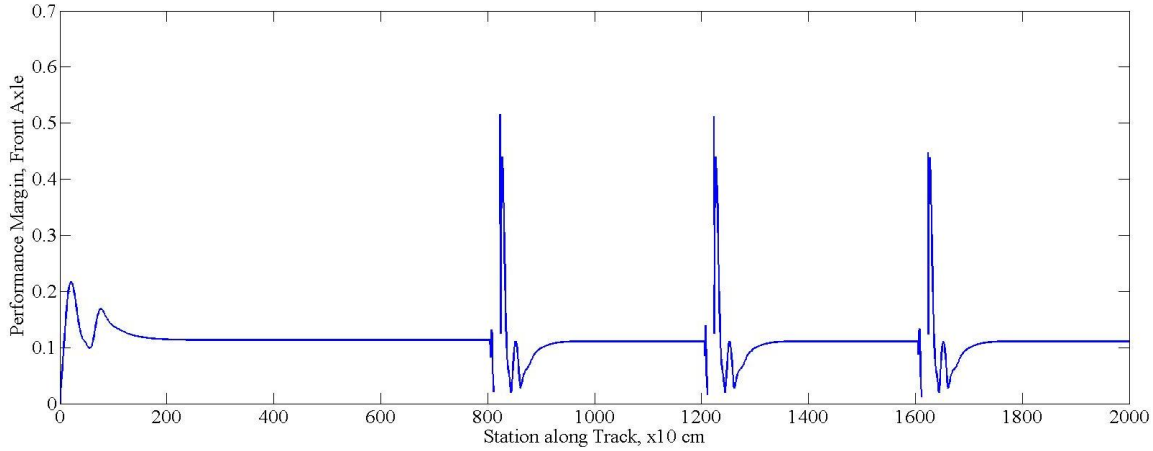

Figure 39: Performance Margin at the Front Axle, 10 cm Bump, 20 km/h

Another obvious continuation of this work is to continue using impulse response functions to approximate changes in vertical force and to validate the relationship between those changes in vertical force and their corresponding changes in longitudinal force as suggested in Appendix E: Relationship Between $\Delta \boldsymbol{F}_{z,terrain}$ and $\Delta \boldsymbol{F}_{x}$. The possibility of estimating vertical forces by impulse response functions depends on the quality of data received from CarSim and the inclusion of some form of tire model – either a point-follower approximation in CarSim or a version of CarSim's model implemented in the impulse response algorithm.

The actual interface between the linear chassis model developed here and the previously developed linear powertrain model [43] [44] as shown in Figure 3 is outside the scope of this work and has yet to be completed. Also left to be completed is the

finalization of the driving simulator which is intended to act as a proof of concept in lieu of implementation in a prototype vehicle.

The feasibility of this work and the LAAVDS Project as a whole is entirely dependent on real-time estimations or measurements of friction at the terrain-tire interface. It is assumed in this thesis that such measurements are available, either because they have been prescribed in simulation or from V2I communications, but in practice this is not yet the case. Celli [39] gives an excellent review of friction estimation techniques that are currently available, but this area is ripe for further investigation.

Also of interest is the area of steering control through either path planning or driver prediction. Coupled with the existing throttle and brake modulation schemes, steering control would be an additional step towards autonomous driving and would allow for more complete control of the vehicle's handling during test maneuvers. It is entirely possible that maneuvers which cannot be safely traversed at this time by the IS alone could be completed with the addition of some form of steering control. The addition of vehicle dynamics control (e.g. active damping) would also allow for fuller control of the vehicle's handling margins and add to the robustness of the IS.

The final goal of course remains to implement the IS in a prototype vehicle after a successful showing by the driving simulator currently under development. By testing this proposed system with actual vehicle data, as opposed to the CarSim results used here, a wider variety of driving maneuvers can be investigated and the full potential of the system can be realized.

References

1. Ryu, J. and J.C. Gerdes, *Integrating inertial sensors with GPS for vehicle dynamics control.* Journal of Dynamic Systems, Measurement, and Control, 2004. **126**(2): p. 243-254.
2. Yih, P. and J.C. Gerdes, *Modification of vehicle handling characteristics via steer-by-wire.* Control Systems Technology, IEEE Transactions on, 2005. **13**(6): p. 965-976.
3. Hong, D.W. and R.J. Cipra, *Visualization of the Contact Force Solution Space for Multi-Limbed Robots.* Journal of Mechanical Design, 2005. **128**(1): p. 295-302.
4. Beiker, S., et al., *GPS augmented vehicle dynamics control.* SAE TEchnical Paper 2006-01-1275, 2006.
5. Matthews, C.C., et al., *Using Performance Margin and Dynamic Simulation for Location Aware Adaptation of Vehicle Dynamics.* SAE International Journal of Passenger Cars-Mechanical Systems, 2013. **6**(1): p. 225-230.
6. van Zanten, A., R. Erhardt, and G. Pfaff, *VDC- The Vehicle Dynamics Control System of Bosch.* SAE Technical Paper 950759, 1994.
7. Dietsche, K.-H., ed. *Automotive Handbook*. 8th ed. 2011, Robert Bosch GmbH: Plochingen.
8. SAE, *J670: Vehicle Dynamics Technology*. 2008.
9. Greenwood, D.T., *Principles of Dynamics, 2nd Edition*. 1988, Englewood Cliffs, New Jersey 07632: Prentice-Hall, Inc.
10. Beer, F.P., et al., *Vector Mechanics for Enginers Dynamics*. Eighth ed. 2007, New York: McGraw-Hill.
11. Milliken, W.F. and D.L. Milliken, *Race Car Vehicle Dynamics*. 1995, Warrendale, PA: Society of Automotive Engineers, Inc.
12. Stone, R. and J.K. Ball, *Automotive Engineering Fundamentals*. 2004, Warrendale, PA: Society of Automotive Engineers, Inc.
13. Heissing, B. and M. Ersoy, eds. *Chassis Handbook*. 1st ed. 2011, Vieweg + Teubner.
14. Wong, J.Y., *Theory of Ground Vehicles*. 4 ed. 2008, Hoboken, NJ: John Wiley & Sons, Inc.
15. Pacejka, H.B., *Tire and Vehicle Dynamics*. 2 ed. 2006, Warrendale, PA: Society of Automotive Engineers, Inc.
16. Benmimoun, M., et al. *Incident detection based on vehicle CAN-data within the large scale field operational test "euroFOT"*. in *22nd Enhanced Safety of Vehicles Conference (ESV 2011), Washington, DC/USA*. 2011.
17. Weiss, C., *simTD überzeugt: Car ‑to ‑X Technologie bereit für den Markt*, in *http://www.simtd.de/index.dhtml/object.media/deDE/8022/CS/-/backup_publications/Informationsmaterial/simTD_prsentation_2013_de_web.pdf*, simTD, Editor. 2013.
18. Naylor, N., *USDOT to Move Forward with Vehicle To Vehicle Communication Technology for Light Vehicles*. 2014, National Highway Traffic Safety Administration.

19. Cole, D.J., A.J. Pick, and A.M.C. Odhams, *Predictive and linear quadratic methods for potential application to modelling driver steering control.* Vehicle System Dynamics: International Journal of Vehicle Mechanics and Mobility, 2006. **44**(3): p. 259-284.
20. Ali, M., et al., *Multi-Objective Collision Avoidance*, in *ASME 2013 Dynamic Systems and Control Conference*. 2013: Palo Alto, CA, USA.
21. Sayers, M.W. and S.M. Karamihas, *The Little Book of Profiling*. 1998, Ann Arbor, MI: The Regent of the University of Michigan.
22. Rainey, C., *Error Estimations in the Design of a Terrain Measurement System*, in *Mechanical Engineering*. 2013, Virginia Polytechnic Institute and State University: Blacksburg, VA.
23. Gimmler, H., D. Ammon, and J. Rauh, *Road profiles: Mobile measurement, data processing for efficient simulation and assessment of road properties.* VDI BERICHTE, 2005. **1912**: p. 335.
24. Chemistruck, H.M., et al., *A Galerkin Approach to Define Measured Terrain Surfaces with Analytic Basis Vectors to Produce a Compact Representation*. 2010, DTIC Document.
25. Robson, J.D., *Deductions From The Spectra of Vehicle Response Due to Road Profile Excitation.* Journal of Sound and Vibration, 1968. **7**(2): p. 156-158.
26. Robson, J. and C. Dodds. *The response of vehicle component to random road-surface undulations*. in *13th FISITA Congress, Brussels, Belgium*. 1970.
27. Virchis, V.J., *Response of an Accelerating Vehicle to Random Road Undulation.* Journal of Sound and Vibration, 1971. **18**(3): p. 423-427.
28. Dodds, C.J. and J.D. Robson, *The description of road surface roughness.* Journal of Sound and Vibration, 1973. **31**(2): p. 175-183.
29. Robson, J.D. and C.J. Dodds, *Stochastic Road Inputs and Vehicle Response.* Vehicle System Dynamics, 1976. **5**(1-2): p. 1-13.
30. Robson, J.D. and K.M.A. Kamash, *Road Surface Description in Relation to Vehicle Response.* International Journal of Vehicle Mechanics and Mobility, 1977. **6**(2-3): p. 153-157.
31. SAE, *Surface Vehicle Information Report*, in *Automotive Stability Enhancement Systems*. 2004, SAE.
32. Tseng, H.E., et al., *The development of vehicle stability control at Ford.* Mechatronics, IEEE/ASME Transactions on, 1999. **4**(3): p. 223-234.
33. Tjonnas, J. and T.A. Johansen, *Stabilization of Automotive Vehicles Using Active Steering and Adaptive Brake Control Allocation.* Control Systems Technology, IEEE Transactions on, 2010. **18**(3): p. 545-558.
34. Anubi, O. and C.D. Crane, III, *Vehicle Roll Stabilization Enhancement Using a Variable Stiffness Architecture: Kinematic Control*, in *ASME 2013 Dynamic Systems and Control Conference*. 2013: Palo Alto, CA, USA.
35. Davoudi, M., M.B. Menhaj, and M. Davoudi, *A Fuzzy Based Vehicle Dynamic Stability Control (FDSC).* SAE Technical Paper 2006-01-3483, 2006.
36. Yoon, Y., et al., *Model-predictive active steering and obstacle avoidance for autonomous ground vehicles.* Control Engineering Practice, 2009. **17**(7): p. 741-750.

37. Minoiu Enache, N., et al., *Driver steering assistance for lane departure avoidance.* Control Engineering Practice, 2009. **17**(6): p. 642-651.
38. Mejia, J.P.S., P.A. Theodosis, and J.C. Gerdes, *Using a Path-Fitting Algorithm to Analyze the Racing Techniques of a Skilled Driver*, in *ASME 2013 Dynamic Systems and Control Conference*. 2013: Palo Alto, CA, USA.
39. Celli, J.M., *An Investigation for a Location Aware Adaptation of a Vehicle Dynamics Controller using Friction Estimation*, in *Mechanical Engineering*. 2012, Virginia Polytechnic Institute and State University: Blacksburg, VA.
40. Milliken, W.F., P.G. Wright, and D.L. Milliken, *Moment Method - A Comprehensive Tool for Race Car Development.* SAE Technical Paper 942538, 1994.
41. Pasterkamp, W.R. and H.B. Pacejka, *The tyre as a sensor to estimate friction.* Vehicle System Dynamics, 1997. **27**(5-6): p. 409-422.
42. Hsu, Y.-H., S.M. Laws, and J. Gerdes, *Estimation of tire slip angle and friction limits using steering torque.* Control Systems Technology, IEEE Transactions on, 2010. **18**(4): p. 896-907.
43. Cho, S., et al., *Location-Aware Adaptive Vehicle Dynamics System: Throttle Modulation.* SAE International Journal of Passenger Cars-Mechanical Systems, 2014.
44. Cho, S., et al., *Location-Aware Adaptive Vehicle Dynamics System: Brake Modulation.* SAE International Journal of Passenger Cars-Mechanical Systems, 2014. **7**(2).
45. Ferris, J., *Location-Aware Adaptive Vehicle Dynamics (LAAVD) System*. 2013.
46. Cho, S., *Development of a Real-Time Powertrain and Yaw Control Strategy for a Location-Aware Adaptive Vehicle Dynamics System*, in *Mechanical Engineering*. 2013, Virginia Polytechnic Institute and State University: Blacksburg, VA.
47. Bandy, R.A., et al., *Location-Aware Adaptive Vehicle Dynamics System: Concept Overview.* SAE International Journal of Passenger Cars-Mechanical Systems, 2014. **7**(1).

Appendix A: CarSim and MATLAB User's Guide

This user's guide is meant to accompany Rebecca Bandy's thesis work and to allow for easy reproduction of her results. All of the code developed by Rebecca and Dr. Ferris is stored at: node1.me.vt.edu:\\DataShare\Code\2013 Development Code\chassis validation.

There are two paths that can be taken through this guide. To use a track that is constructed in CarSim, follow Setting up CarSim Simulations, CarSim2Track, track_builder, and then chassis_prediction. To create a track in MATLAB and use it as the excitation for CarSim simulations, follow track_builder, Track2CarSim, Setting up CarSim Simulations, then chassis_prediction.

A.1 Setting up CarSim Simulations

CarSim is a powerful piece of software with the ability to simulate a wide variety of vehicles, driving maneuvers, and track conditions. It is highly recommended to complete the CarSim Quick Start Guide before running any simulations such as those used in this thesis.

A.1.1 Vehicle Setup

For the LAAVD System Research, a previously built model of a VW CC will be used. Do not modify this model in any way! The vehicle setup can be viewed by clicking on the "Vehicle configuration" button on the CarSim main screen.

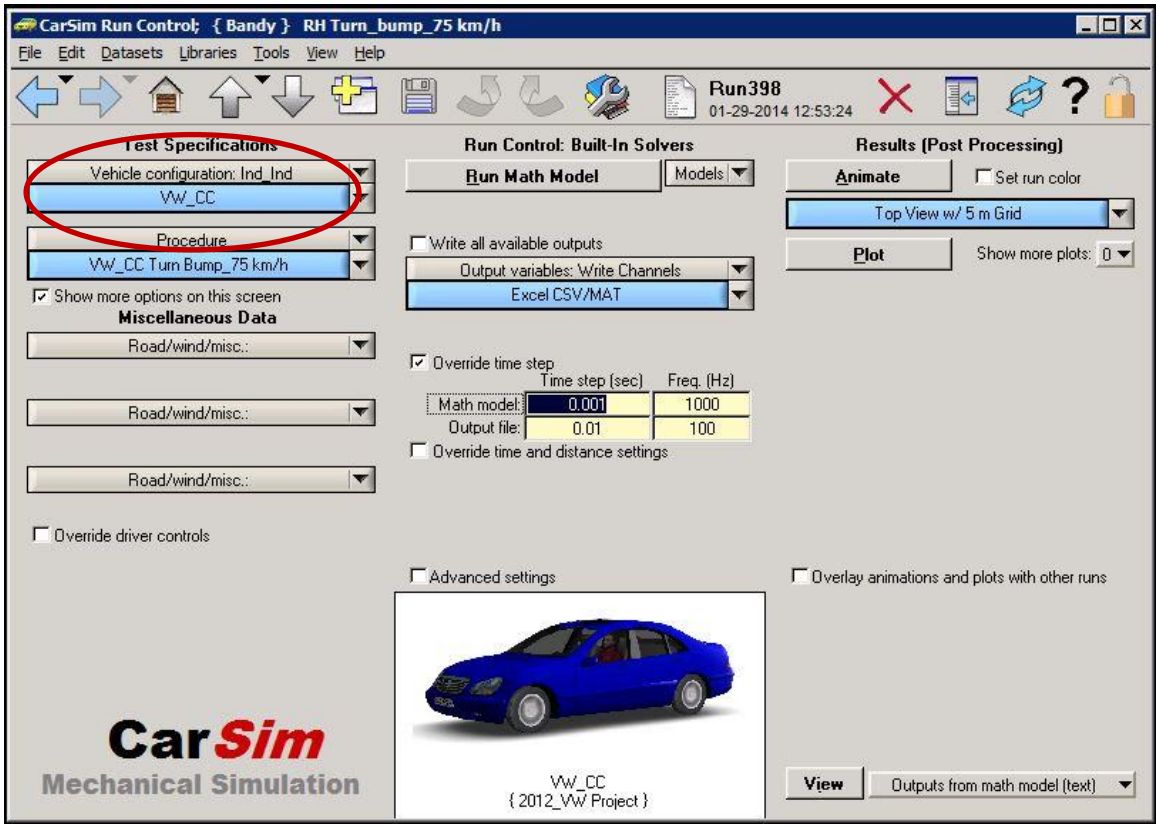

Figure 40: CarSim Main Screen

This brings up the vehicle assembly screen, Figure 41. From the vehicle assembly screen, clicking on the "Sprung mass" button will bring up sprung mass screen, shown in Figure 42. Clicking on the "Powertrain" button will bring up the corresponding powertrain screen, shown in Figure 43. Clicking on the "Front kinematics" and "Rear kinematics" will bring up the corresponding screens shown in Figure 44 and Figure 45. These buttons are all circled on Figure 41. All of the physical data necessary for the estimation calculations in this thesis are found on the following screens.

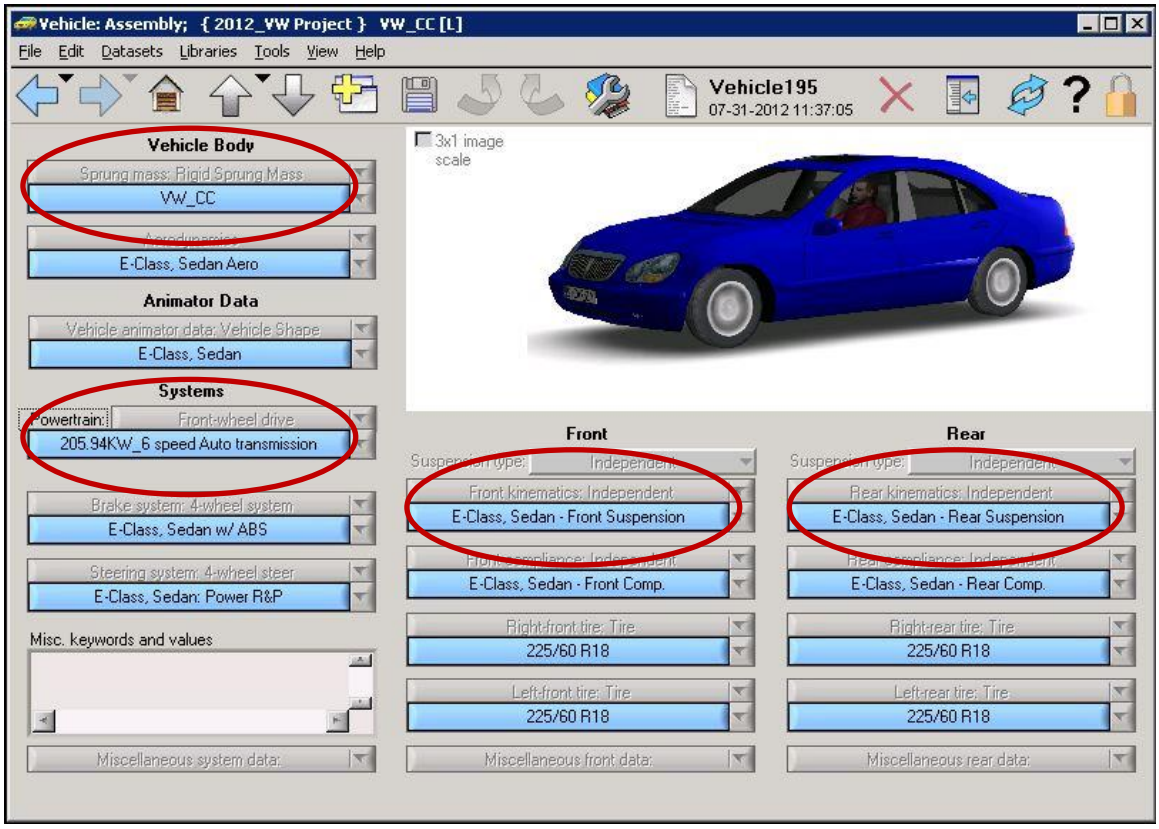

Figure 41: Vehicle Assembly Screen

The CG height, wheelbase, and sprung mass necessary for the estimations of roll, pitch, yaw, and road influences can all be found in Figure 42. For the vehicle model particular to the LAAVD Research, the CG height is 590 mm, the wheelbase is 2710 mm, and the sprung mass is 1536 kg.

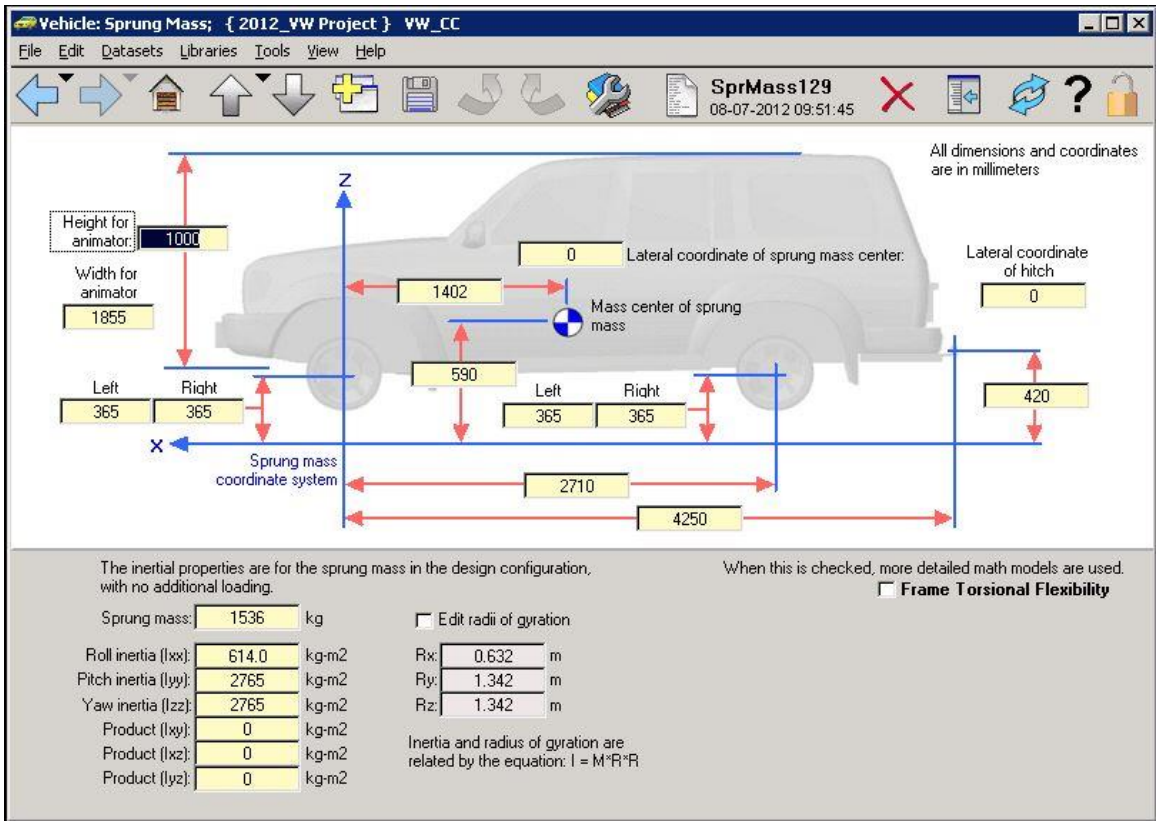

Figure 42: Sprung Mass Screen

Figure 43 shows the powertrain configuration for the LAAVD Research vehicle. While not directly referenced in the chassis dynamic estimations derived here, it is nonetheless important to understand the system with which this thesis will ultimately communicate. The vehicle model is that of a 205.94 kW, 6 speed, automatic transmission. The vehicle is also modeled with front wheel drive. Eventually, the necessary changes in longitudinal force to effect desired changes in PM will be read into a predictive powertrain model. These connected models will give the necessary changes in torque (achieved brake, throttle, or steering changes in the Intervention Strategy) to obtain the desired changes in PM.

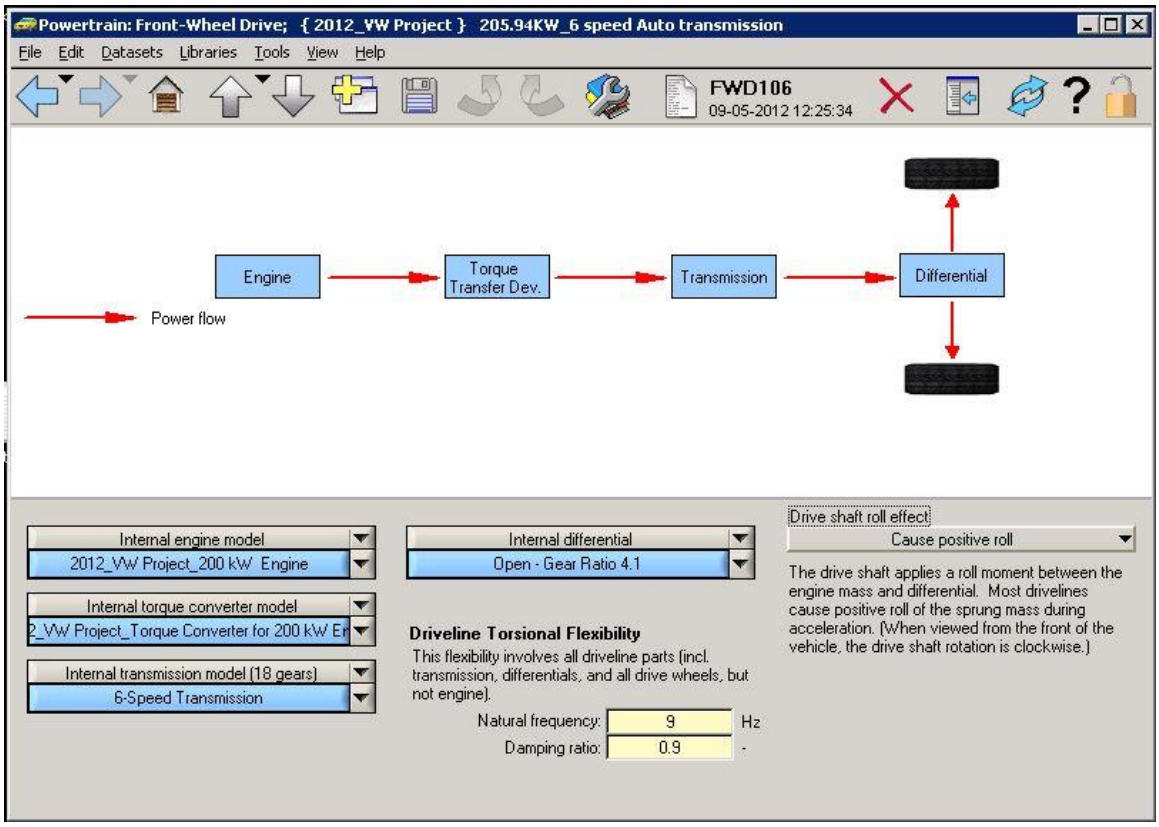

Figure 43: Powertrain Screen

Among other parameters, the suspension screens, Figure 44 and Figure 45, show the track width of the vehicle. This value is necessary to properly estimate the pitch and yaw effects.

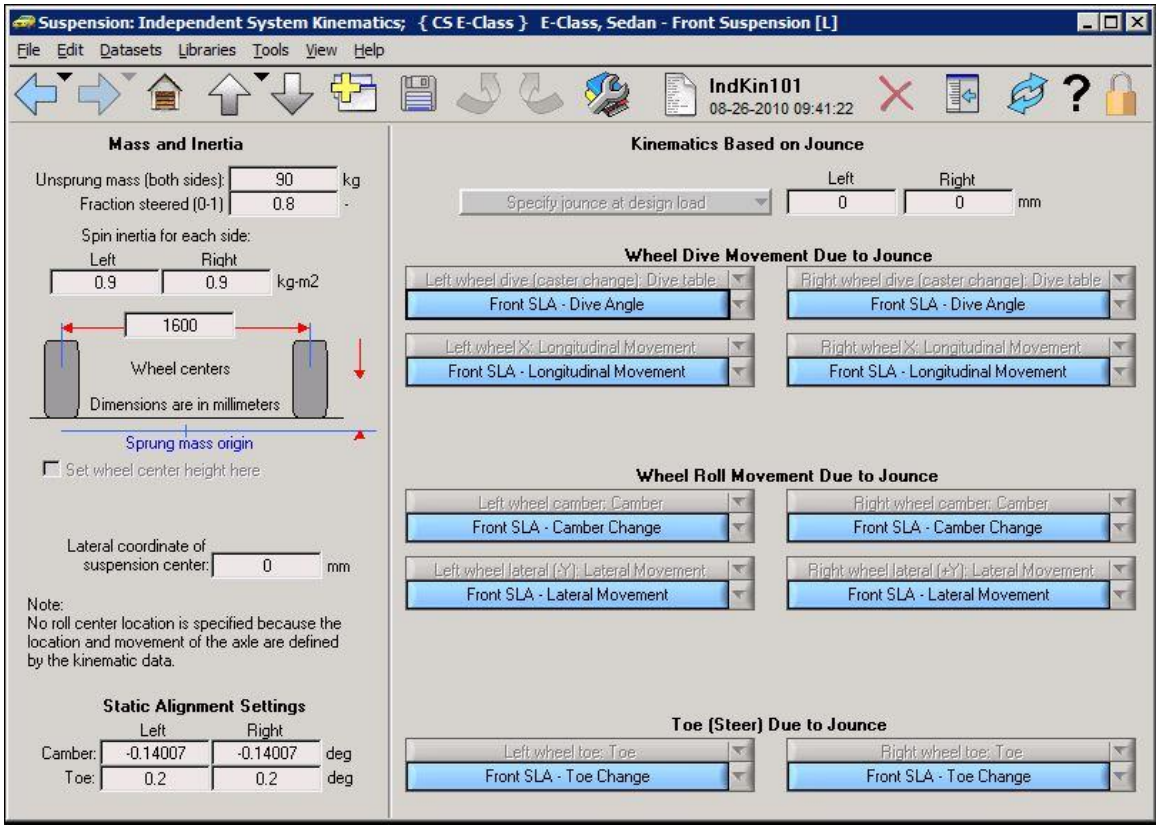

Figure 44: Front Suspension Screen

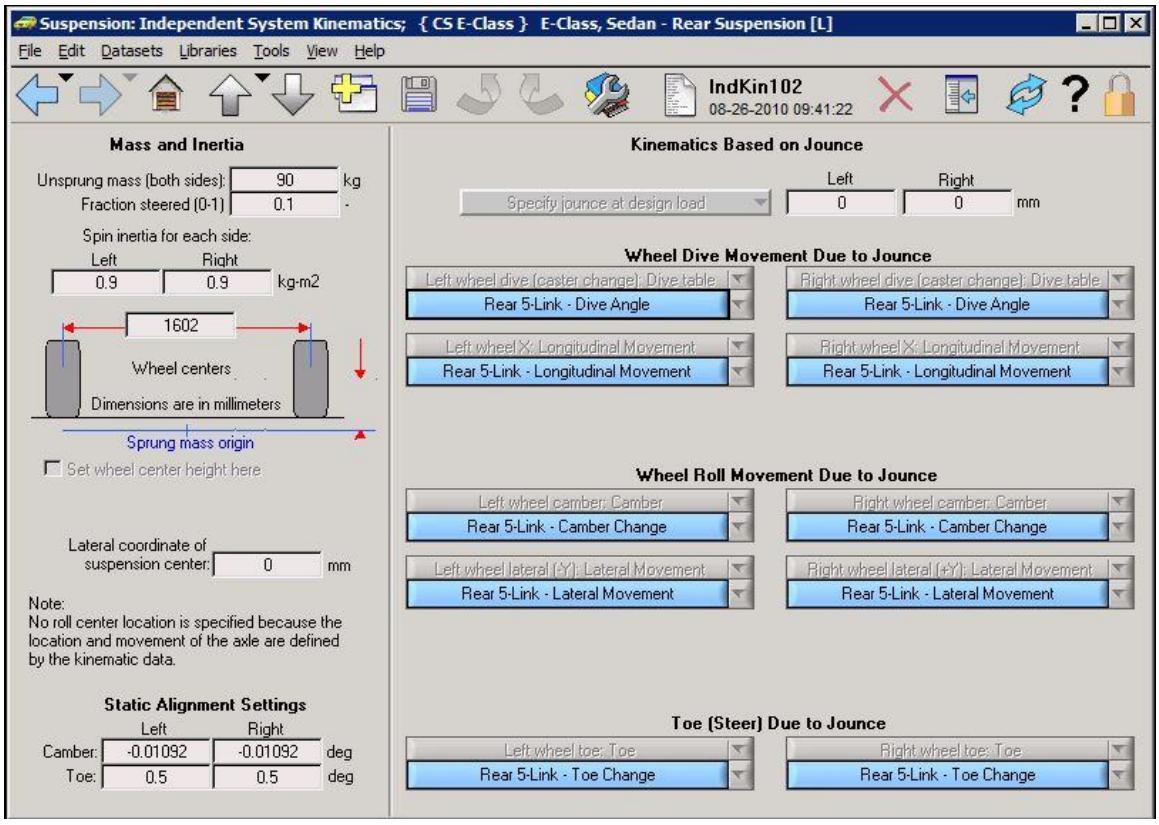

Figure 45: Rear Suspension Screen

A.1.2 Procedure Setup

All procedures used in this thesis were set up following the Quick Start Guide. Special attention was paid to the brake, throttle, and driver commands on the "Procedures" screen. Specifically, a constant target velocity was specified, the brake control was set to "no braking", the shifting control was set to automatic 6-speed, and the simulation stop time was set so that the entire track could be traversed before the end of the simulation. These parameters are shown in Figure 46.

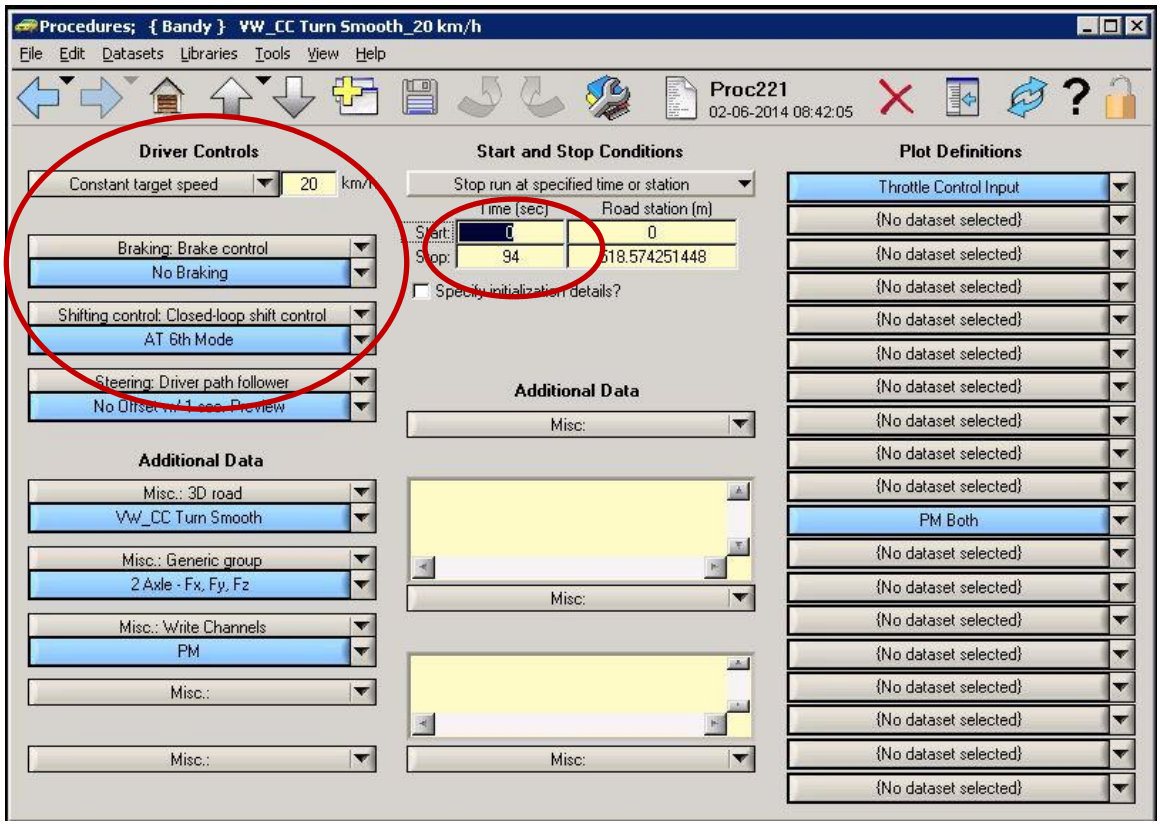

Figure 46: Procedures Screen

A.2 CarSim2Track

This code acts as a translator between CarSim track data files (.csv format) and the Track structure used for various projects internal to VTPL. The CarSim track data is read into MATLAB, renamed with respect to the Track structure convention, and then saved as a .mat structure. The resultant Track structure should be input to track_builder to be further populated.

1. There are two versions of this code to be used depending on the type of track being converted. To deal with a 2D track (only XY coordinates), run CarSim2Track_2014_01_13_bandy:
    a. Type "Track = CarSim2Track_2014_01_09_bandy" in the MATLAB command window.
    b. Select the CarSim track file that you would like to convert, push enter
2. To deal with a 3D track, run CarSim2Track_2014_01_21_bandy following the same steps as above.

This program will save the original CarSim filename, the vectors of x and y data points, and the new filename and directory to the Track structure.

A.3 track_builder

This piece of code was developed by John Ferris and Brian Davidson. This code takes an existing Track structure and further populates it with z (height), mu (friction), theta (bank angle), and phi (heading angle) values, as well as creates a path, u, by interpolating qx, qy, and qz (the input data points). Alternatively, it can create an altogether new track.

To run (with existing Track structure):

1. Type "Track = track_builder_2014_01_08b(Track, 'whatever you want your new track to be saved as', 0)" or "Track = track_builder_2014_01_08b(Track, 'whatever you want your new track to be saved as', 1)" in the MATLAB command window. Typing 1 turns on silent mode and does not prompt the user to add more x and y data points manually.
2. If silent mode = 0:
    a. User will be prompted to add more path points, type y or n, depending on if more path points are desired.
    b. If user types 'y', more path points can be entered using the left mouse button and the accompanying figure. Press 'enter' to exit path point selection.
    c. Enter z, mu, and theta values for each path point.
3. If silent mode = 1:
    a. No further input from the user is necessary.

To run (without existing track):

1. Type "Track = track_builder_2014_01_08b" in the MATLAB command window. You will be prompted to select data points and enter their z, mu, and theta values as in step 2 above.

This will save the full track structure to the filename specified in the function call. The resulting Track structure can be used as the input to chassis_prediction, in order to compare multiple vehicle test runs over the same track.

A GUI for the track_builder code is currently under development that will allow for 2D and 3D tracks (by setting all *z* heights to zero in the 2D case) with split-mu conditions to be automatically generated by the same piece of code. The interface will also incorporate the Track2CarSim functionality described in the next section, allowing for tracks to be saved in a variety of formats. At the time of this writing however, the GUI is not complete and the workarounds described above are still necessary.

A.4 Track2CarSim

You may wish to use your newly created track as a road profile in CarSim. To do this, either load the desired Track structure in MATLAB and type "Track2CarSim_2014_01_20(Track)" into the MATLAB command window, or simply type "Track2CarSim_2014_01_20([])". The second option will prompt you to choose an existing track_builder output file which will then be loaded to the workspace.

This piece of code gleans the x, y, and z values from the Track structure and saves them as columns 1, 2, and 3 respectively in a .csv file. The .csv file is saved with the filename "road_(time index from original track file)" for ease of comparison. This .csv file can be imported to CarSim and saved as a new road using the following steps:

1. On the CarSim Roads Screen, choose "Centerline geometry X-Y-Z table"

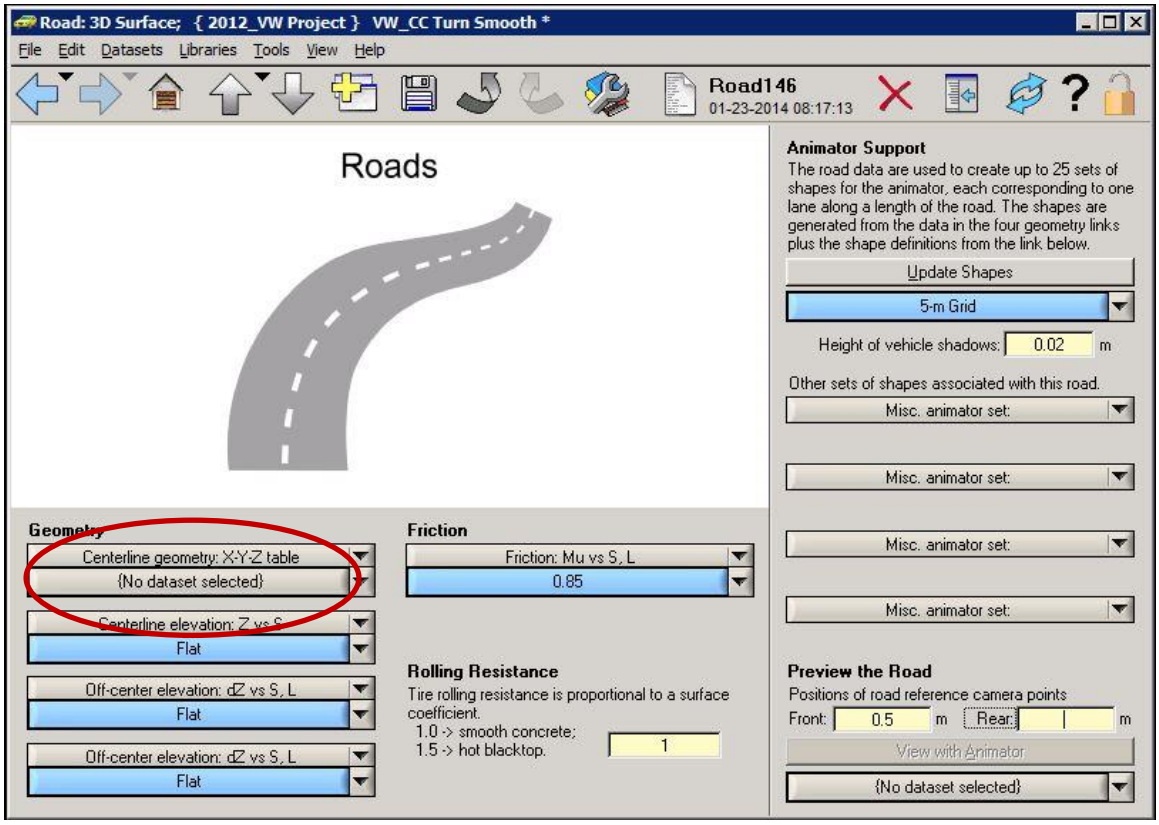

Figure 47: Road Screen

2. Create and link a new dataset using the drop down arrow next to (No dataset selected).

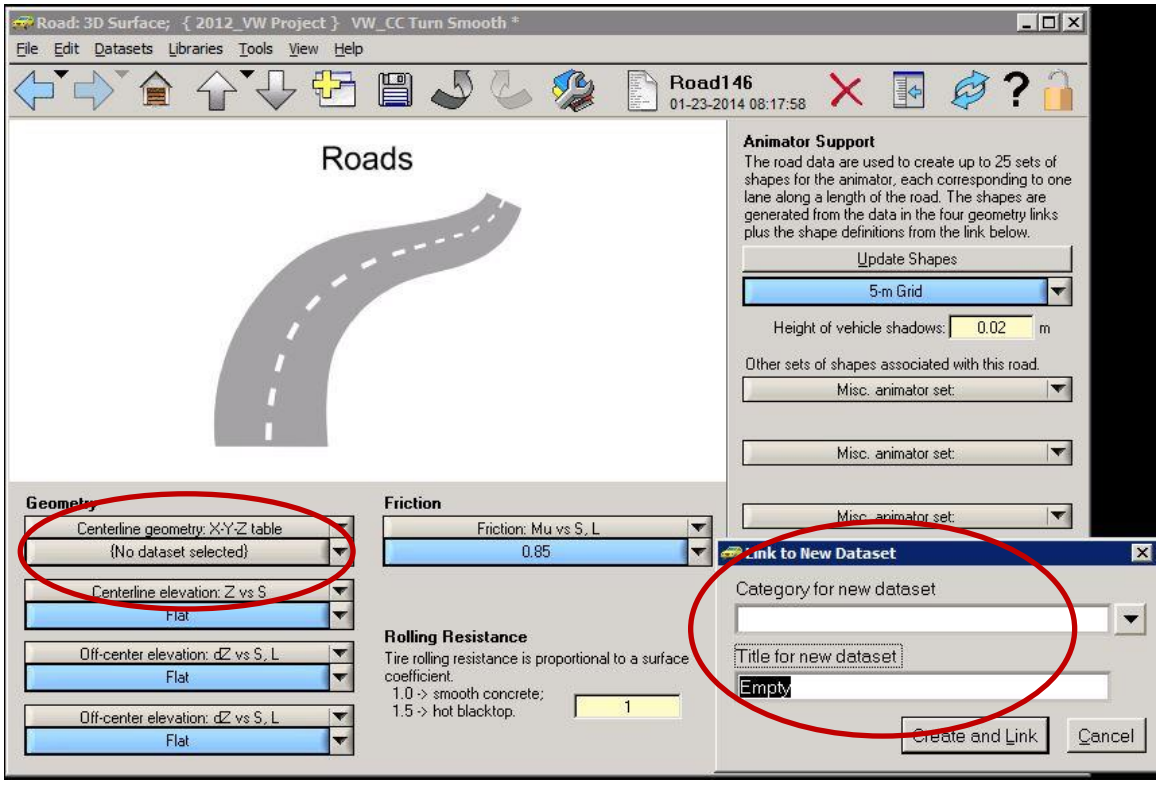

Figure 48: Link to New Dataset

3. Double-click on the new centerline geometry dataset name and a blank road geometry screen will appear.

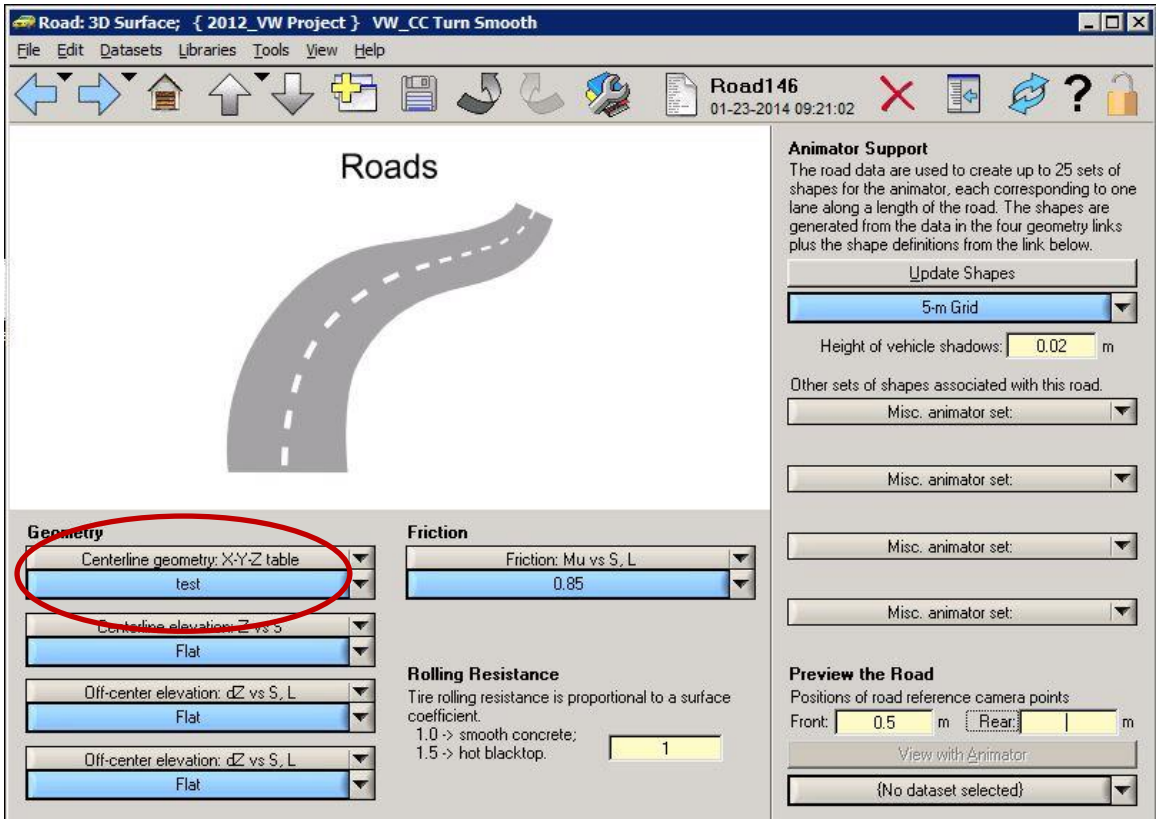

Figure 49: New Dataset Linked

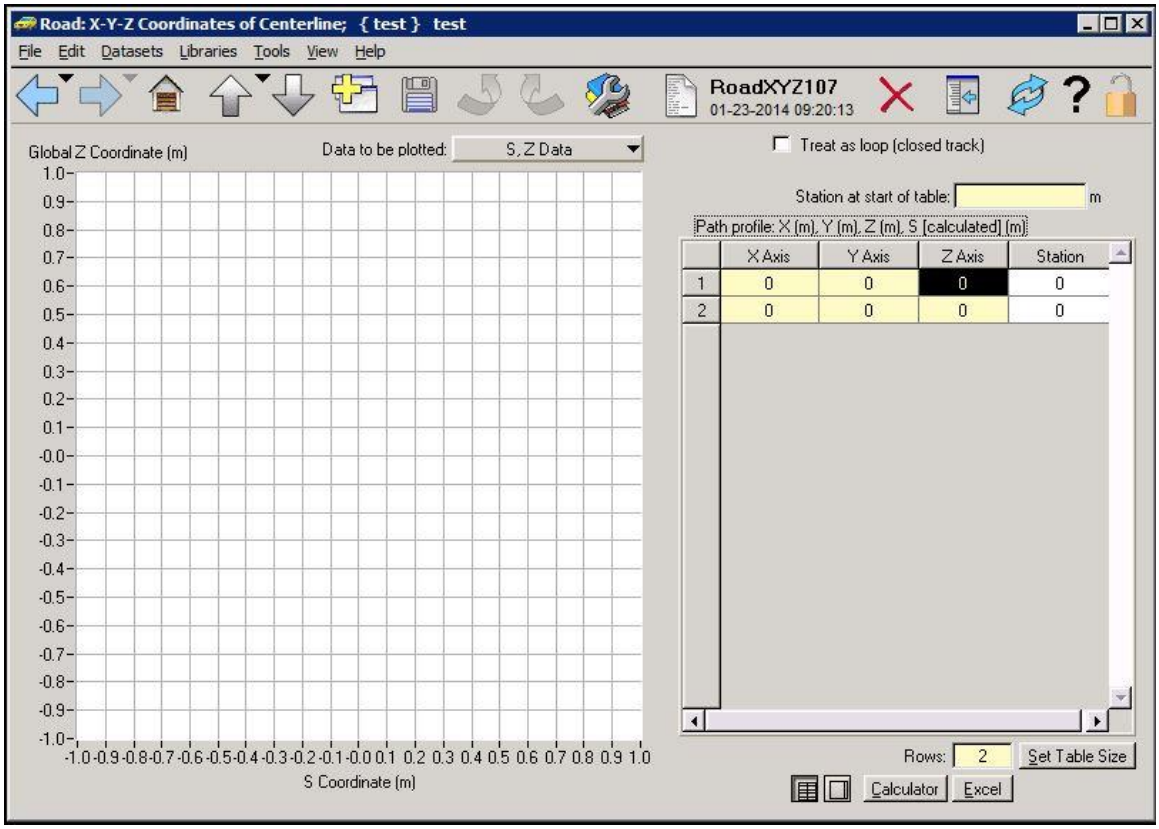

Figure 50: Road Geometry Screen

4. Click the Excel button to bring up the new .csv file.

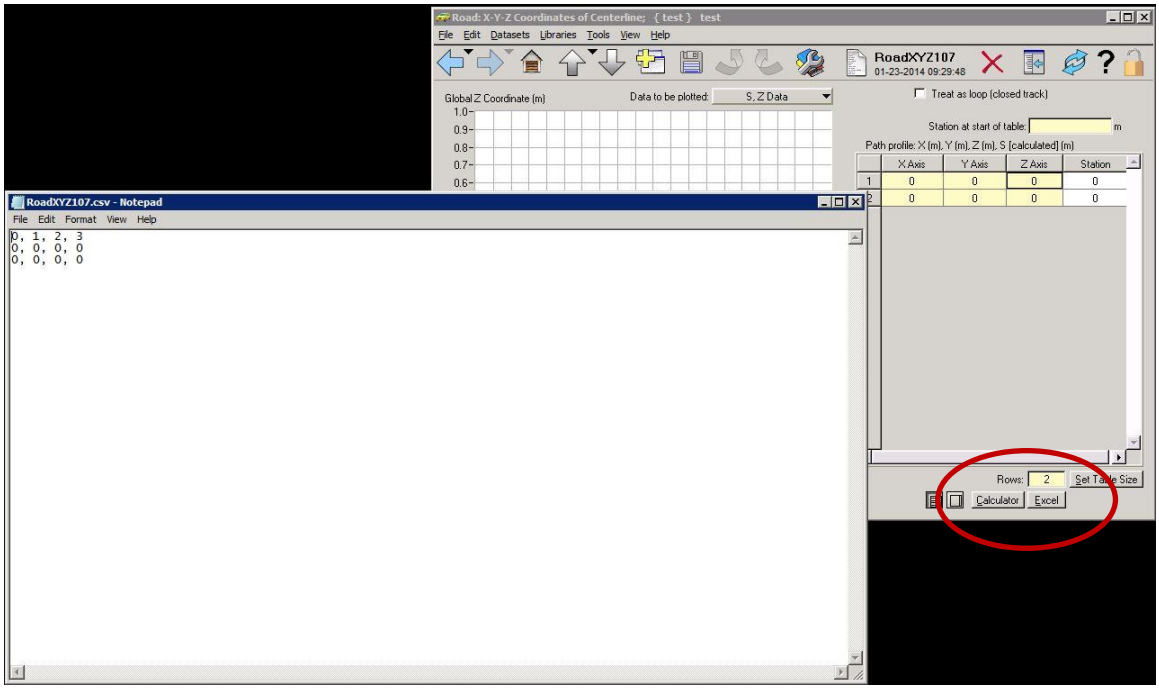

Figure 51: New .csv File

5. Copy and paste your .csv file from track_builder into this window, save, and close. CarSim will automatically calculate and assign Stations (in meters) along the length of the track. You can also plot different orientations of the track from this screen.
6. Your track is now ready for use in CarSim. Go back to the home screen and run a simulation as usual.

A.5 chassis_prediction

This is the code that takes the previously created Track structure, all of the outputs from the CarSim runs, and in the future, driver inputs, and uses them to predict changes to the PM at a given speed. This code automatically generates four plots – the actual and estimated changes in PM at the front axle, the same at the rear axle, the actual PM values at the front axle for the two CarSim runs, and the same at the rear axle. These plots are used to determine the validity of the Taylor Series approximation to changes in PM, the estimation of roll, pitch, yaw, and finally, the impact of road excitations on changes in PM.

Like CarSim2Track, there are several iterations of this code, each with a specific purpose.

1. To validate the Taylor Series approximation, use the function call "chassis_prediction_2014_01_22". The user will be prompted to choose the track file as well as two CarSim runs – the original and perturbed velocity runs corresponding to the chosen track file.
2. To validate the estimation of F_z due to roll and pitch, use the function call "chassis_prediction_2014_01_31." This prompts the user to choose a track file and two CarSim runs as before. Be careful to only choose a 2D (XY coordinate) track file, as this code does not account for the impact of road excitations to changes in PM.
3. To validate the estimation of roll, pitch, and yaw, use the function call "chassis_prediction_2014_03_30." As before, this prompts the user to choose a track and two CarSim runs. Be sure to only use a 2D track file, as this code does not account for the impact of road excitations.

Appendix B: Lateral Force Anomaly

An anomaly is apparent in the PM estimation at speeds of 25 km/h and below. The estimations track very closely the actual PM of the higher speed runs, but drop off in the center of the turn and estimate little to no change in PM, before estimating the PM on the final straightaway. An investigation is conducted to determine which force (or forces) at which tire is responsible for this estimation error. The longitudinal, lateral, and vertical forces returned by the CarSim simulation are plotted for each tire across the range of test velocities. It becomes apparent that the estimation error is coming from the lateral force at the front left tire in the 20 and 25 km/h simulations. Figure 52 shows the lateral force at the front left tire for each velocity tested. In the 20 and 25 km/h tests, the lateral force becomes less negative through the cornering maneuver, while the lateral force at all other velocities becomes more negative.

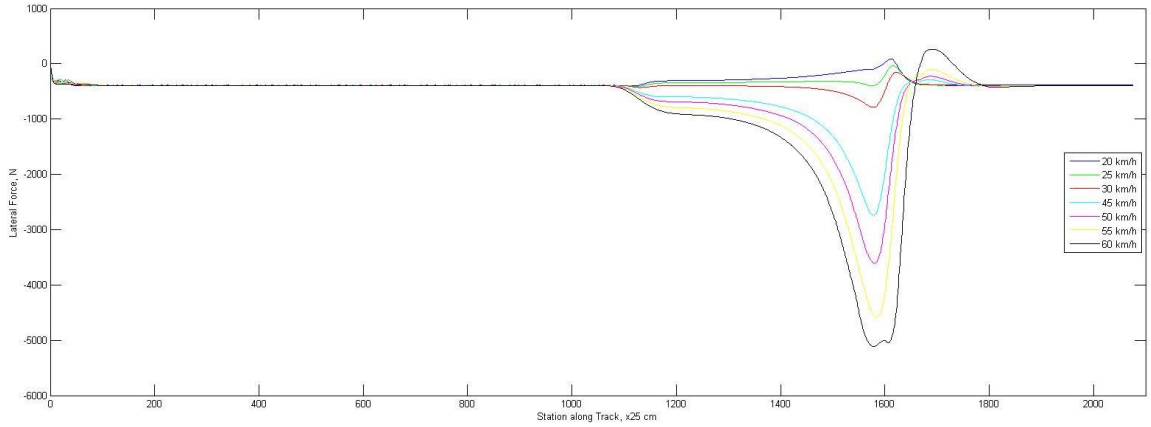

Figure 52: Lateral Force at Front Left Tire

What is not initially apparent is the underlying cause of this anomaly, since the vehicle parameters and CarSim track are unchanged throughout all simulations. It is expected that if there were an underlying problem with the vehicle parameters that an anomaly would be apparent in more than just one force at one tire at one speed.

Appendix C: Additional Results

This appendix presents additional results beginning with the Taylor Series estimation discussed in Section 3.1.1. Below the results for the 20 km/h perturbed to 25 km/h, 30 km/h to 35 km/h, 35 km/h to 40 km/h, 45 km/h to 50 km/h, and 50 km/h to 55 km/h runs.

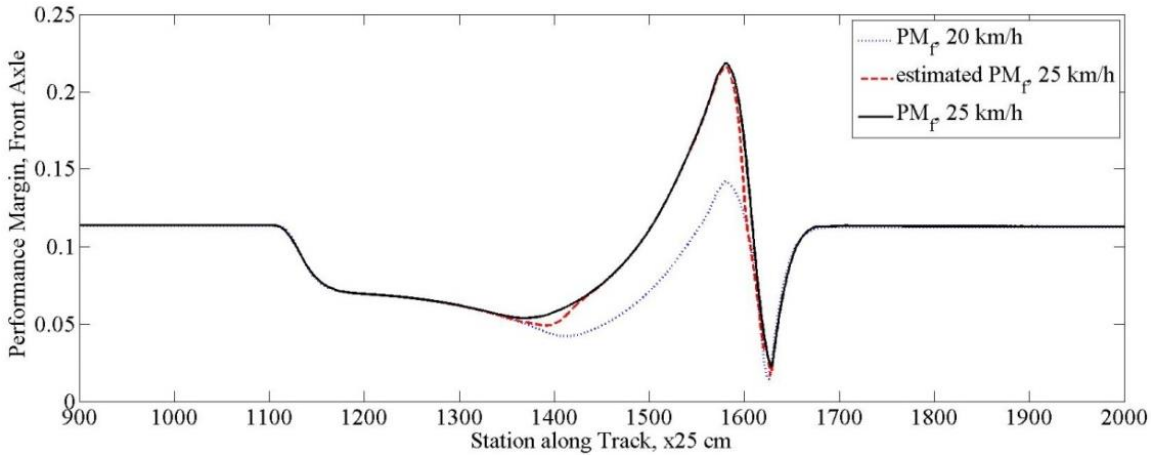

Figure 53: Estimated and Actual PM, Front Axle, 20 to 25 km/h

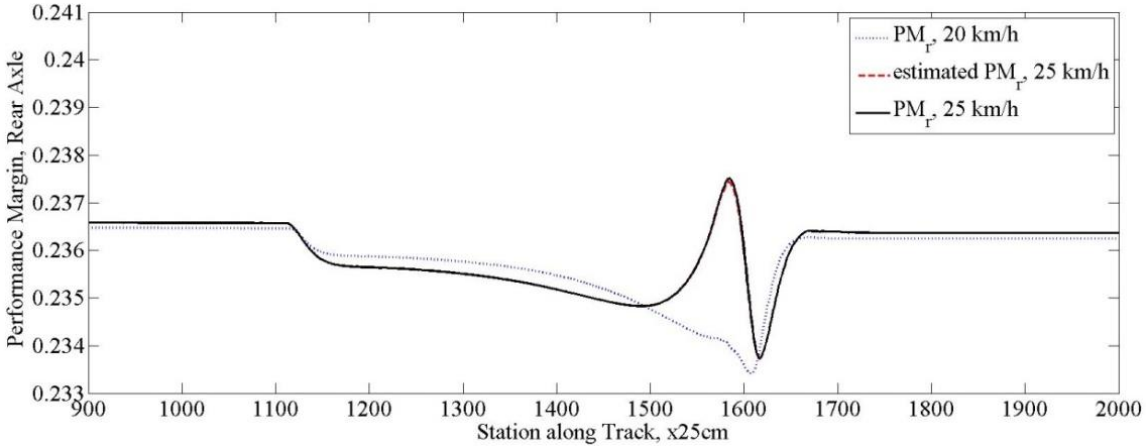

Figure 54: Estimated and Actual PM, Rear Axle, 20 to 25 km/h

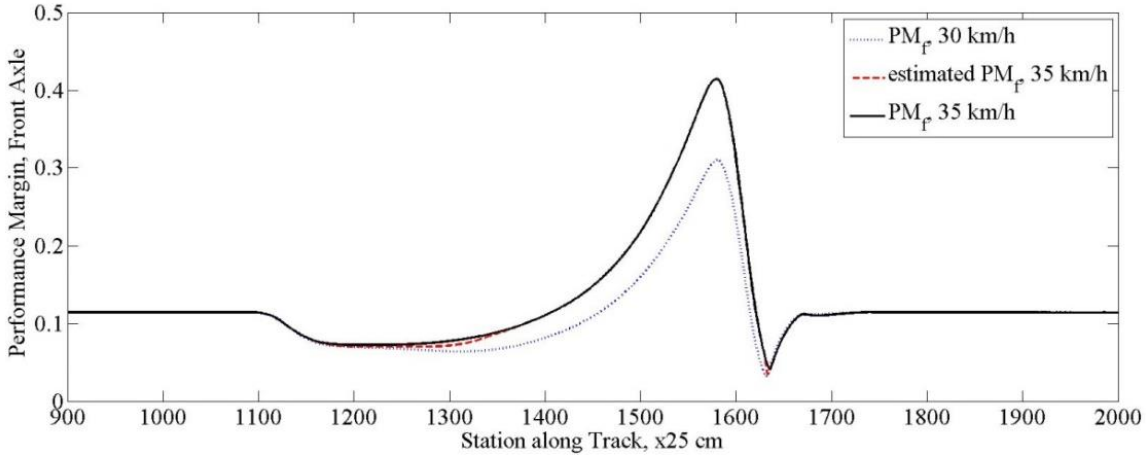

Figure 55: Estimated and Actual PM, Front Axle, 30 to 35 km/h

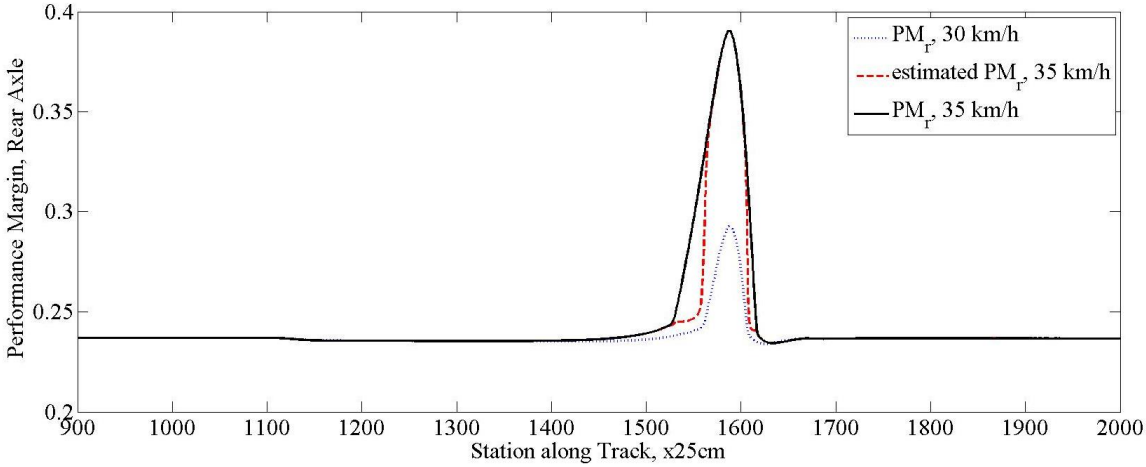

Figure 56: Estimated and Actual PM, Rear Axle, 30 to 35 km/h

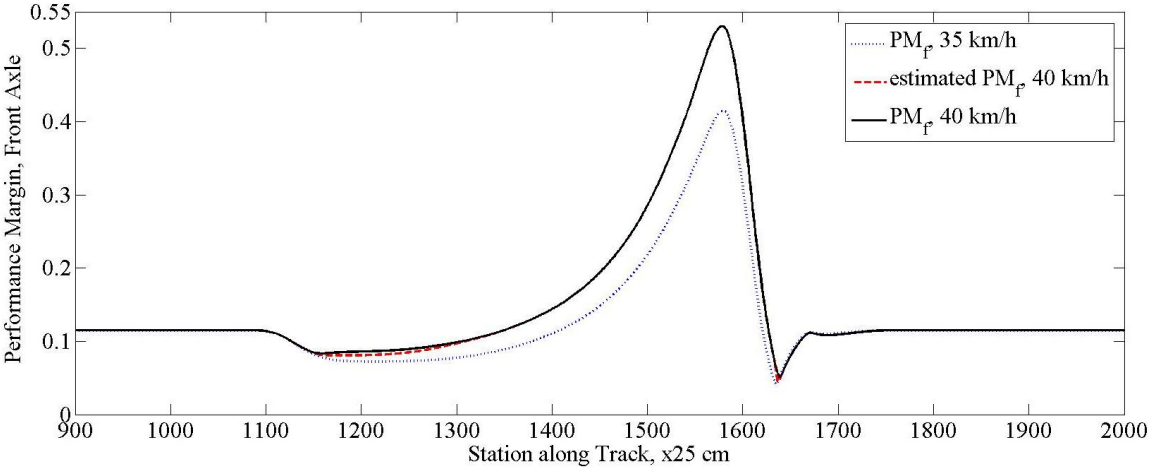

Figure 57: Estimated and Actual PM, Front Axle, 35 to 40 km/h

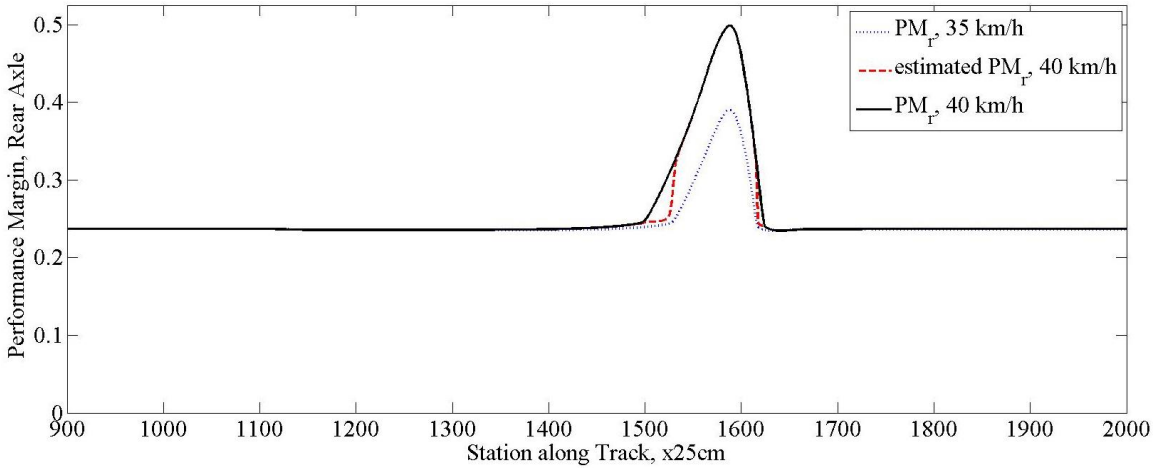

Figure 58: Estimated and Actual PM, Rear Axle, 35 to 40 km/h

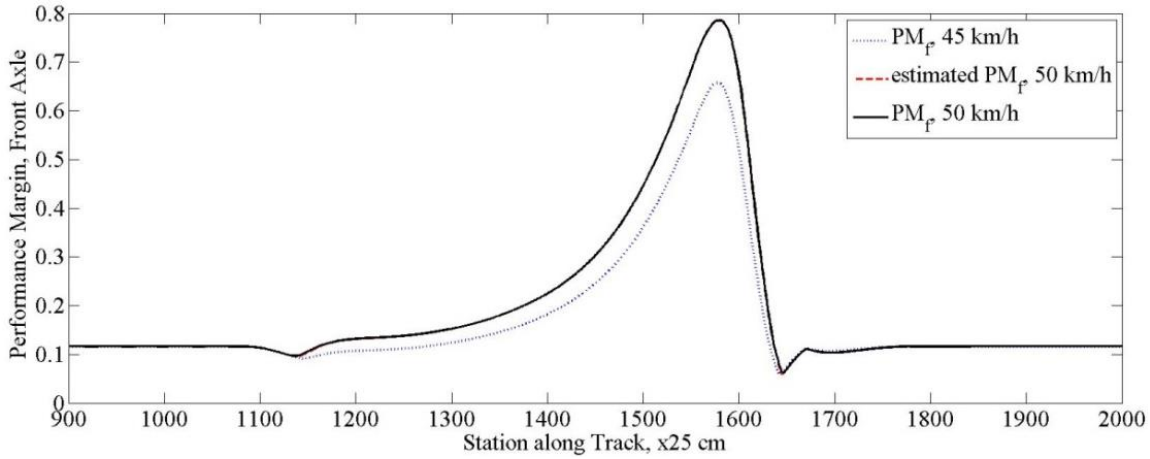

Figure 59: Estimated and Actual PM, Front Axle, 45 to 50 km/h

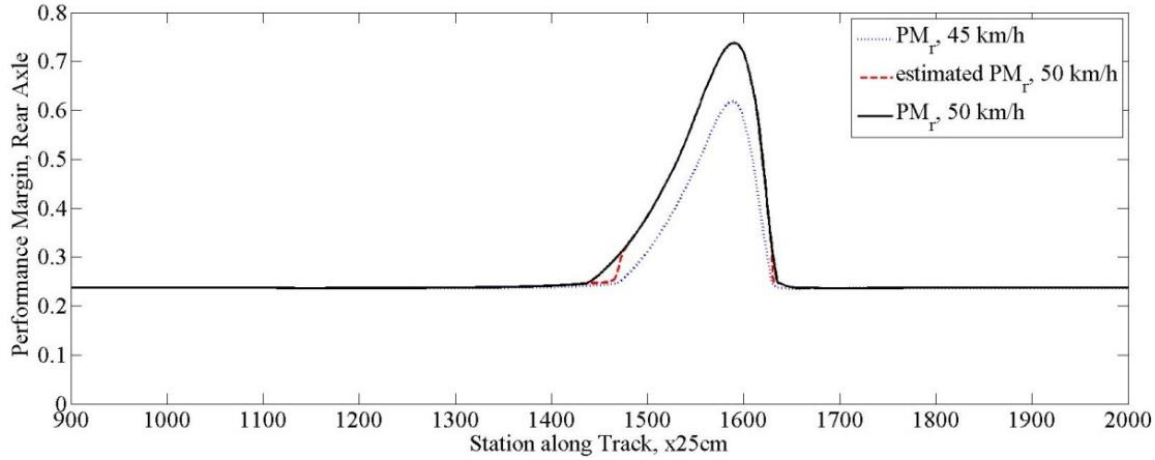

Figure 60: Estimated and Actual PM, Rear Axle, 45 to 50 km/h

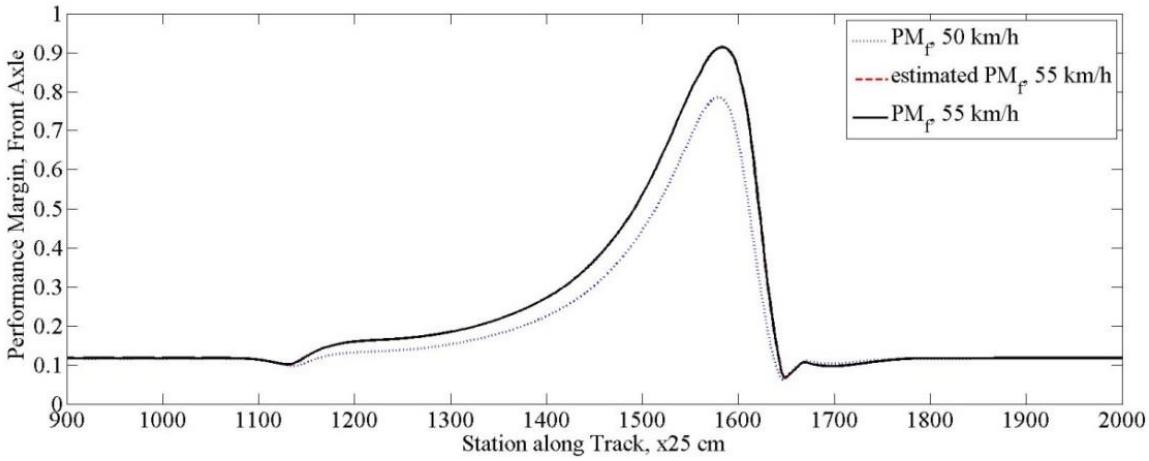

Figure 61: Estimated and Actual PM, Front Axle, 50 to 55 km/h

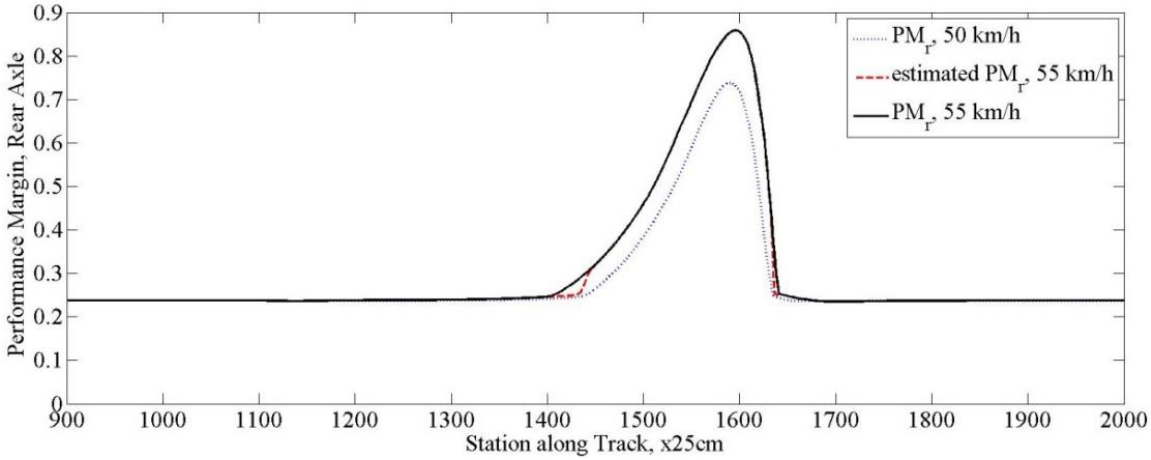

Figure 62: Estimated and Actual PM, Rear Axle, 50 to 55 km/h

Next, results of the estimation of ΔF_z due to roll and pitch are presented.

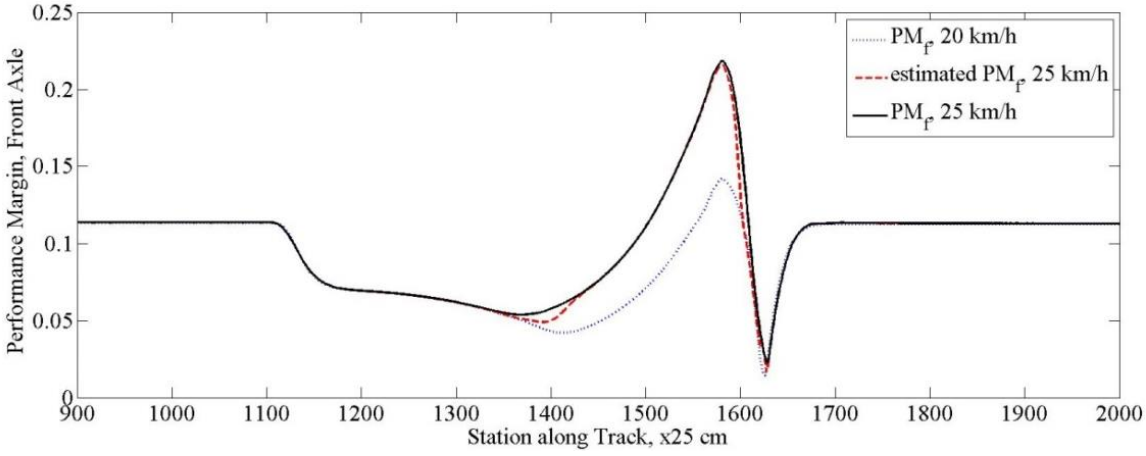

Figure 63: Estimated and Actual PM, Front Axle, 20 to 25 km/h

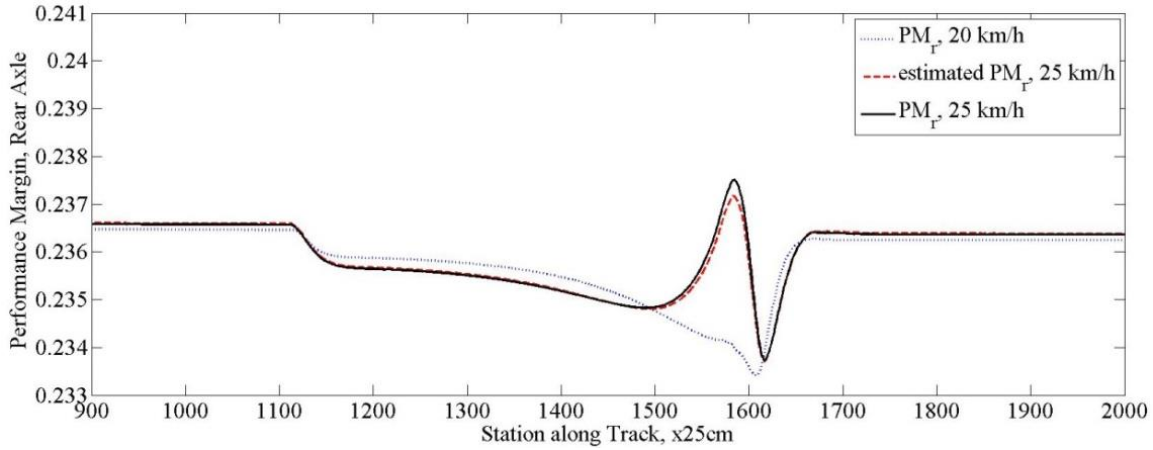

Figure 64: Estimated and Actual PM, Rear Axle, 20 to 25 km/h

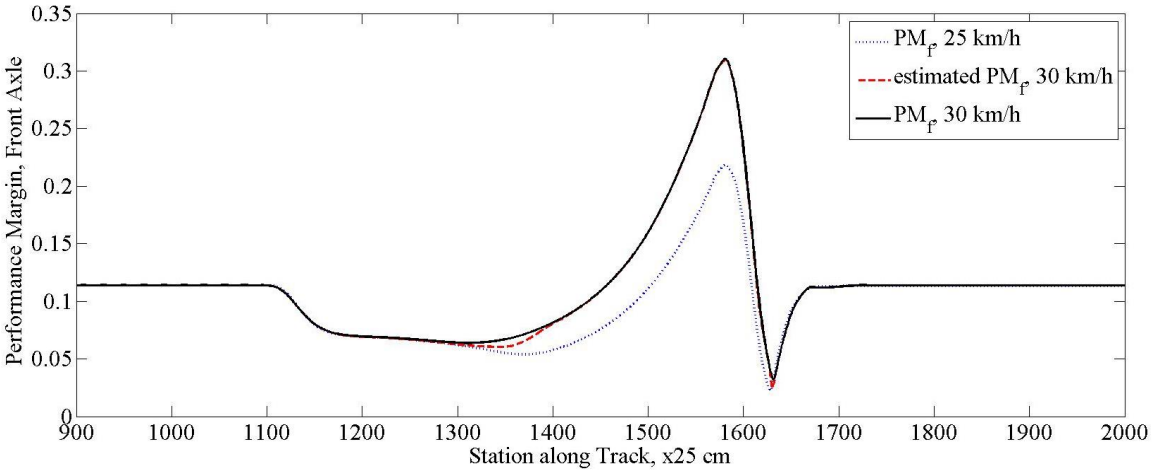

Figure 65: Estimated and Actual PM, Front Axle, 25 to 30 km/h

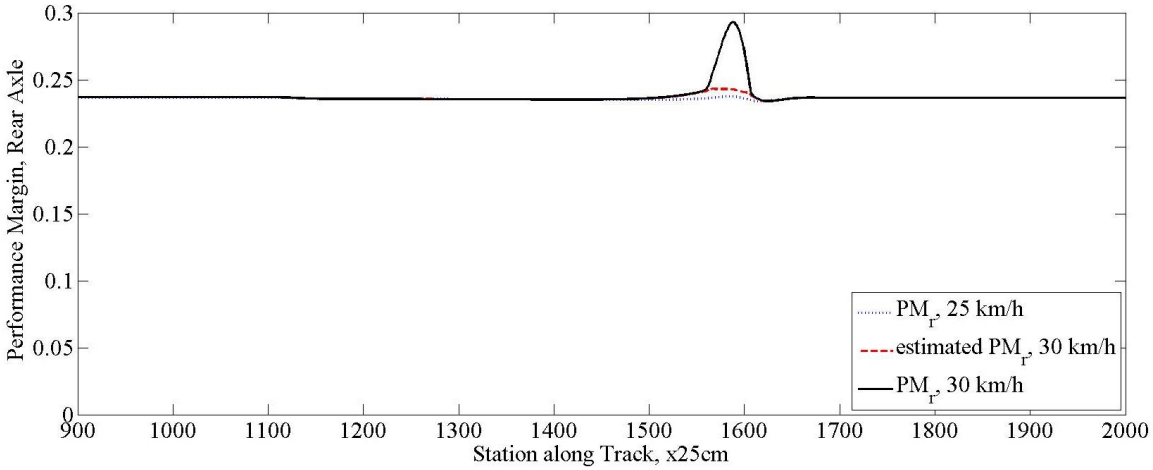

Figure 66: Estimated and Actual PM, Rear Axle, 25 to 30 km/h

Again, the anomaly discussed in Appendix B: Lateral Force Anomaly is apparent only in the 25 to 30 km/h rear axle estimation.

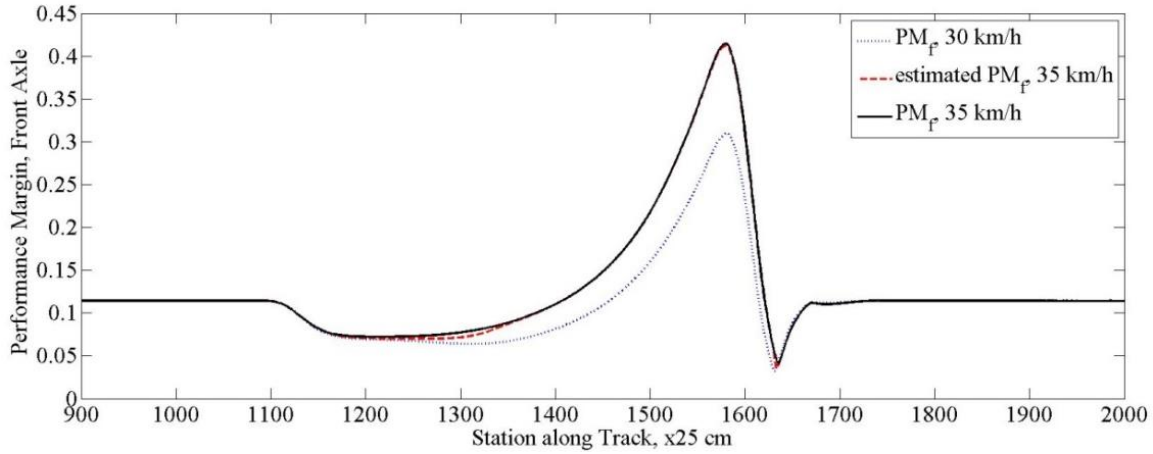

Figure 67: Estimated and Actual PM, Front Axle, 30 to 35 km/h

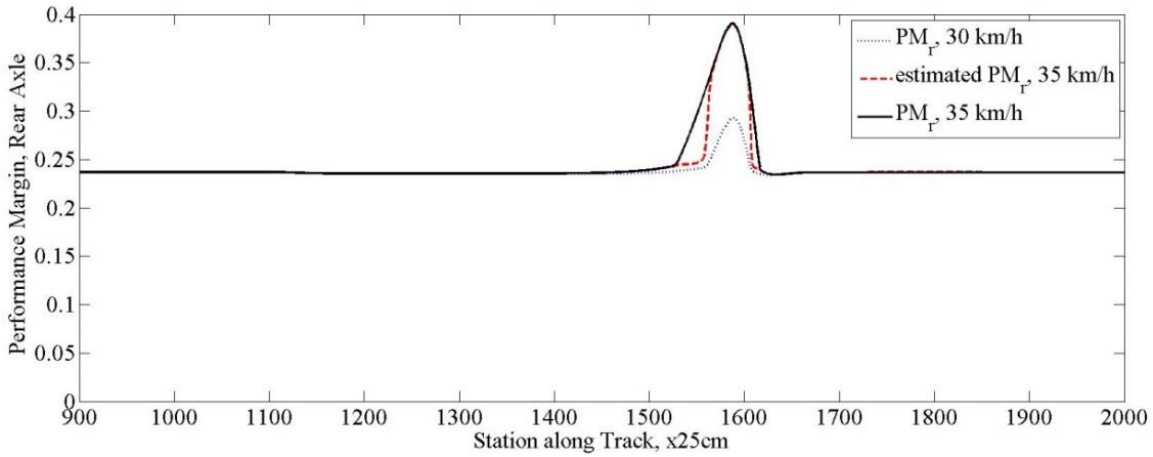

Figure 68: Estimated and Actual PM, Rear Axle, 30 to 35 km/h

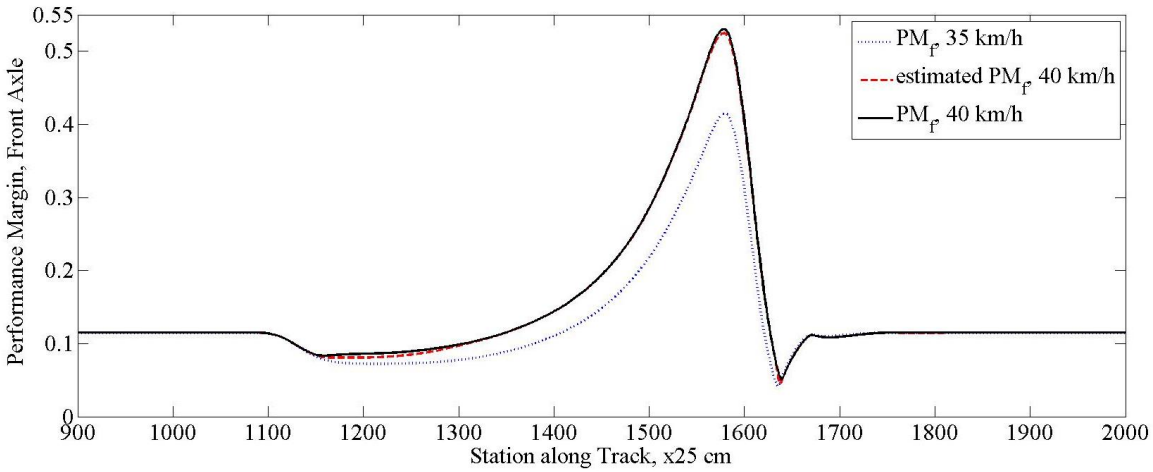

Figure 69: Estimated and Actual PM, Front Axle, 35 to 40 km/h

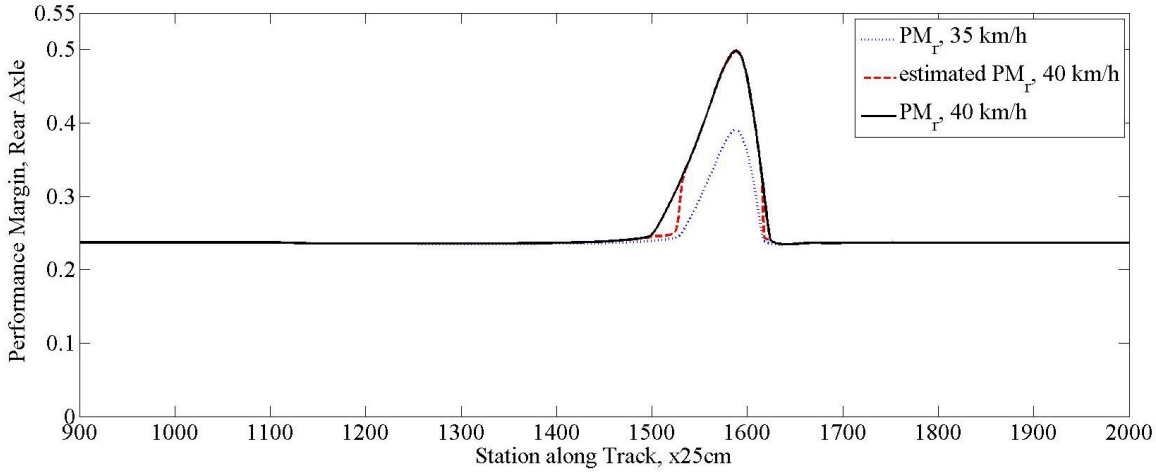

Figure 70: Estimated and Actual PM, Rear Axle, 35 to 40 km/h

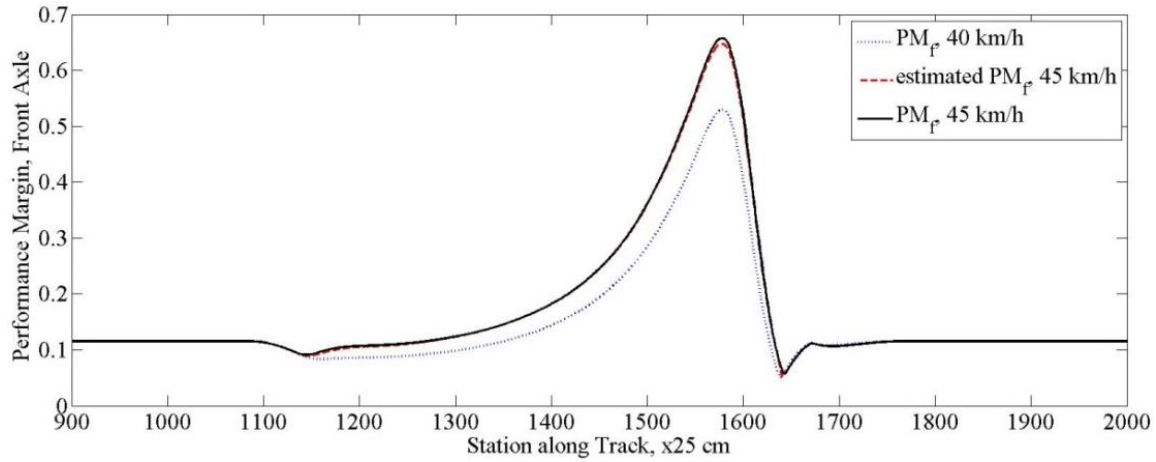

Figure 71: Estimated and Actual PM, Front Axle, 40 to 45 km/h

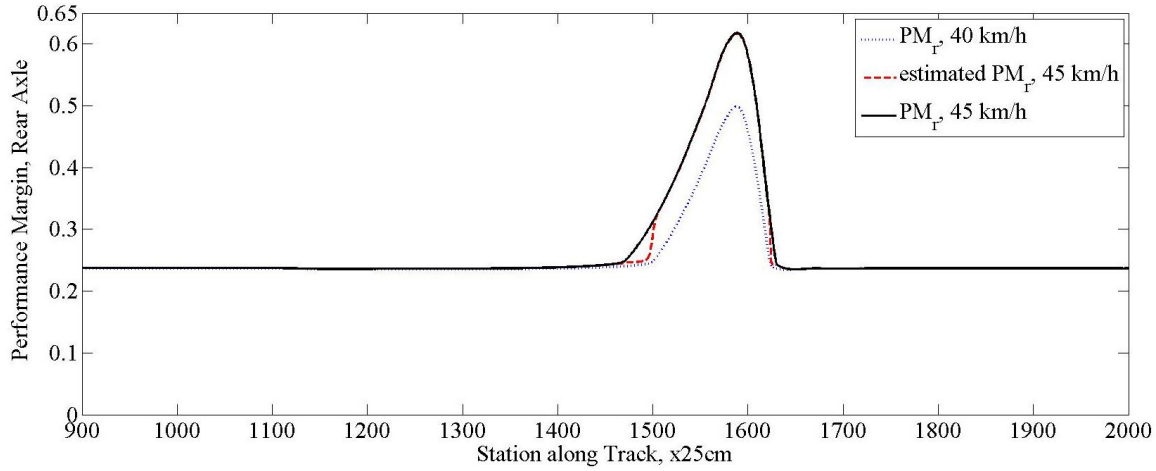

Figure 72: Estimated and Actual PM, Rear Axle, 40 to 45 km/h

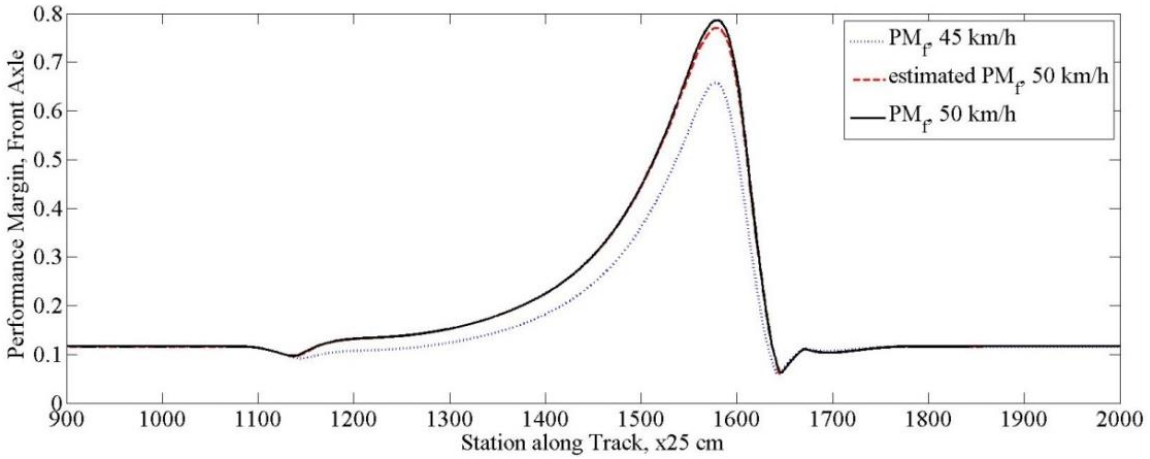

Figure 73: Estimated and Actual PM, Front Axle, 45 to 50 km/h

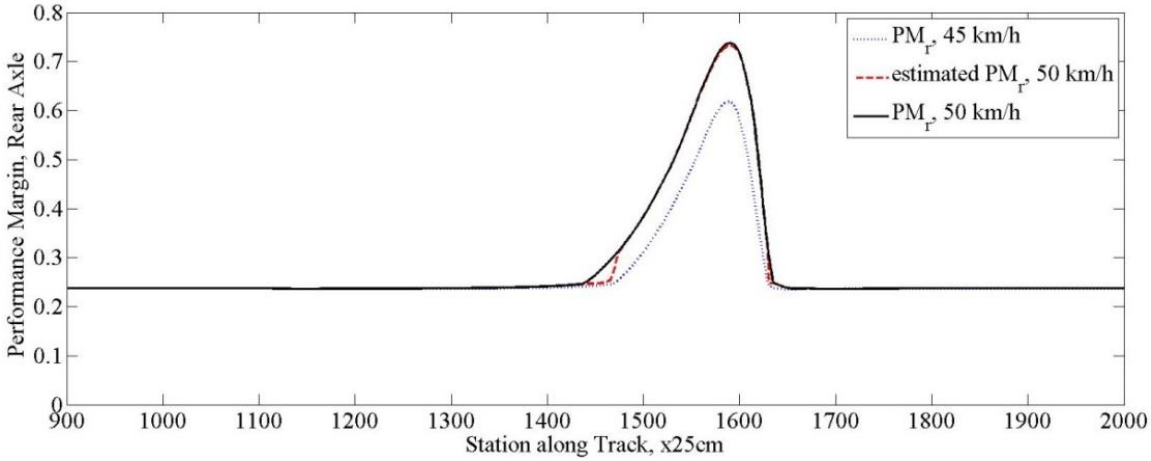

Figure 74: Estimated and Actual PM, Rear Axle, 45 to 50 km/h

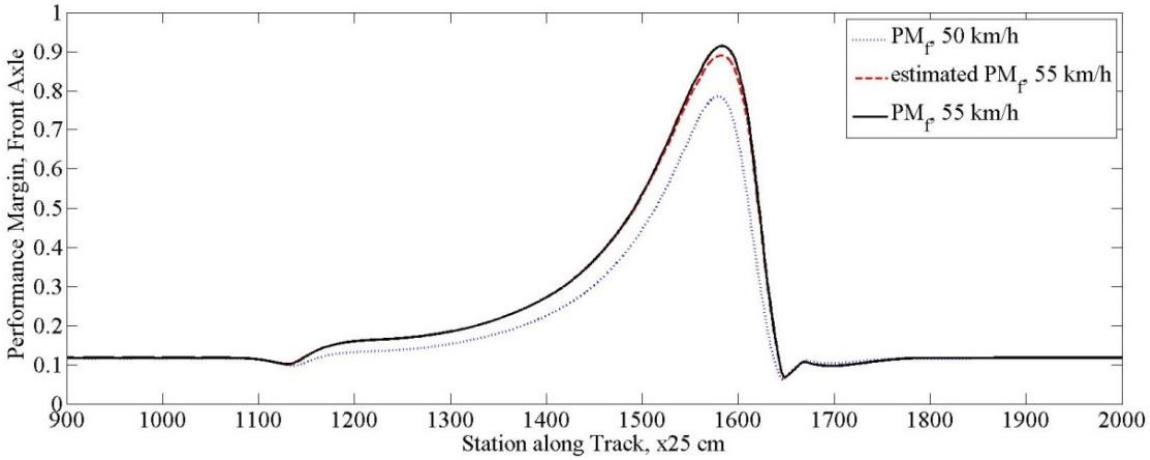

Figure 75: Estimated and Actual PM, Front Axle, 50 to 55 km/h

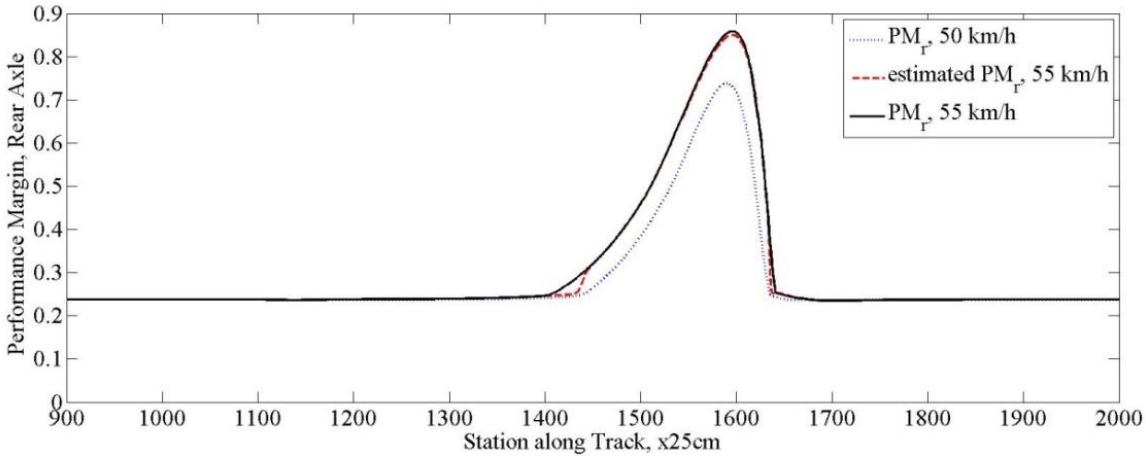

Figure 76: Estimated and Actual PM, Rear Axle, 50 to 55 km/h

Next, the results of the estimation of ΔF_y due to velocity and yaw are presented.

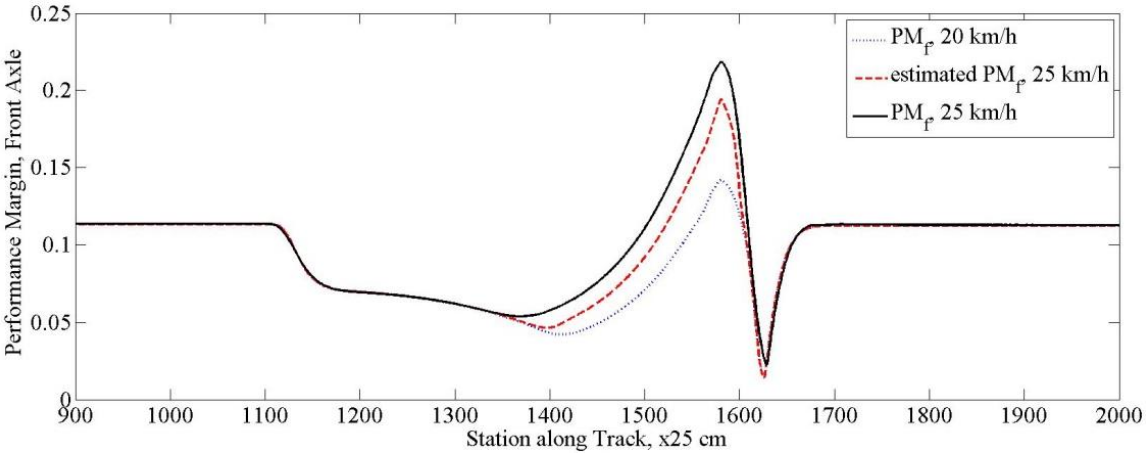

Figure 77: Estimated and Actual PM, Front Axle, 20 to 25 km/h

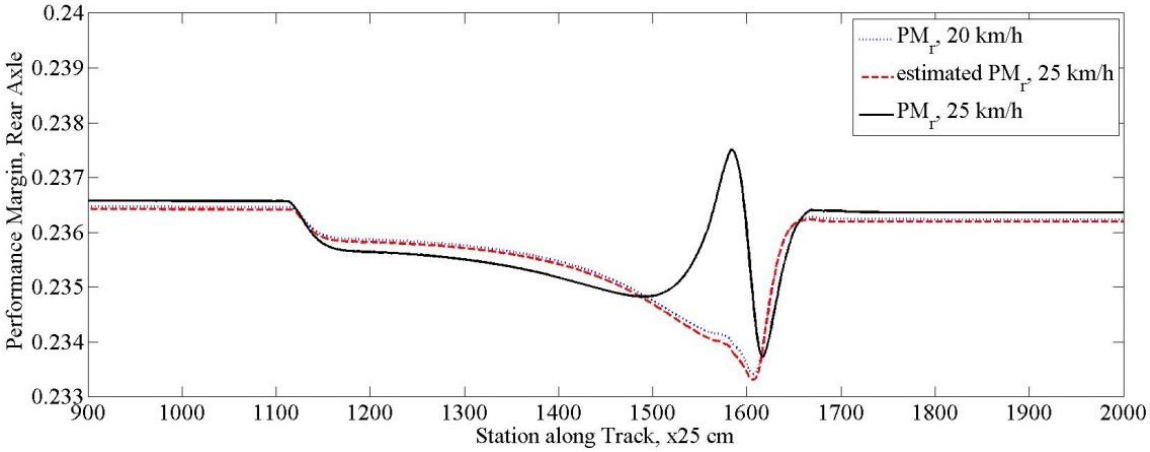

Figure 78: Estimated and Actual PM, Rear Axle, 20 to 25 km/h

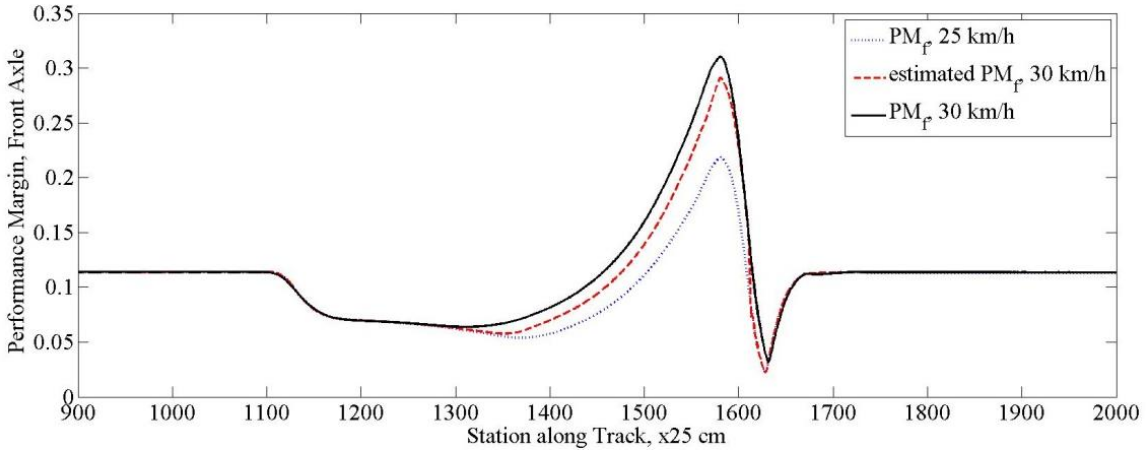

Figure 79: Estimated and Actual PM, Front Axle, 25 to 30 km/h

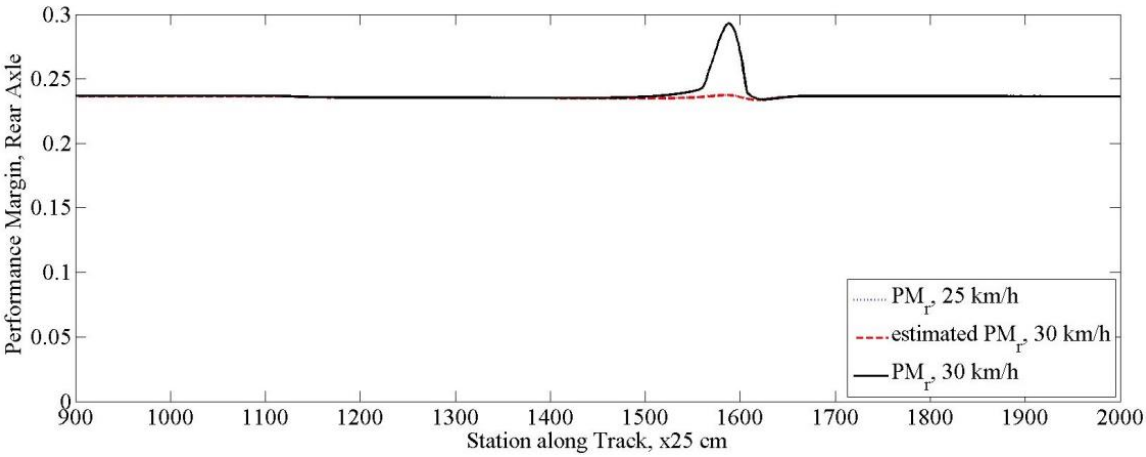

Figure 80: Estimated and Actual PM, Rear Axle, 25 to 30 km/h

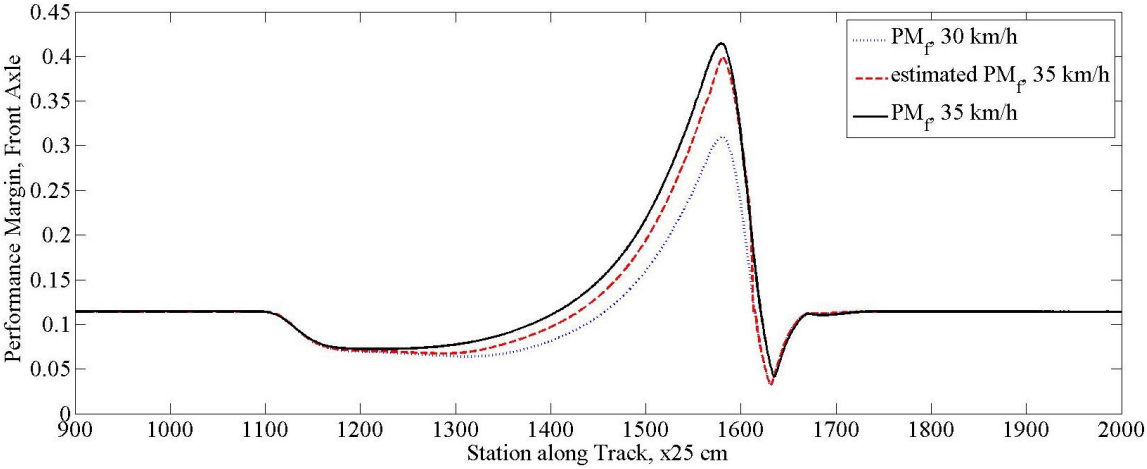

Figure 81: Estimated and Actual PM, Front Axle, 30 to 35 km/h

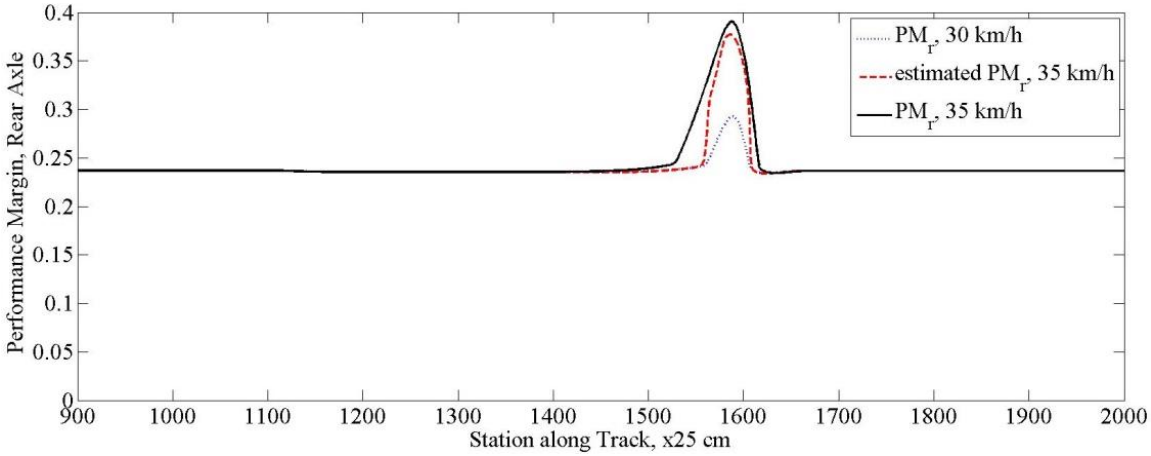

Figure 82: Estimated and Actual PM, Rear Axle, 30 to 35 km/h

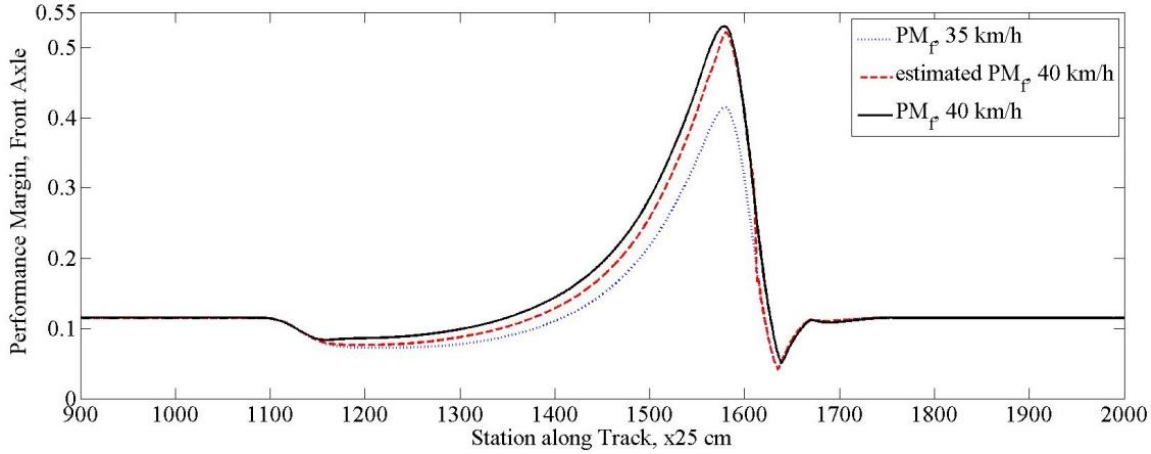

Figure 83: Estimated and Actual PM, Front Axle, 35 to 40 km/h

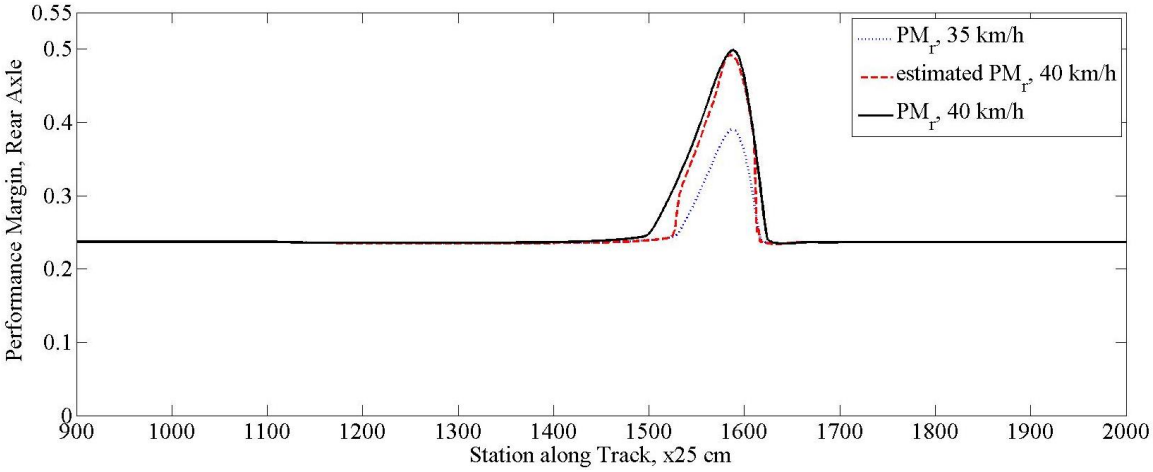

Figure 84: Estimated and Actual PM, Rear Axle, 35 to 40 km/h

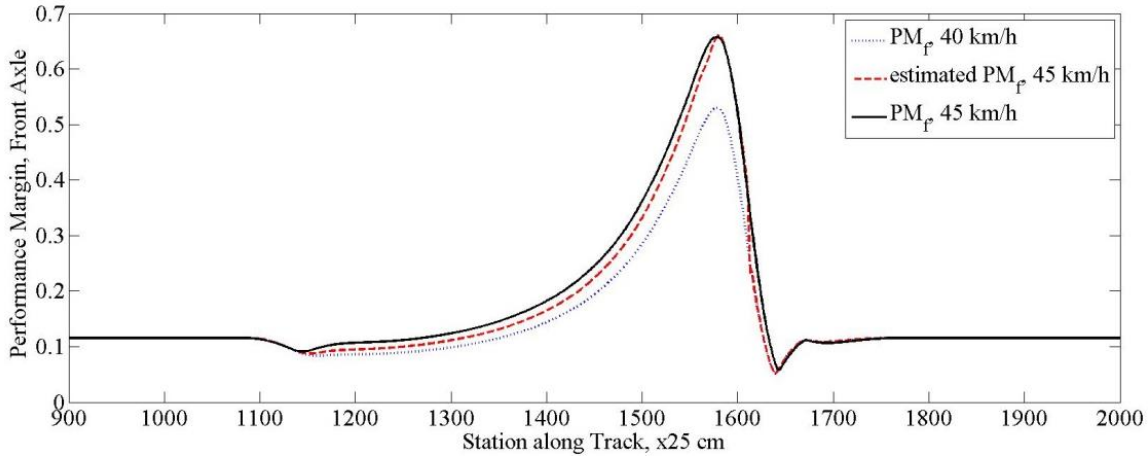

Figure 85: Estimated and Actual PM, Front Axle, 40 to 45 km/h

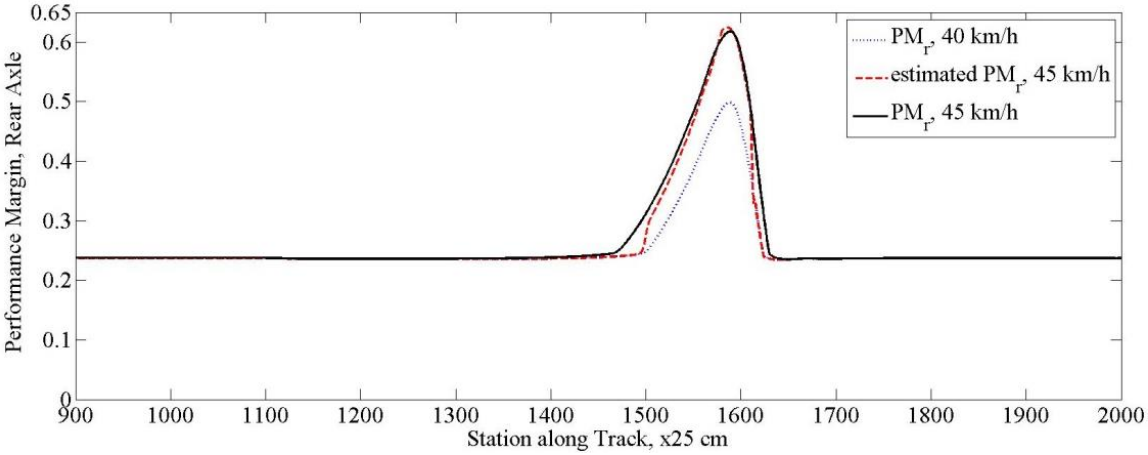

Figure 86: Estimated and Actual PM, Rear Axle, 40 to 45 km/h

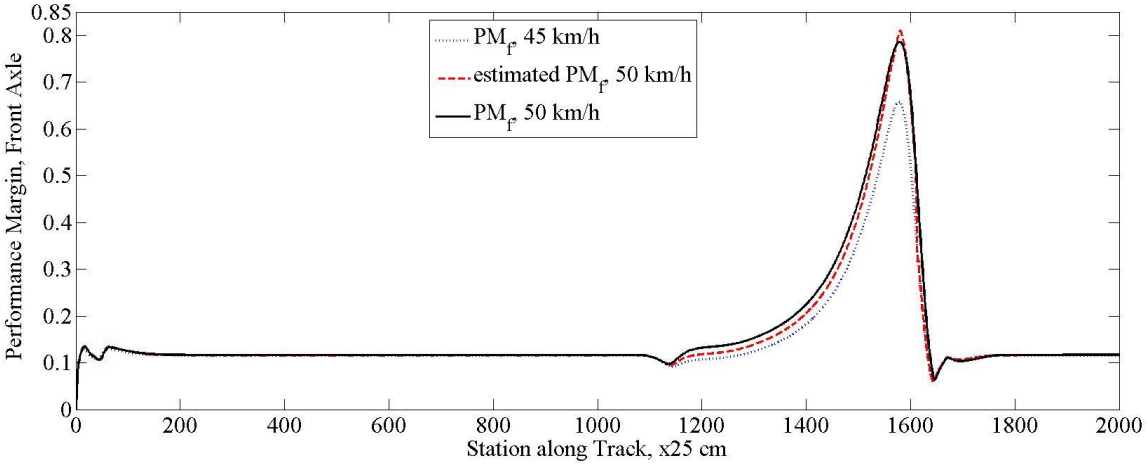

Figure 87: Estimated and Actual PM, Front Axle, 45 to 50 km/h

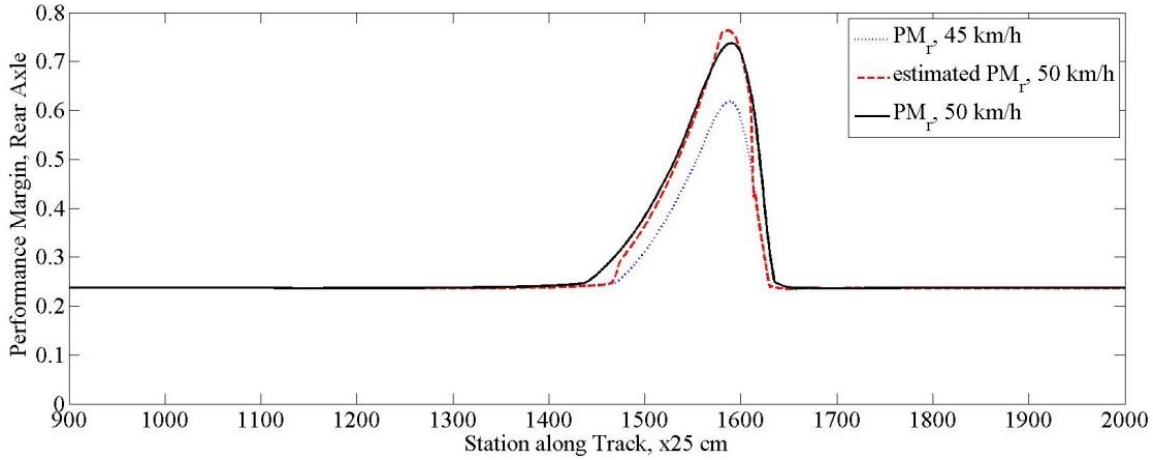

Figure 88: Estimated and Actual PM, Rear Axle, 45 to 50 km/h

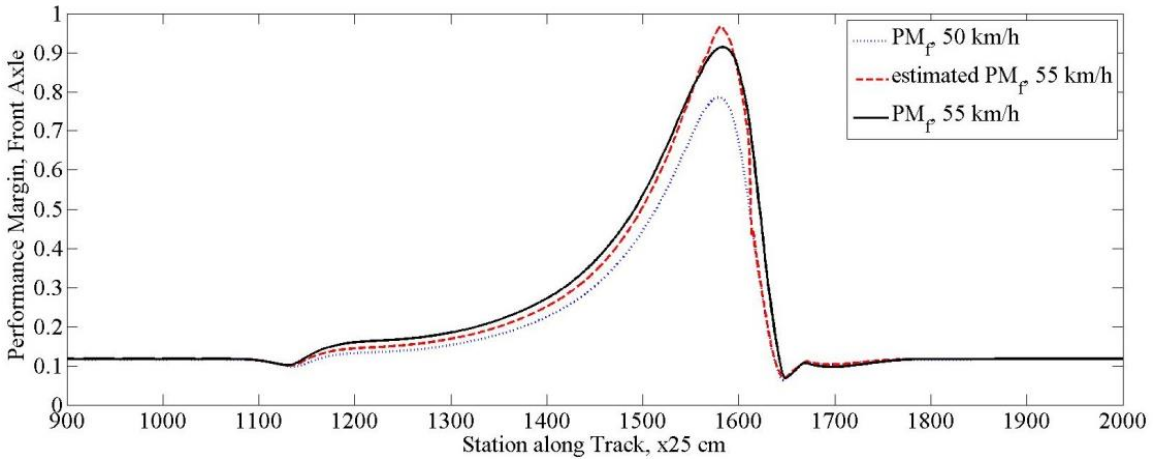

Figure 89: Estimated and Actual PM, Front Axle, 50 to 55 km/h

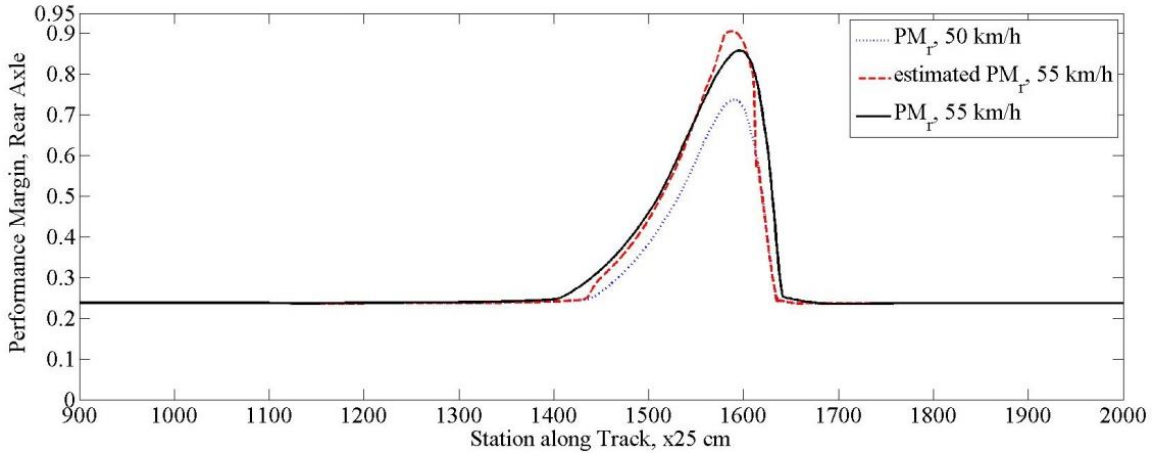

Figure 90: Estimated and Actual PM, Rear Axle, 50 to 55 km/h

Next, the results of the roll, pitch, and yaw estimations on Track 2 are presented.

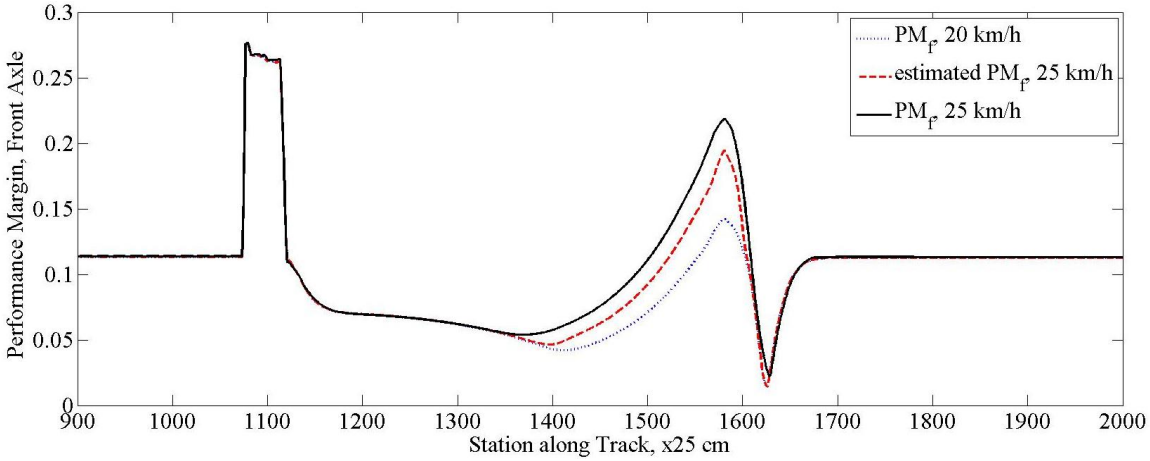

Figure 91: Estimated and Actual PM, Front Axle, 20 to 25 km/h

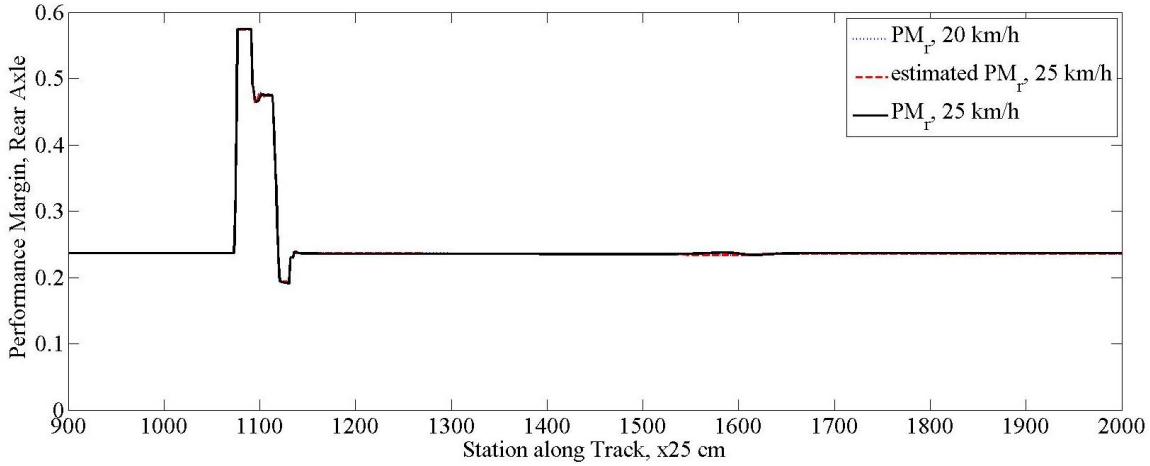

Figure 92: Estimated and Actual PM, Rear Axle, 20 to 25 km/h

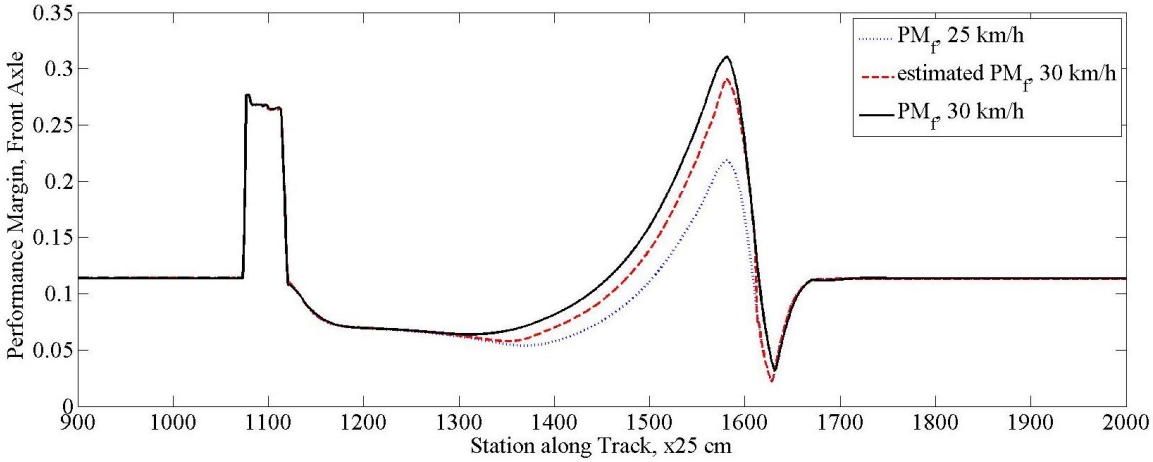

Figure 93: Estimated and Actual PM, Front Axle, 25 to 30 km/h

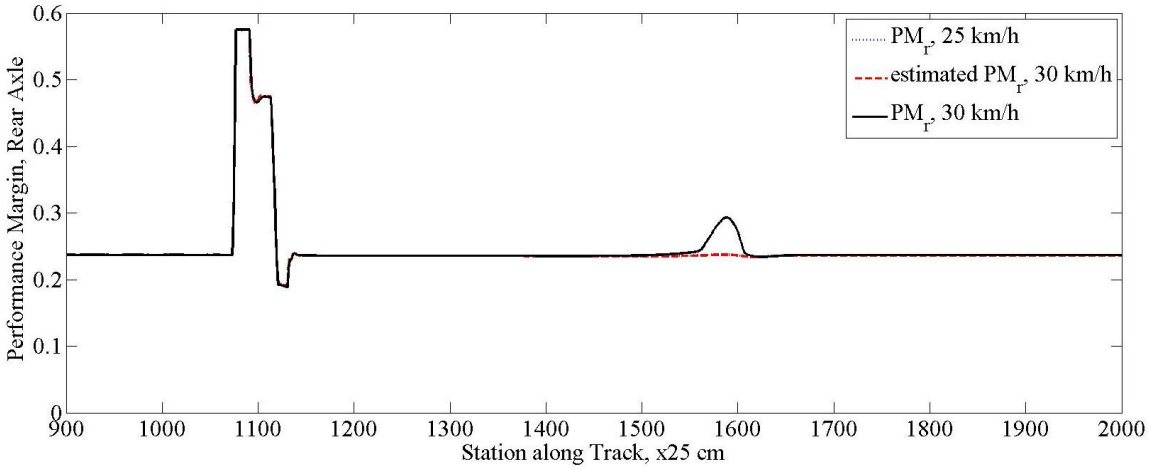

Figure 94: Estimated and Actual PM, Rear Axle, 25 to 30 km/h

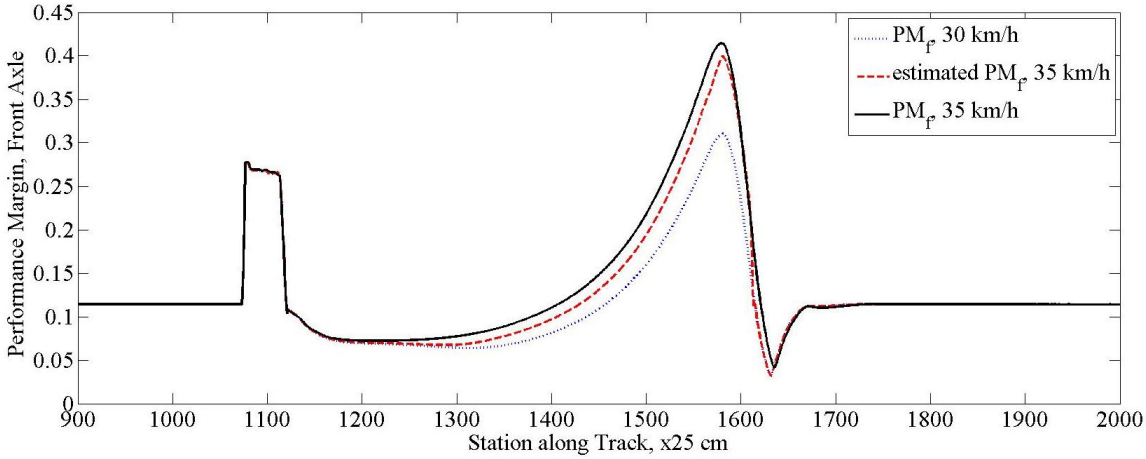

Figure 95: Estimated and Actual PM, Front Axle, 30 to 35 km/h

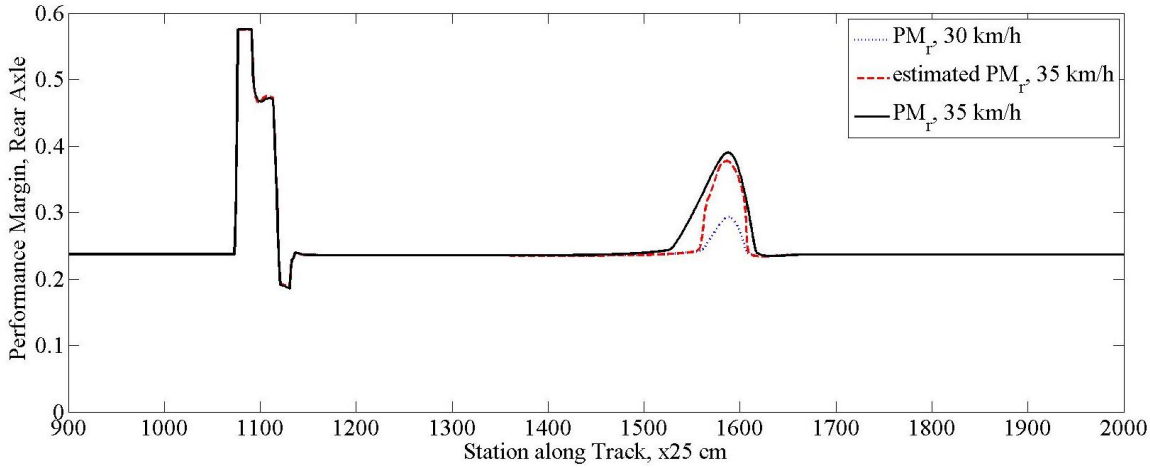

Figure 96: Estimated and Actual PM, Rear Axle, 30 to 35 km/h

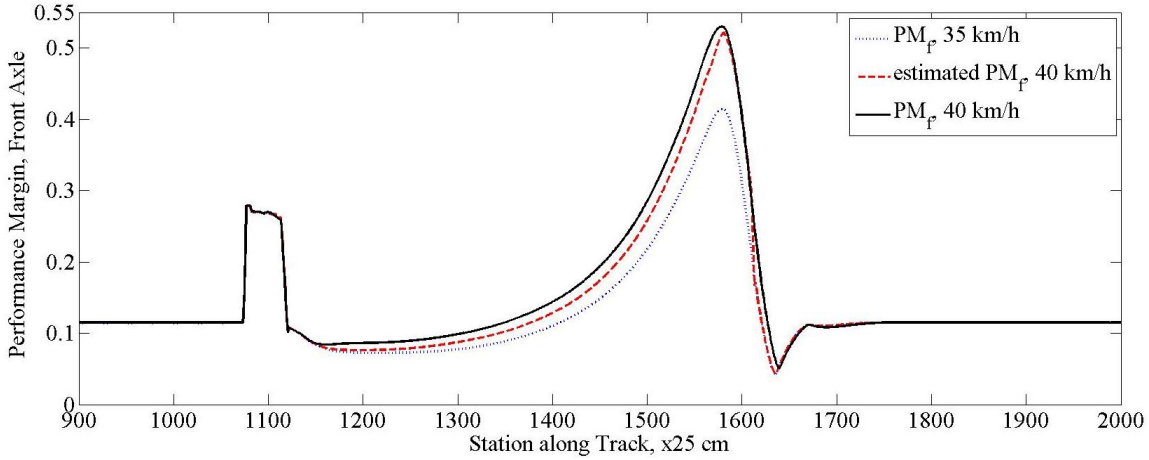

Figure 97: Estimated and Actual PM, Front Axle, 35 to 40 km/h

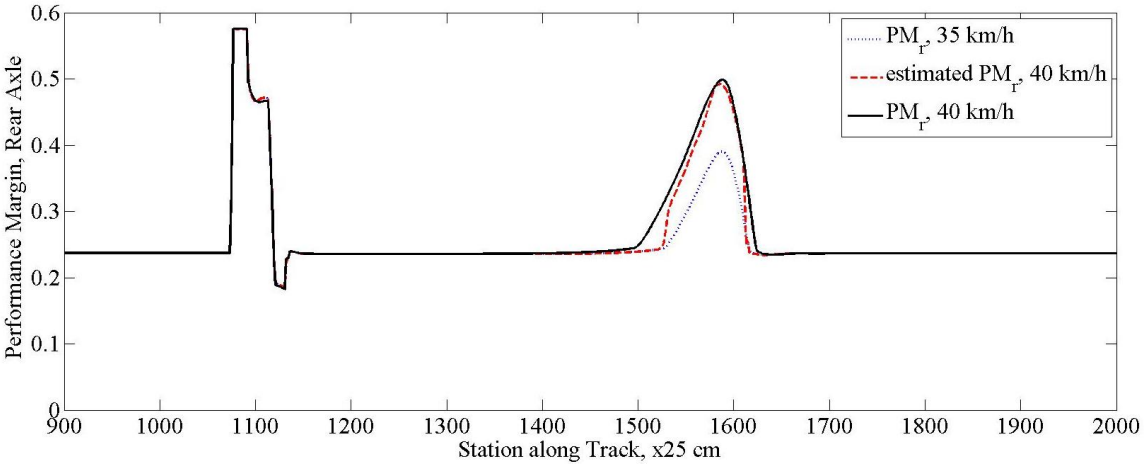

Figure 98: Estimated and Actual PM, Rear Axle, 35 to 40 km/h

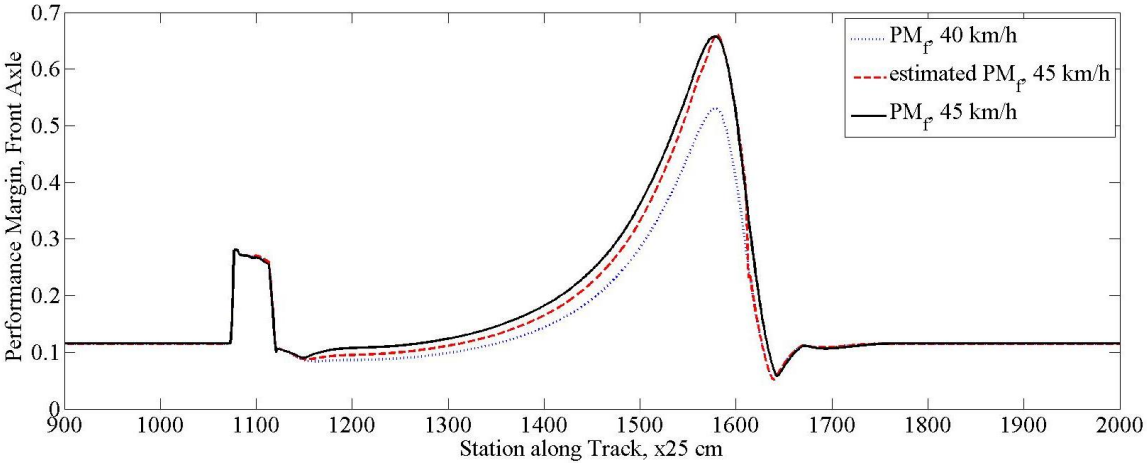

Figure 99: Estimated and Actual PM, Front Axle, 40 to 45 km/h

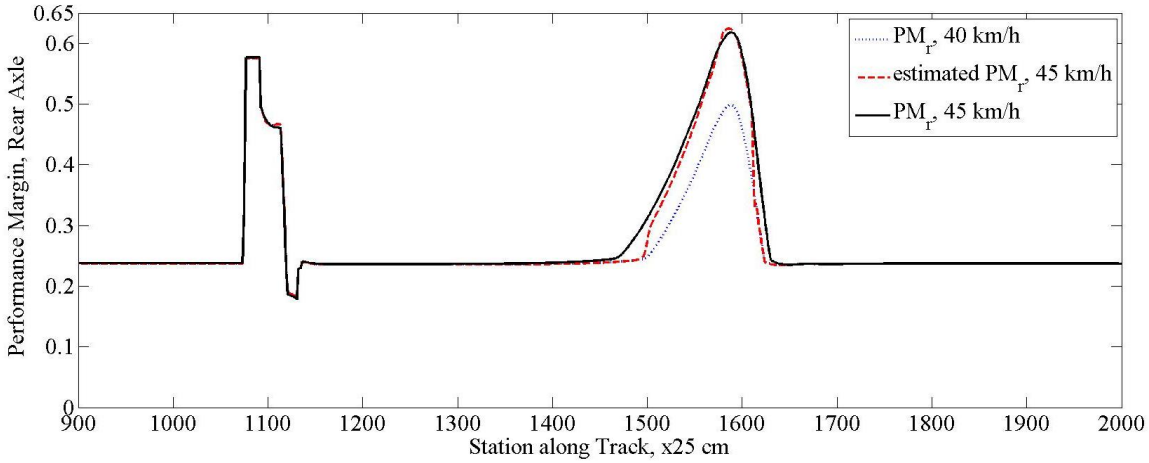

Figure 100: Estimated and Actual PM, Rear Axle, 40 to 45 km/h

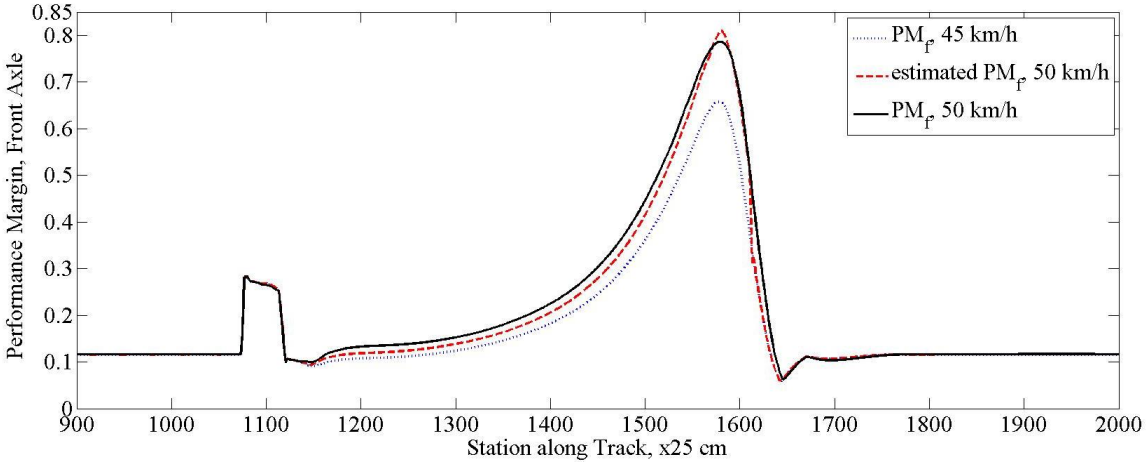

Figure 101: Estimated and Actual PM, Front Axle, 45 to 50 km/h

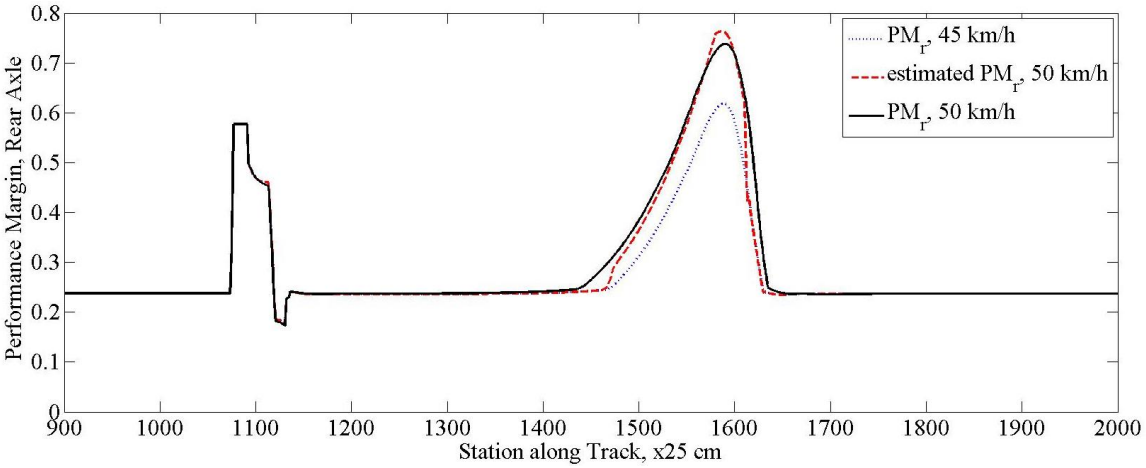

Figure 102: Estimated and Actual PM, Rear Axle, 45 to 50 km/h

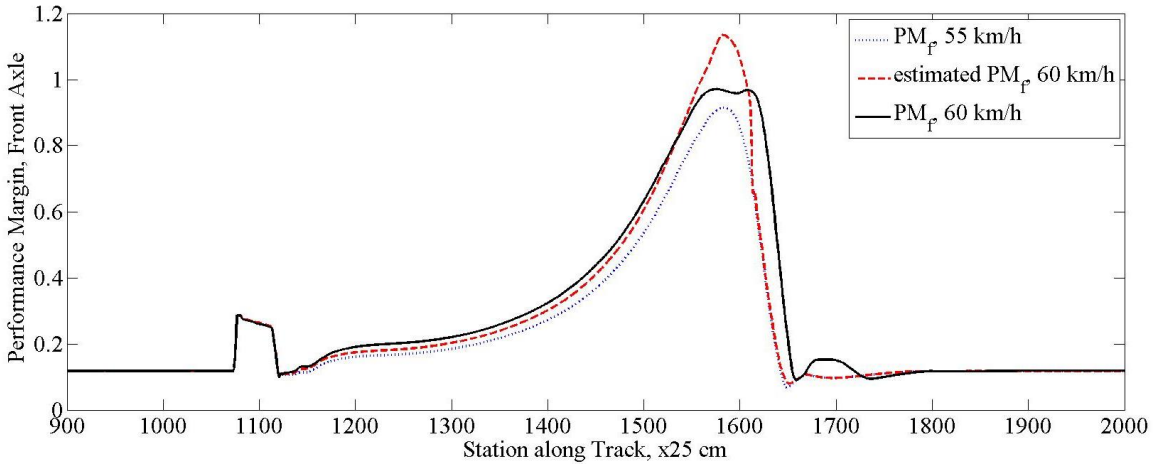

Figure 103: Estimated and Actual PM, Front Axle, 55 to 60 km/h

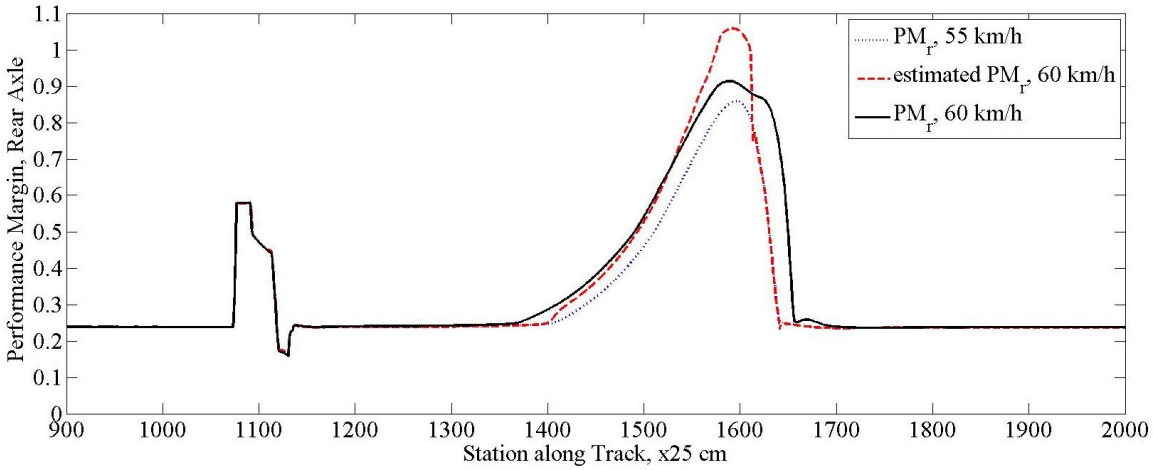

Figure 104: Estimated and Actual PM, Rear Axle, 55 to 60 km/h

Lastly, the estimations of vertical forces due to terrain excitations are presented.

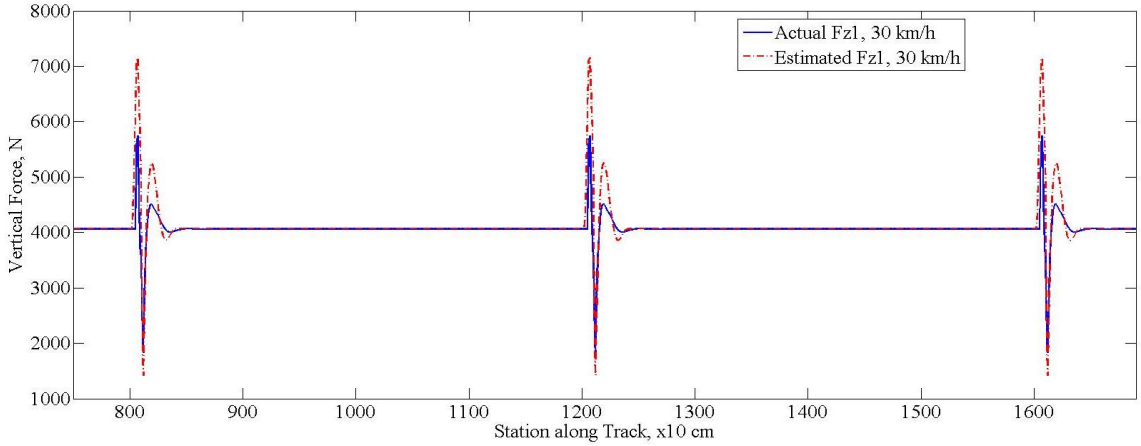

Figure 105: Estimated and Actual Vertical Force, Left Front Tire, 30 km/h

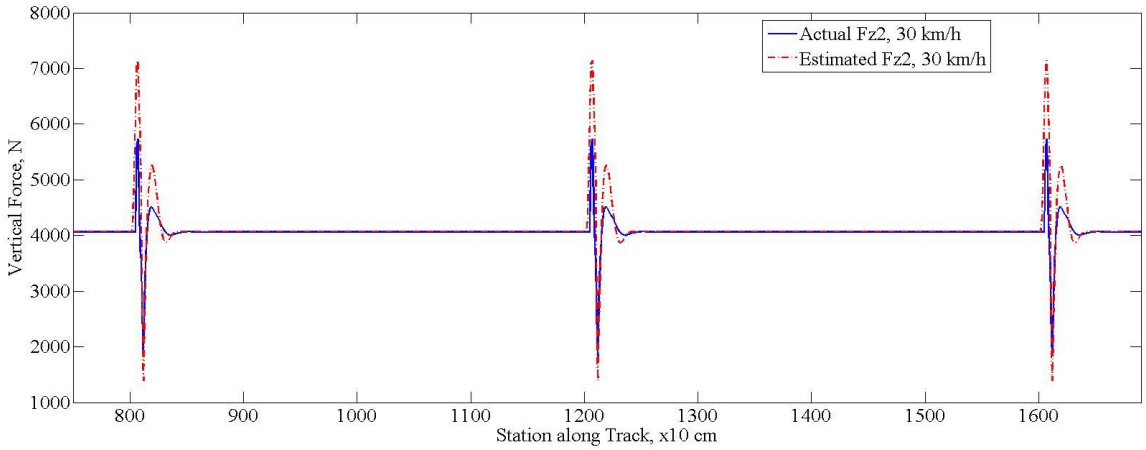

Figure 106: Estimated and Actual Vertical Force, Right Front Tire, 30 km/h

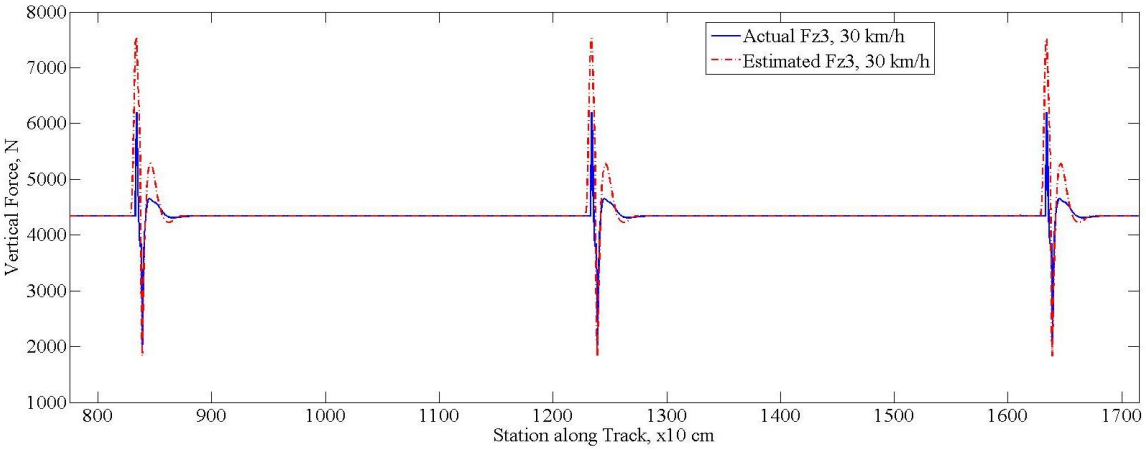

Figure 107: Estimated and Actual Vertical Force, Left Rear Tire, 30 km/h

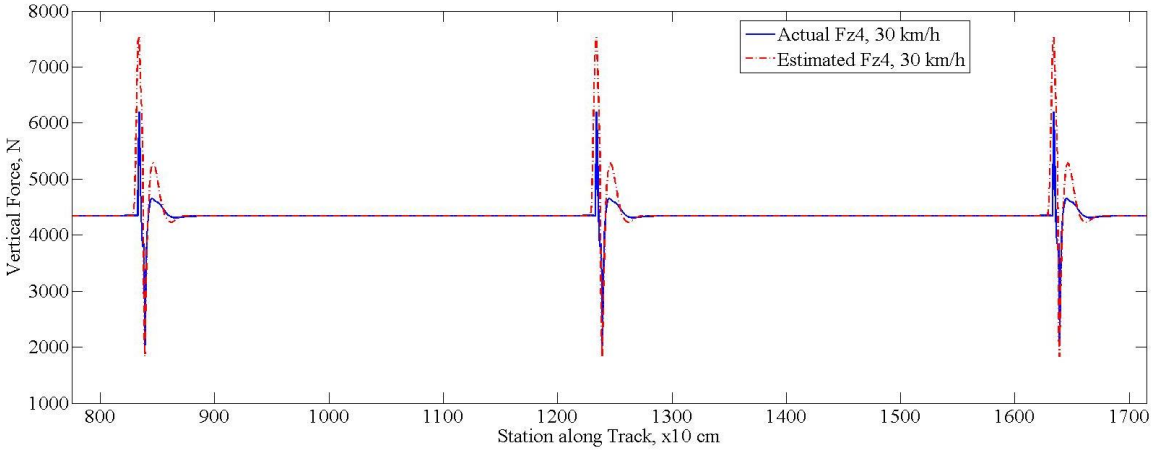

Figure 108: Estimated and Actual Vertical Force, Right Rear Tire, 30 km/h

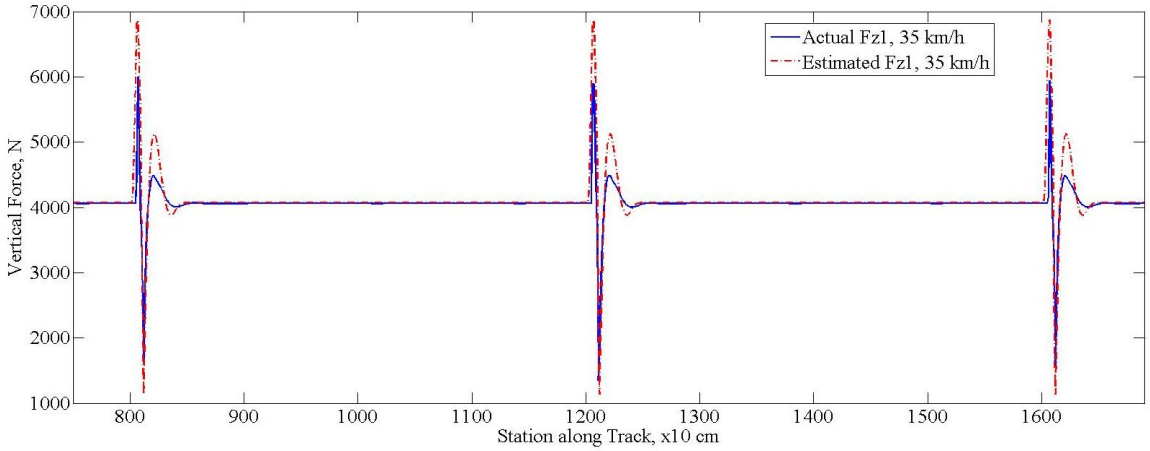

Figure 109: Estimated and Actual Vertical Force, Left Front Tire, 35 km/h

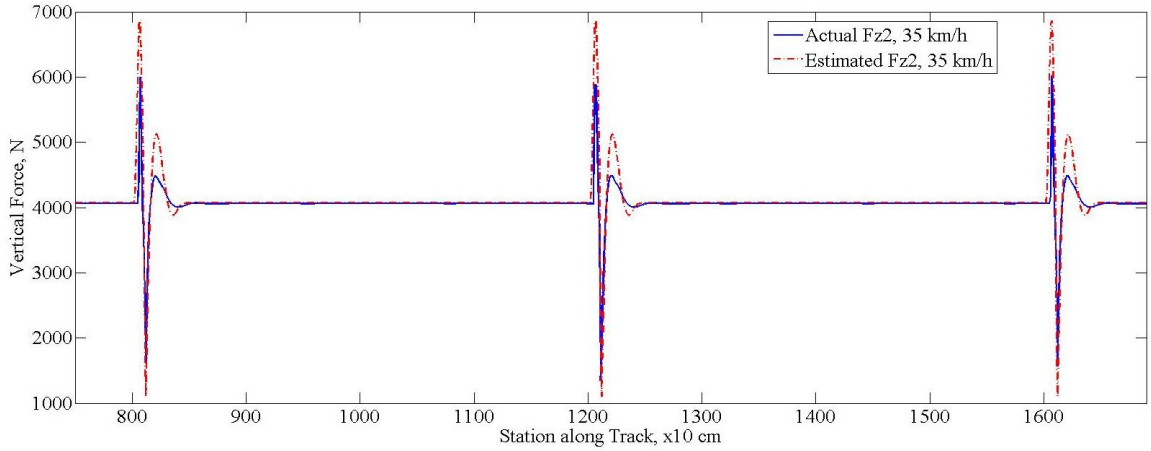

Figure 110: Estimated and Actual Vertical Force, Right Front Tire, 35 km/h

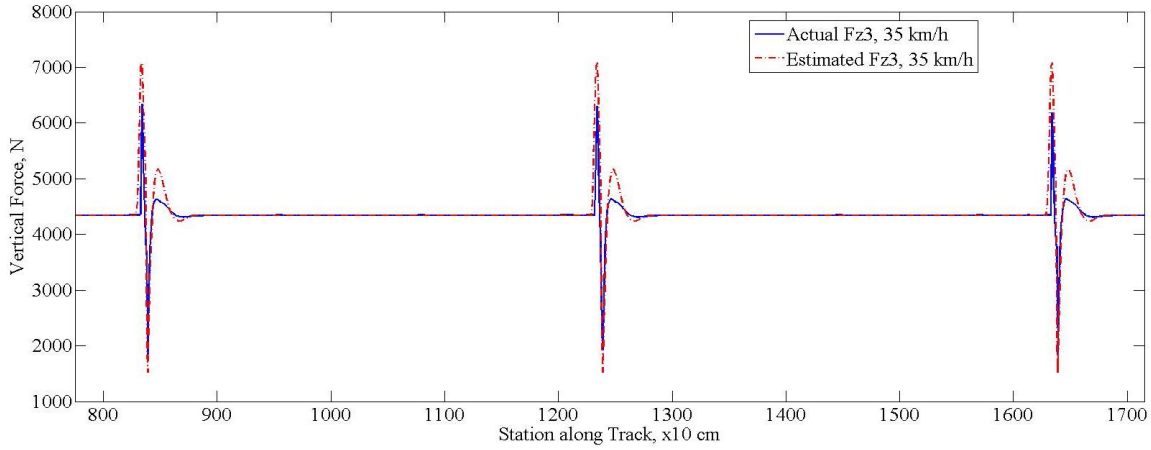

Figure 111: Estimated and Actual Vertical Force, Left Rear Tire, 35 km/h

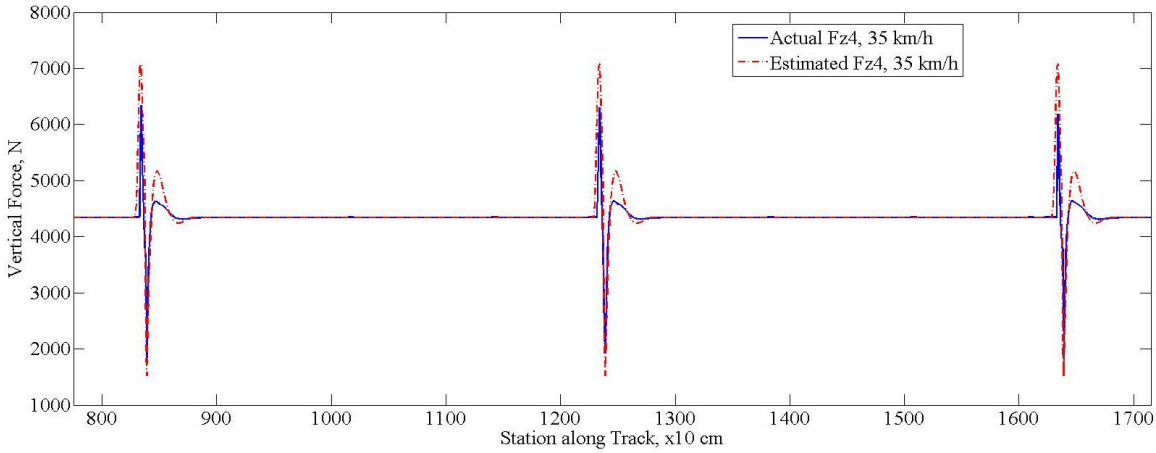

Figure 112: Estimated and Actual Vertical Force, Right Rear Tire, 35 km/h

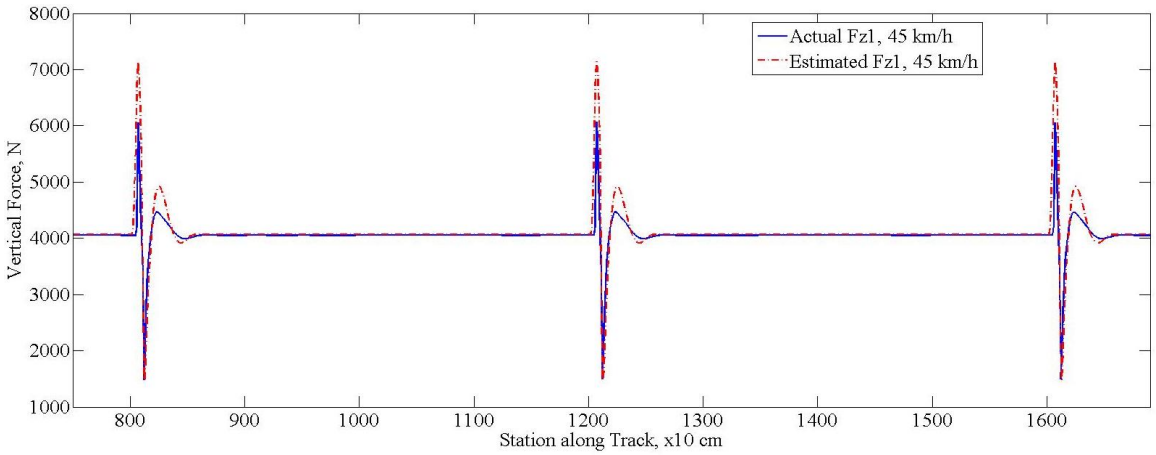

Figure 113: Estimated and Actual Vertical Force, Left Front Tire, 45 km/h

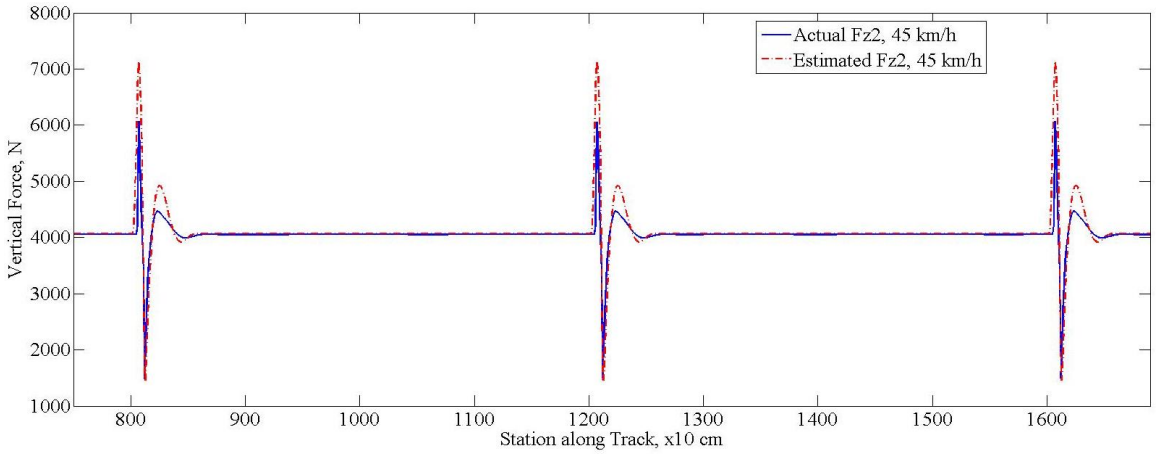

Figure 114: Estimated and Actual Vertical Force, Right Front Tire, 45 km/h

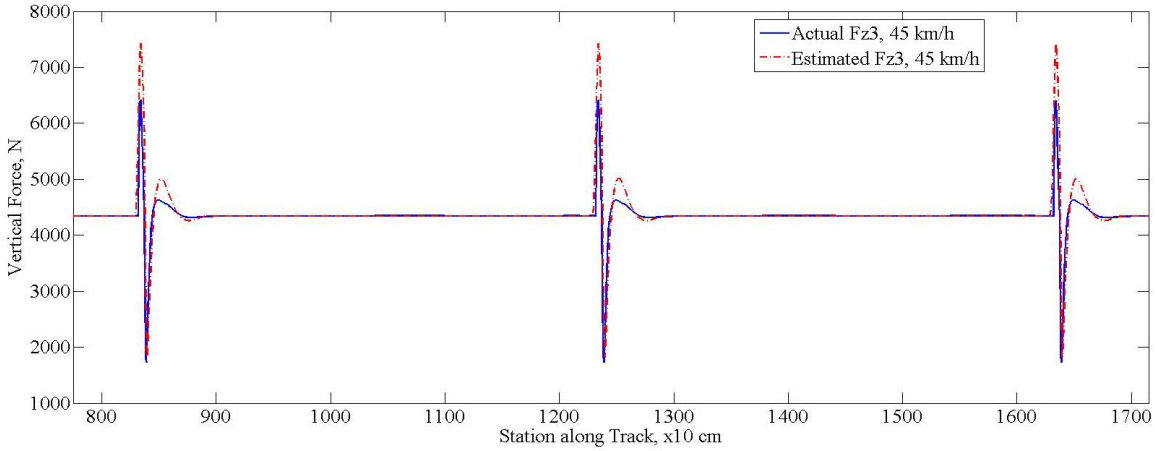

Figure 115: Estimated and Actual Vertical Force, Left Rear Tire, 45 km/h

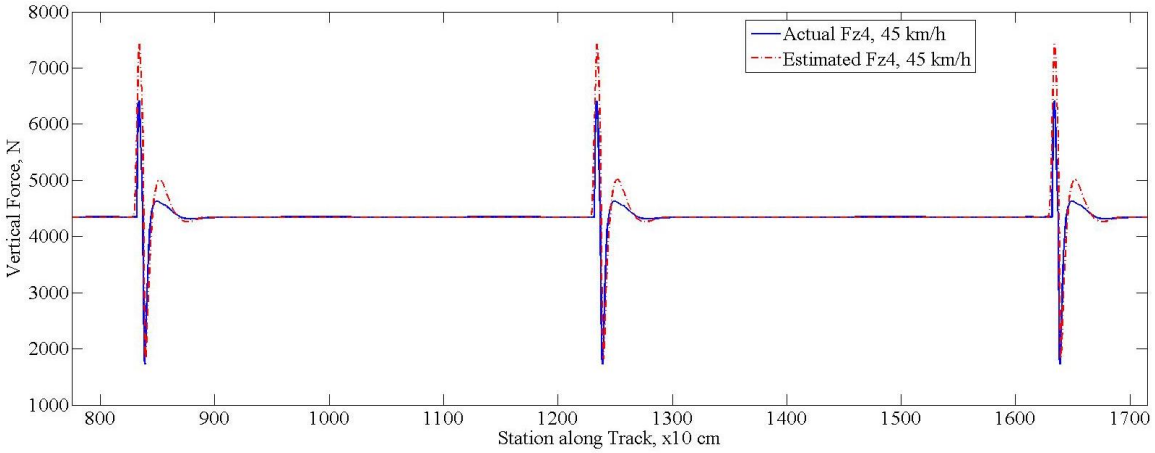

Figure 116: Estimated and Actual Vertical Force, Right Rear Tire, 45 km/h

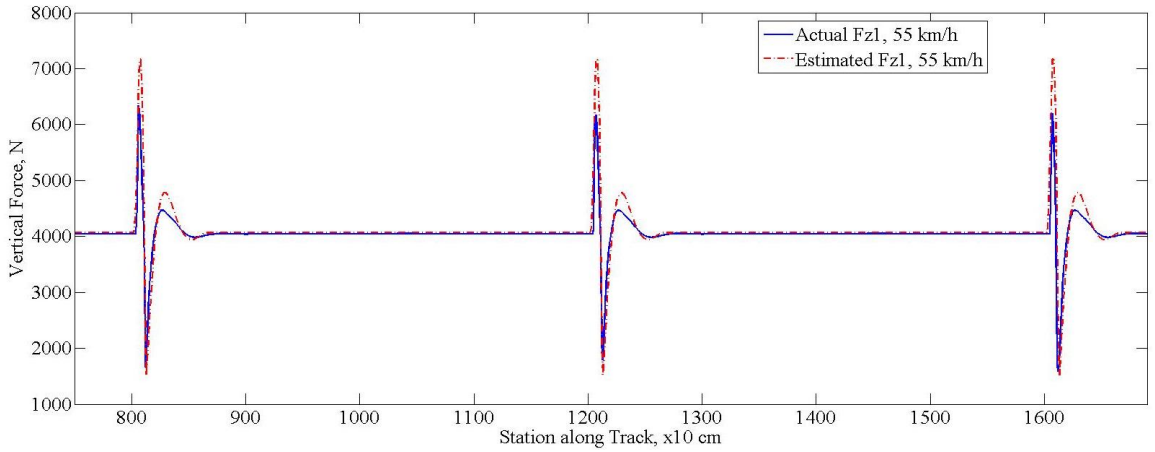

Figure 117: Estimated and Actual Vertical Force, Left Front Tire, 55 km/h

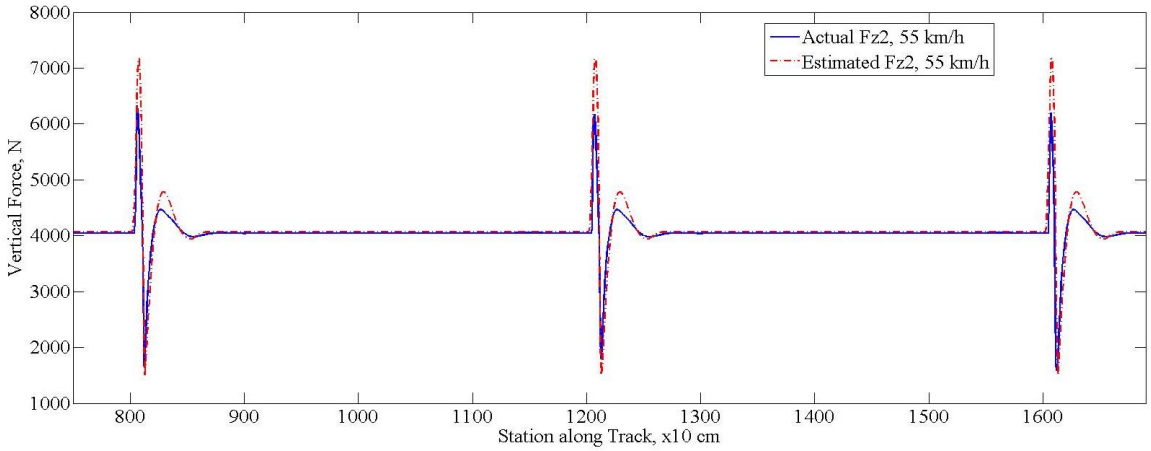

Figure 118: Estimated and Actual Vertical Force, Right Front Tire, 55 km/h

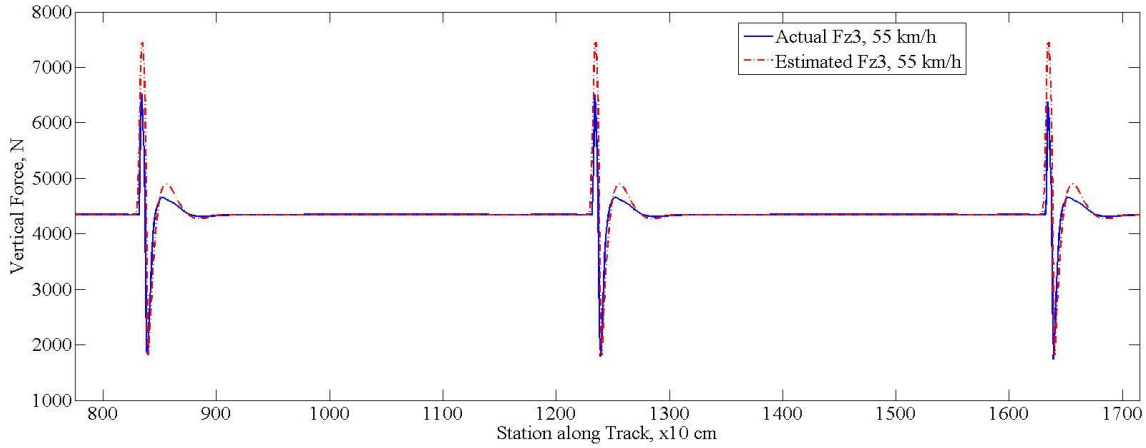

Figure 119: Estimated and Actual Vertical Force, Left Rear Tire, 55 km/h

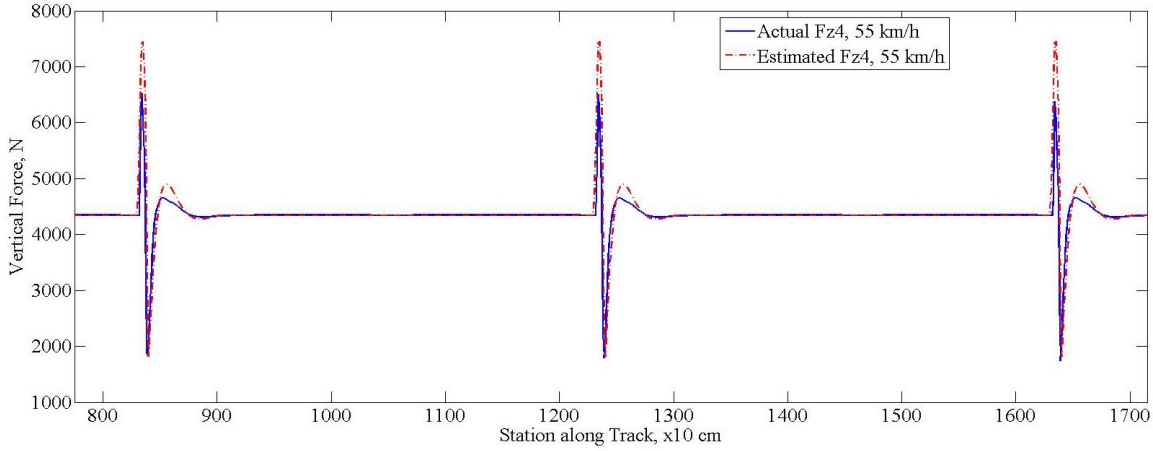

Figure 120: Estimated and Actual Vertical Force, Right Rear Tire, 55 km/h

Appendix D: Impulse Response Anomaly

Initially, a bump 10 mm in height and 25 cm in duration is modeled in CarSim and used as the input excitation to several different velocity runs. The definition of the bump in CarSim is shown in Figure 121.

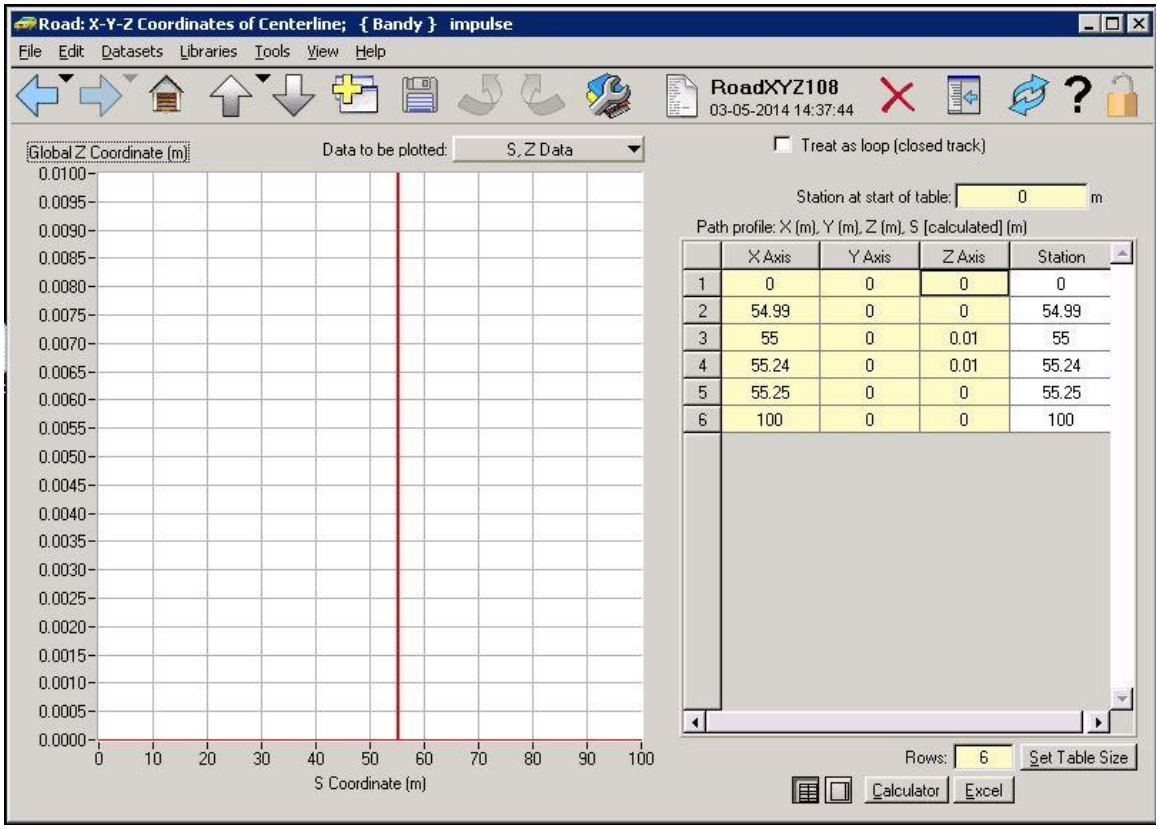

Figure 121: Definition of Impulse 1

The physical results from CarSim are encouraging, showing that the physical displacement of the tires and the vertical force at the tires both increase at the prescribed distance of 55 m (or stations) down the road.

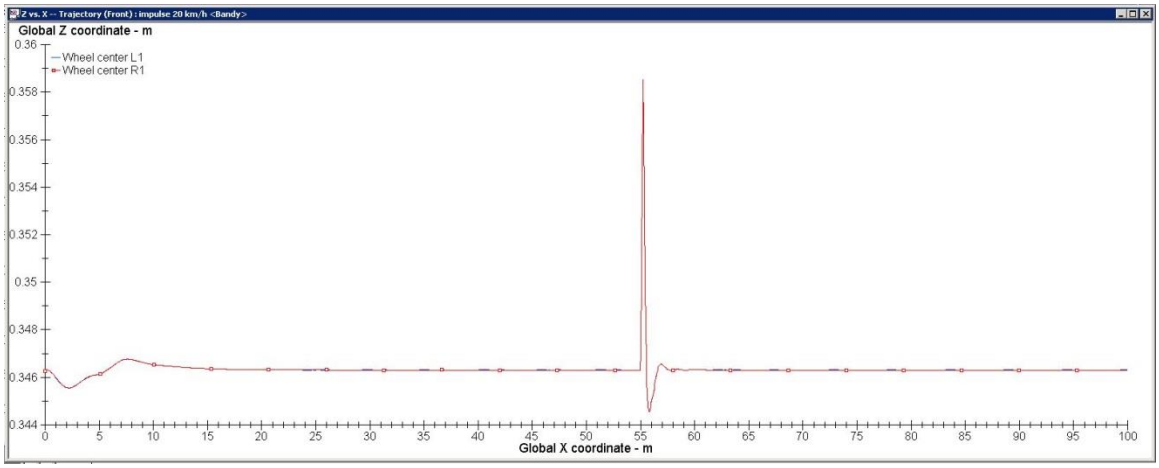

Figure 122: Physical Displacement of Front Tires, Impulse 1

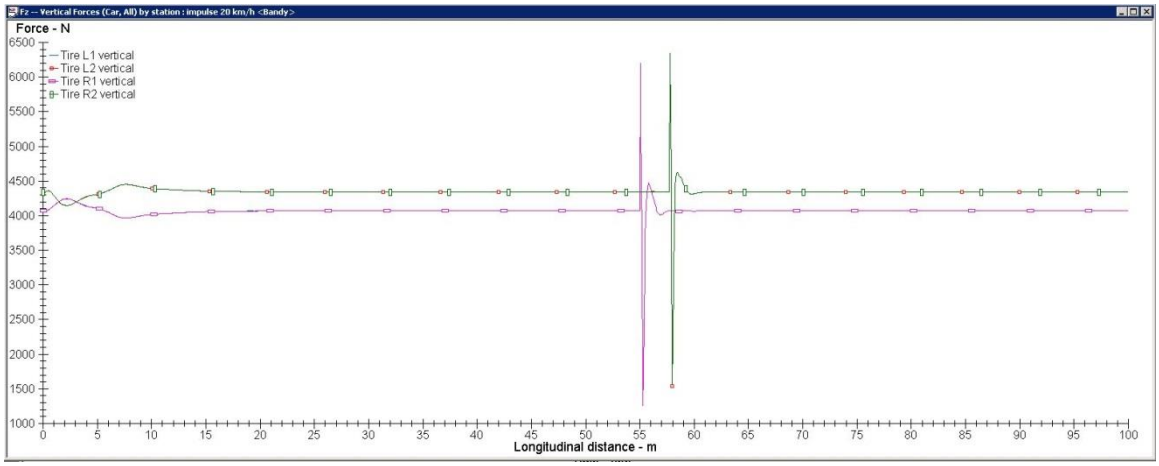

Figure 123: Force Response of All Tires, Impulse 1

There are two main issues with these CarSim responses that are discovered when they are used to predict a perturbed response. Firstly, the vertical force as measured at the center of the tire contact patch reacts before that point ever physically contacts the excitation. Figure 124 is zoomed in on the beginning of the excitation and shows the premature force response.

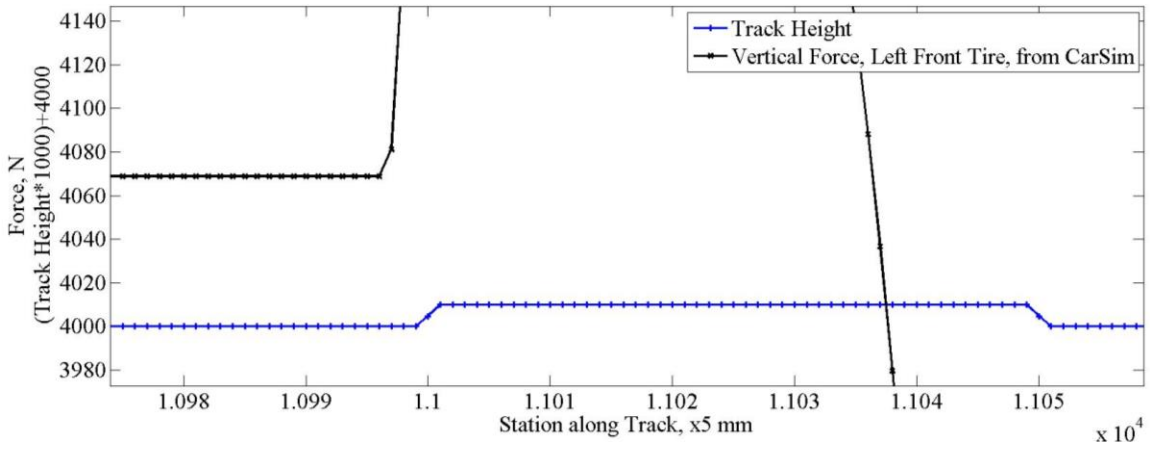

Figure 124: Vertical Force Response to Impulse 1

Secondly, the 25 cm duration is too long to be classified as an impulse – the vertical force at the tires peaks and begins to decrease before the tire is fully over the event. The first issue is due to the difference in tire modeling between the CarSim model and the algorithm developed here. CarSim allows for a variety of tires and tire models, but not for the point-follower model that the impulse response equations above assume. In this scenario, as in the roll, pitch, and yaw estimations, 220/60 R18 tires are simulated. It appears in this figure that the leading edge of the tire is interacting with the bump and causes the force at the tire contact patch to increase before the center of the tire has ever encountered the bump itself.

The second issue is easier to address, so a second bump was defined in CarSim with a height of 1 mm and duration of 2 cm.

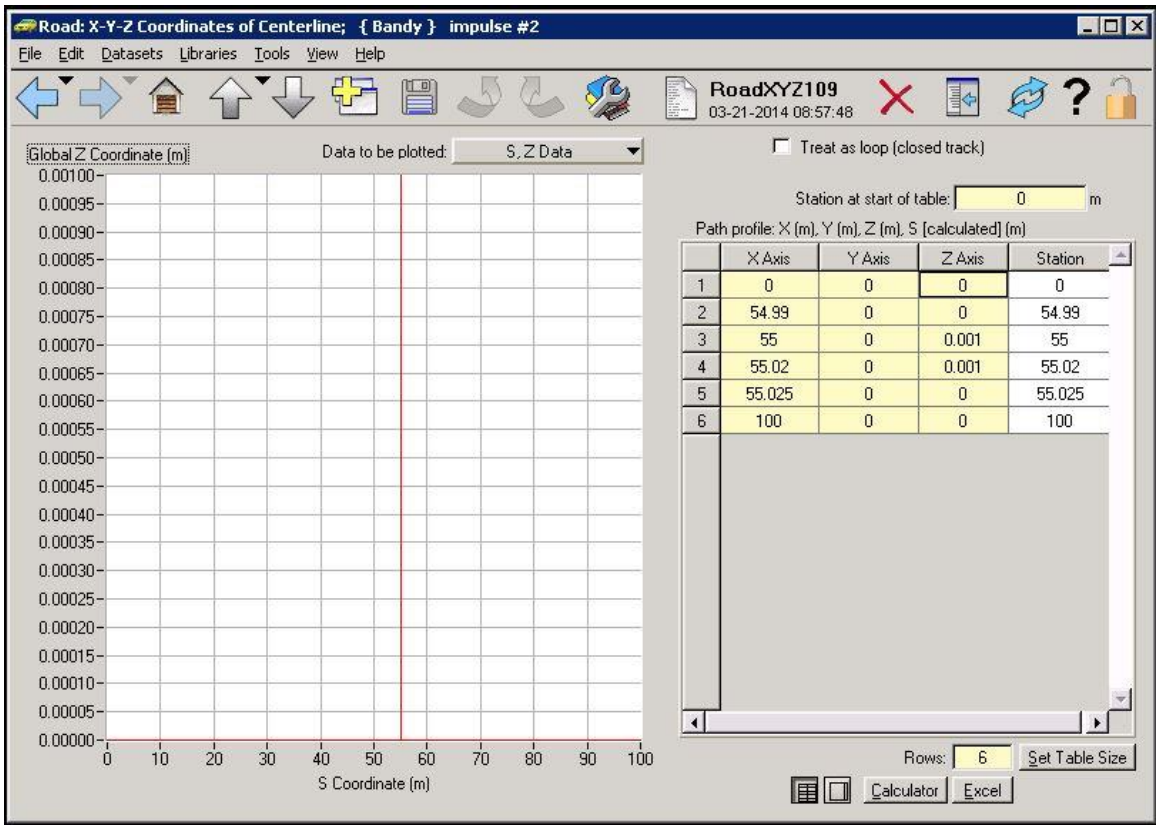

Figure 125: Definition of Impulse 2

The physical displacement of the front tires is in the positive direction as expected, albeit with a much smaller magnitude due to the decrease in height of the excitation. This is shown in Figure 126.

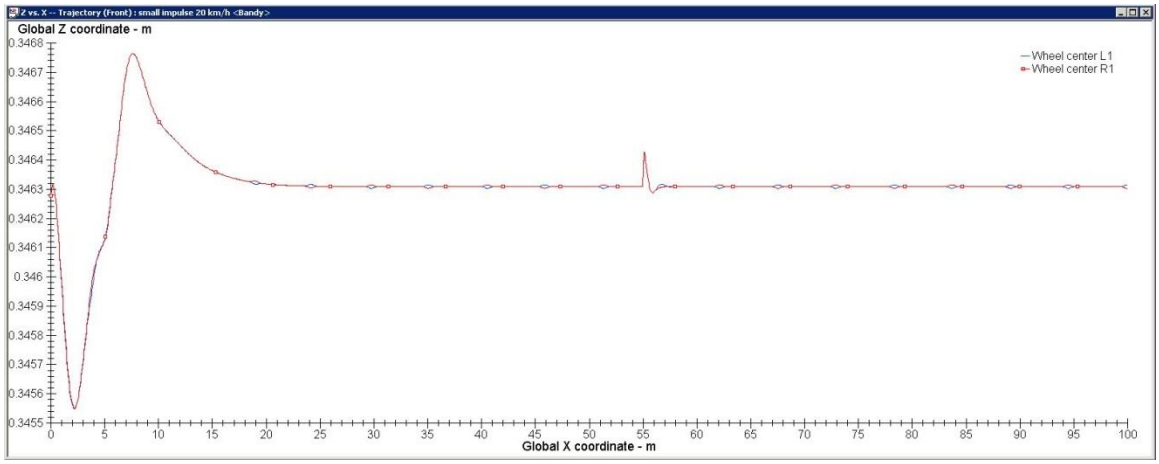

Figure 126: Physical Displacement of Front Tires, Impulse 2

Unfortunately, the vertical force response at the tires is in the negative direction, and this is physically implausible. These results are shown in Figure 127.

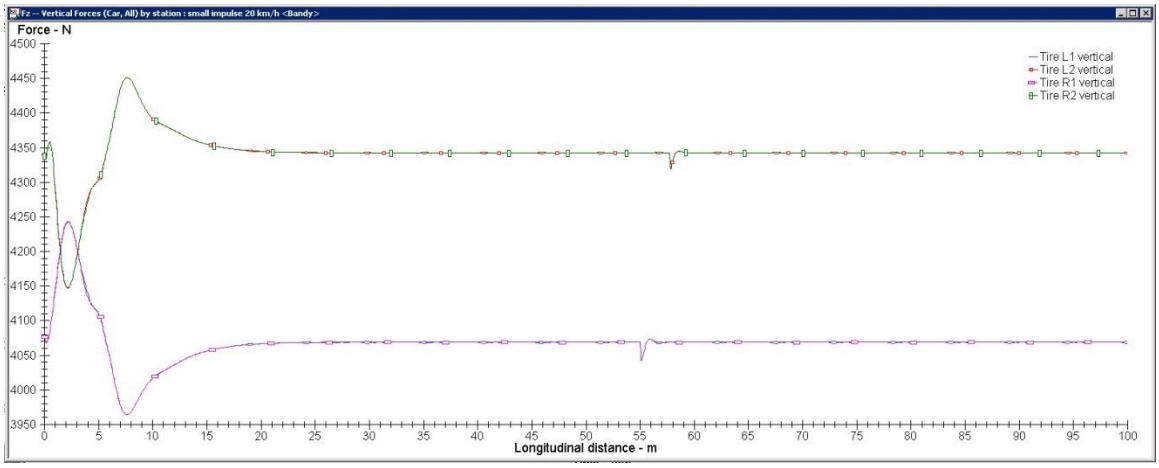

Figure 127: Force Response of All Tires, Impulse 2

A third attempt is made, defining a bump with a height of 10 mm and a duration of 3 cm in the hopes that the 2 cm duration of the second excitation event was too short for CarSim to properly interpolate the results. Figure 128 shows the definition of the event.

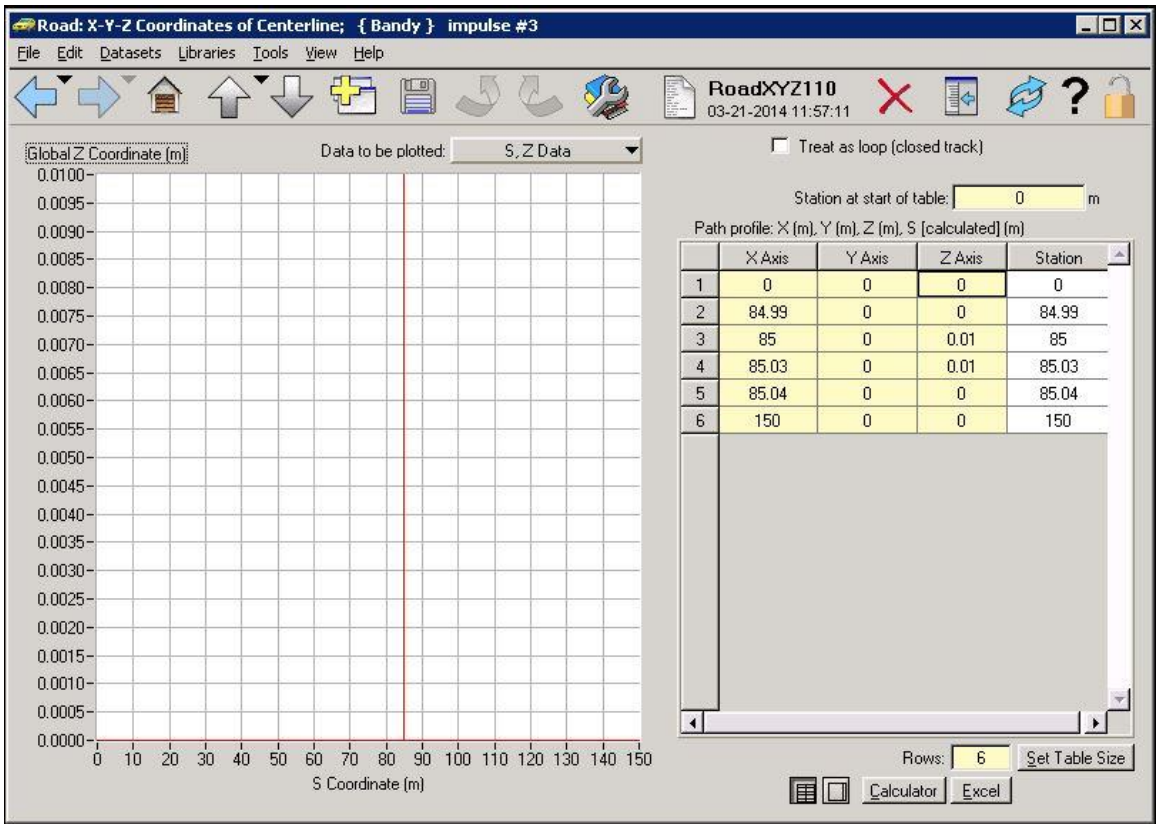

Figure 128: Definition of Impulse 3

This particular excitation gives promising results at 25 km/h – the displacement and force response are both physically plausible, but the tire model in CarSim is still causing the vertical force to increase before the center of the tire, where the force is measured, ever reaches the excitation. Figure 129, Figure 130, and Figure 131 show these results.

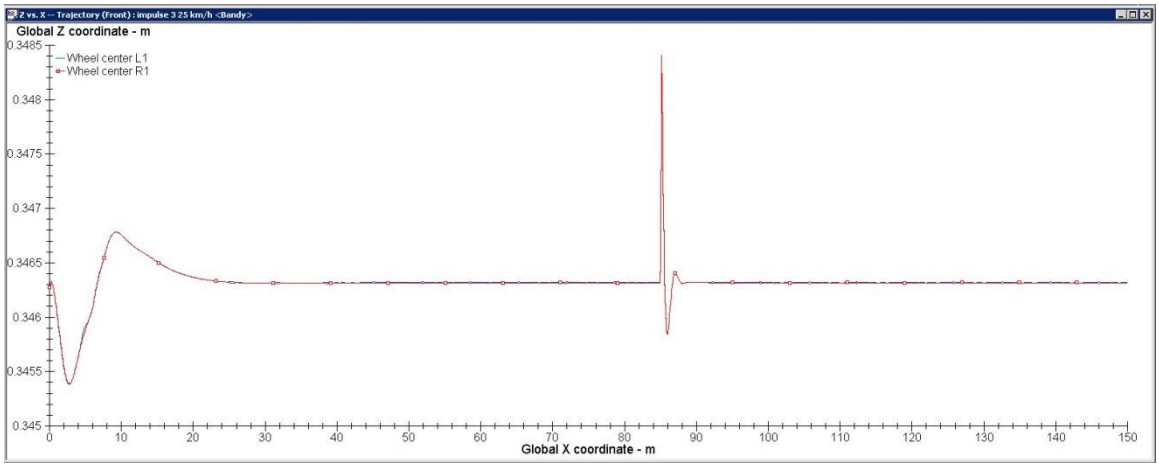

Figure 129: Physical Displacement of Front Tires, Impulse 3, 25 km/h

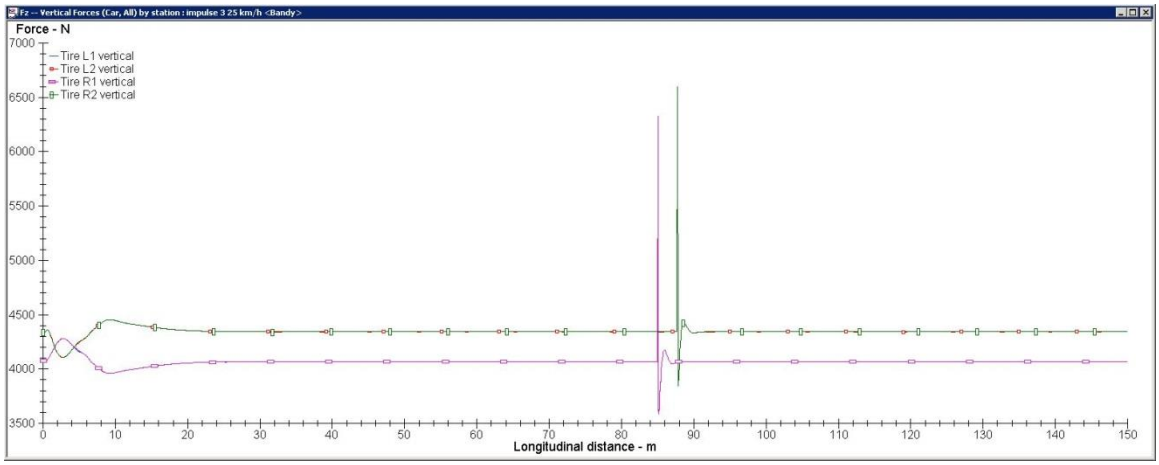

Figure 130: Force Response of All Tires, Impulse 3, 25 km/h

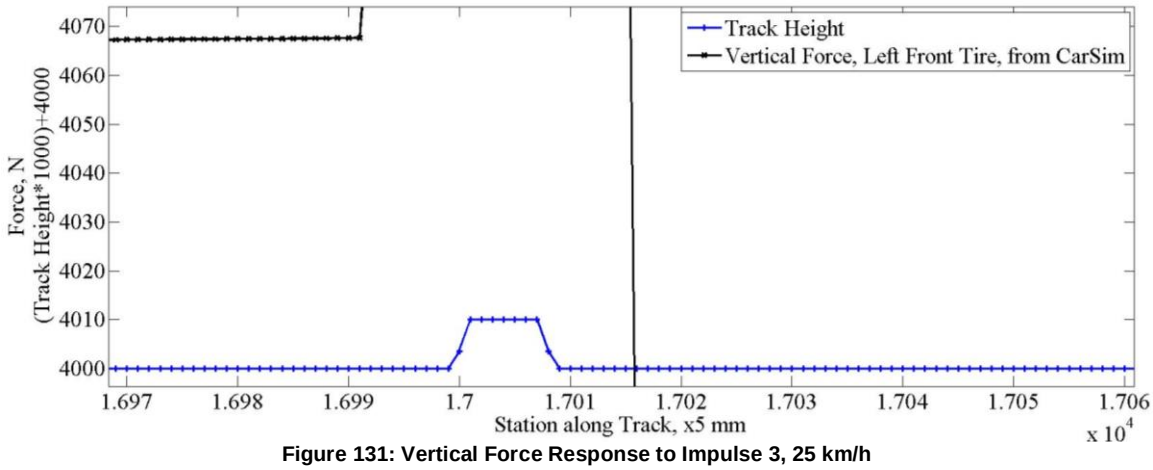

Figure 131: Vertical Force Response to Impulse 3, 25 km/h

This result could be accepted as a remnant of the tire geometry, but the force response at 35 km/h over the same excitation again gives implausible results. When the displacement is in the positive direction, it does not make sound physical sense for the force to change in the negative direction. Figure 132 and Figure 133 show these results.

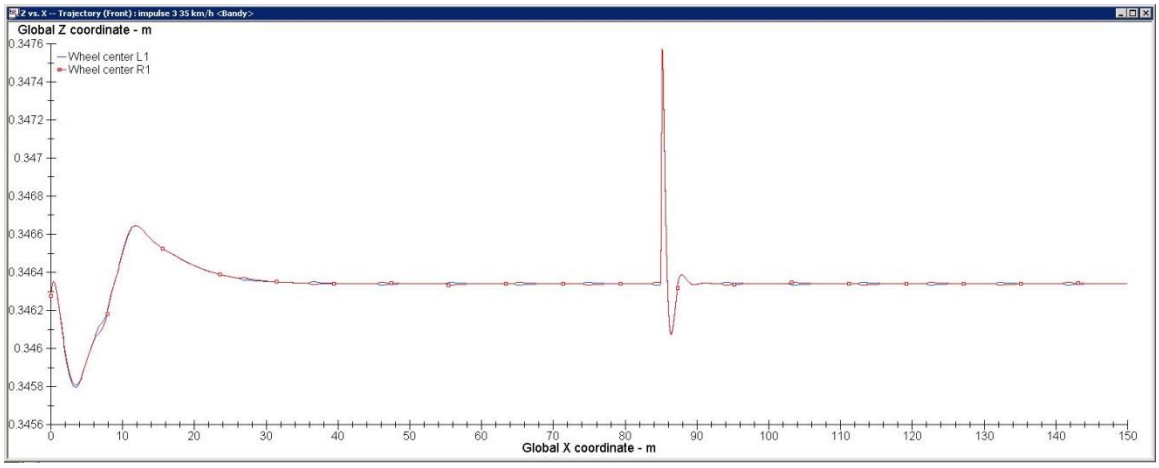

Figure 132: Physical Displacement of Front Tires, Impulse 3, 35 km/h

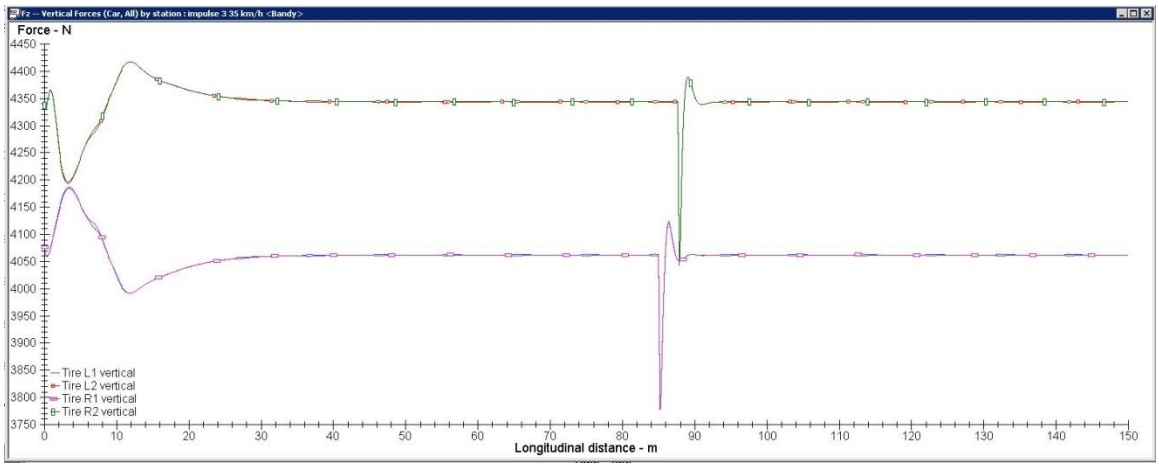

Figure 133: Force Response of All Tires, Impulse 3, 35 km/h

A final attempt is made to define an excitation event which will give physically plausible results for at least 2 separate velocities. The same excitation event is used as in the last case, but this time the tire which is being modeled is no longer specified in CarSim as shown in Figure 134.

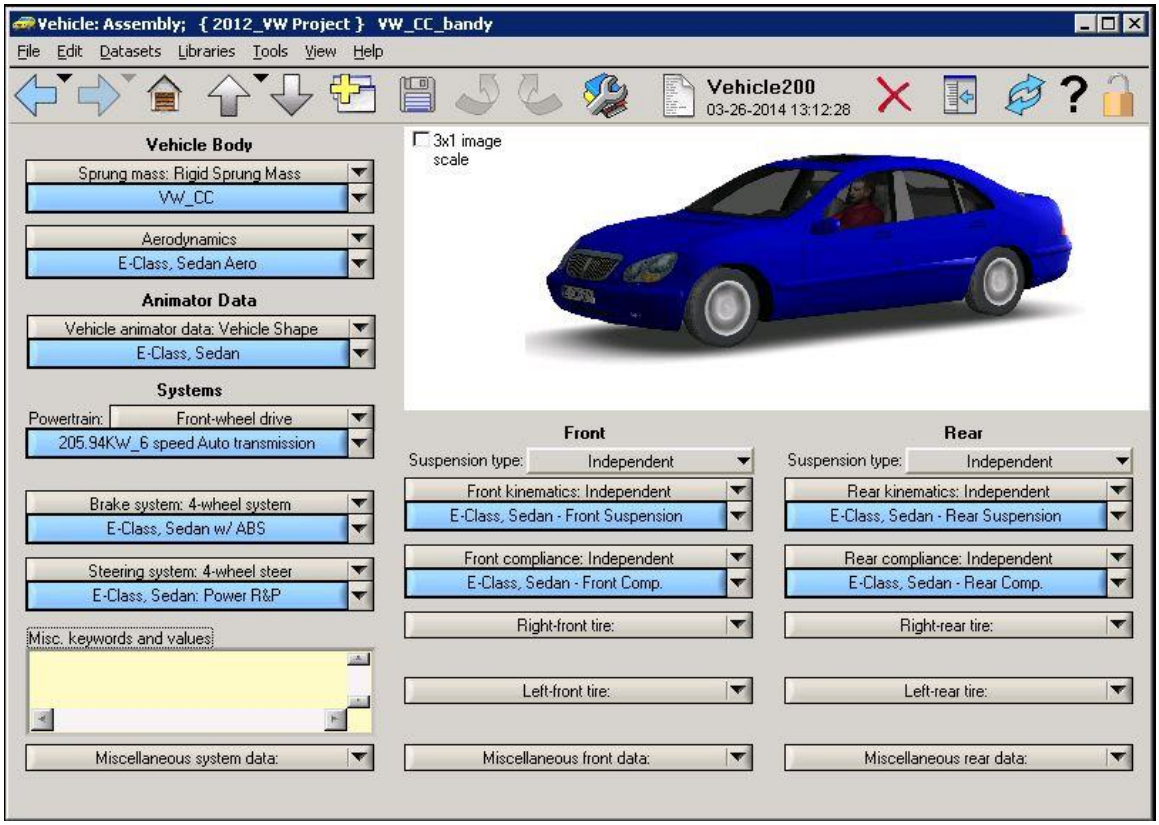

Figure 134: Vehicle Definition with no Tires Specified

While this fourth attempt does provide physically plausible results at the 20 and 25 km/h test scenarios, the force at the center of the tire contact patch is still reacting before that

same point ever reaches the excitation. This proves the point that even when no tires are specified in the CarSim model, there is still an internal tire model that is used. Since this configuration does provide two sets of usable data, it is decided to move forward with these results. Further development is discussed in Section 4.1.1.

Appendix E: Relationship Between $\Delta F_{z,terrain}$ and ΔF_x

This appendix outlines a relationship between changes in vertical force resulting from terrain excitations and the corresponding changes in longitudinal force. The validation of this model is left as future work.

Once again using a Taylor Series to approximate a series of linear perturbations and starting with Equation 72, the following relationship is suggested. First, the perturbed response is written as the known response plus a small linear perturbation.

$$F'_{zi} = F_{zi} + \left.\frac{dF_{zi}}{dv}\right|_{known} \Delta v \tag{73}$$

Next, the change in vertical force can be written as the difference between the perturbed and known forces summed over all stations along the track.

$$\Delta F_{zi} = F'_{zi} - F_{zi} = \left.\frac{dF_{zi}}{dv}\right|_{known} \Delta v \tag{74}$$

$$\Delta F_{zi} = \sum_{j=1}^{i} \frac{dF_{zj}}{dv_j} \Delta v_j \tag{75}$$

Equation 75 can be written in matrix form when the derivative with respect to velocity is solved at each combination of *i* and *j* called c_{ij}.

$$\Delta F_{zi} = [c_{ij}][\Delta v] \tag{76}$$

$$[c_{ij}] = \begin{bmatrix} c_{11} & \cdots & c_{1n} \\ \vdots & \ddots & \vdots \\ c_{n1} & \cdots & c_{nn} \end{bmatrix} \tag{77}$$

$$[\Delta v] = \begin{bmatrix} \Delta v_1 \\ \Delta v_2 \\ \vdots \\ \Delta v_n \end{bmatrix} \tag{78}$$

A relationship between changes in velocity and changes in longitudinal force is originally developed in Equations 48 to 55 and can be used again here. Expanding the change in vertical force to all four tires gives the following.

$$\Delta F_z = \begin{bmatrix} \Delta F_{z1} \\ \Delta F_{z2} \\ \Delta F_{z3} \\ \Delta F_{z4} \end{bmatrix} = \begin{bmatrix} C_1 \\ C_2 \\ C_3 \\ C_4 \end{bmatrix} [\Delta v_x] \tag{79}$$

Equations 63 and 64 can now be expanded to the following forms.

$$\Delta PM_{front} = \left(A_f + C_f D_f\right)\begin{bmatrix}\Delta F_{x1}\\ \Delta F_{x2}\end{bmatrix} + \left(B_f + C_f E_f\right) * \frac{b}{L}[\delta]\left[[I\ I\ I\ I][\Delta F_x][T][U]\right]^T + C_f\begin{bmatrix}C_1\\ C_2\end{bmatrix}\left[\frac{1}{m}[I\ I\ I\ I][\Delta F_x][T][U]\right]^T \quad (80)$$

$$\Delta PM_{rear} = \left(A_r + C_r D_r\right)\begin{bmatrix}\Delta F_{x3}\\ \Delta F_{x4}\end{bmatrix} + \left(B_r + C_r E_r\right) * \frac{b}{L}[\delta]\left[[I\ I\ I\ I][\Delta F_x][T][U]\right]^T + C_r\begin{bmatrix}C_3\\ C_4\end{bmatrix}\left[\frac{1}{m}[I\ I\ I\ I][\Delta F_x][T][U]\right]^T \quad (81)$$

The final form of the equation relating changes in PM and changes in longitudinal force now becomes:

$$\Delta PM_{front} = R_f \Delta F_x \quad (82)$$

$$\Delta PM_{rear} = R_r \Delta F_x \quad (83)$$

Where the *R* matrices are defined as:

$$R_f = \left(\left(A_{f_{expanded}} + C_{f_{expanded}} D_{f_{expanded}}\right) + \left(\left(B_f + C_{f_{original}} E_f\right) G_f U^T T[I\ I\ I\ I]\right) + \left(\frac{1}{m} C_{f_{original}}\begin{bmatrix}C_1\\ C_2\end{bmatrix} U^T T[I\ I\ I\ I]\right)\right) \quad (84)$$

$$R_r = \left(\left(A_{r_{expanded}} + C_{r_{expanded}} D_{r_{expanded}}\right) + \left(\left(B_r + C_{r_{original}} E_r\right) G_r U^T T[I\ I\ I\ I]\right) + \left(\frac{1}{m} C_{r_{original}}\begin{bmatrix}C_3\\ C_4\end{bmatrix} U^T T[I\ I\ I\ I]\right)\right) \quad (85)$$